

**Faculty for Physics and Astronomy  
University Heidelberg**

Master Thesis in Physics  
by

**Michael Winn**

born in Saarbrücken

**2012**



**J/ $\psi$ - Hadron Correlations in Proton-Proton  
Collisions at  $\sqrt{s} = 7$  TeV with ALICE at the LHC**

The Master Thesis was carried out by Michael Winn at the

**Physics Institute of the University Heidelberg**

under the supervision of

**Prof. Dr. Johanna Stachel**



# **J/ $\psi$ - Hadron Correlations in Proton-Proton Collisions at $\sqrt{s} = 7$ TeV with ALICE at the LHC**

## **Abstract**

The azimuthal J/ $\psi$ -hadron correlation is measured for the first time at low transverse momenta of J/ $\psi$  in proton-proton collisions at  $\sqrt{s} = 7$  TeV with ALICE at the LHC. The non-background-free measurement is based on the dielectron decay channel of the J/ $\psi$ -meson and involves extended particle identification. No correlated behavior of charged particles within the same proton-proton collision as the J/ $\psi$  is observed within the achieved precision.

## **Kurzfassung**

Die azimuthale J/ $\psi$ -Hadron Korrelation wurde zum ersten Mal bei niedrigen J/ $\psi$ -Transversalimpulsen in Proton-Proton-Kollisionen bei einer Schwerpunktsenergie von 7 TeV mit ALICE am LHC gemessen. Die nicht untergrundfreie Messung basiert auf dem Dielektronen-Zerfallskanal des J/ $\psi$ -Mesons und umfasst umfangreiche Teilchenidentifizierung. Es konnte kein korreliertes Verhalten der in der gleichen Proton-Proton Kollision auftretenden geladenen Teilchen innerhalb der erreichten Genauigkeit beobachtet werden.



# Contents

<b>Introduction</b> .....	<b>1</b>
<b>I The <math>J/\psi</math> and its Hadronic Production</b> .....	<b>7</b>
I.A The Role of the $J/\psi$ in High-Energy Physics .....	7
I.B Hadroproduction of Charmonium in Theory .....	11
I.C The $J/\psi$ at $pp(p\bar{p})$ Colliders .....	19
I.D $J/\psi$ -Hadron Correlations in $pp(p\bar{p})$ Collisions .....	21
<b>II A Large Ion Collider Experiment at the LHC</b> .....	<b>25</b>
II.A The Large Hadron Collider .....	25
II.B A Large Ion Collider Experiment .....	26
II.B-1 Overview .....	27
II.B-2 The Inner Tracking System .....	29
II.B-3 The Time Projection Chamber .....	30
II.B-4 The Transition Radiation Detector .....	31
II.B-5 The Time of Flight Detector .....	32
II.B-6 The Electro-Magnetic Calorimeter .....	33
II.B-7 The VZERO Detector .....	34
<b>III Data Samples and Analysis Selection Criteria</b> .....	<b>35</b>
III.A EMCAL-Triggered Data 2011 .....	35
III.B Minimum Bias Data 2010 .....	37

III.B-1 Event Selection .....	37
III.B-2 Dielectron Selection .....	37
III.B-2.i PID and Kinematic Basics of $J/\psi \rightarrow e^+e^-$ .....	38
III.B-2.ii Signal Distribution of $J/\psi \rightarrow e^+e^-$ .....	39
III.B-2.iii Correlation Requirements .....	41
III.B-2.iv Cut Variations: PID and ITS Requirements .....	42
III.B-3 Associated Track Selection .....	50
<b>IV Analysis Method.....</b>	<b>53</b>
IV.A Terminology .....	54
IV.B Raw Distributions.....	54
IV.C Corrections on Raw Distributions .....	55
IV.C-1 Corrections via Weighting Factors .....	56
IV.C-2 $\phi$ - and $\eta$ -dependent Corrections via Mixed Events .....	58
IV.C-3 Statistical Uncertainties .....	62
IV.D Background Subtraction.....	65
IV.D-1 General Considerations .....	65
IV.D-2 Fit Approach for Assessing the Background Correlation ...	66
IV.D-3 Statistical Uncertainties .....	67
IV.E $J/\psi$ -Efficiency .....	69
<b>V Systematic Uncertainties.....</b>	<b>73</b>
V.A Uncertainties of the Dielectron-Hadron Correlations .....	73
V.B Signal Extraction Uncertainties .....	74
V.C Uncertainty due to Bremsstrahlung.....	76
<b>VI Results and Discussion.....</b>	<b>77</b>
VI.A Azimuthal Dielectron-Hadron Correlations .....	77
VI.B Azimuthal $J/\psi$ -Hadron Correlations.....	82
VI.C Event Generator Description of $J/\psi$ -Hadron Observables .....	89

<b>VII Conclusion and Prospects</b> .....	<b>91</b>
<b>Appendix A: Mixed Event Correction</b> .....	<b>93</b>
Basic formalism .....	93
Role of pool categories .....	97
<b>Appendix B: Influence of Internal and External Bremsstrahlung     on the Measurement of <math>\phi_{J/\psi}</math></b> .....	<b>101</b>
<b>Bibliography</b> .....	<b>105</b>
<b>Index</b> .....	<b>115</b>



# Introduction

With the advent of proton-proton collisions (pp collisions) at the LHC<sup>1</sup> at CERN<sup>2</sup> in 2009, a new era in particle physics has started. The highest collision energy reached in accelerators increased from a center of mass energy ( $\sqrt{s}$ ) of 1.97 TeV in proton-antiproton ( $p\bar{p}$ ) collisions at the Tevatron accelerator at Fermilab to  $\sqrt{s} = 7$  TeV in 2010 and 8 TeV in 2012 at the LHC. One of the major goals of this large scientific and technological effort is the discovery and characterization of the last missing piece in the Standard Model [1–4] of particle physics: the Higgs Boson, which is the particle associated with the Higgs field (see for a review [5]). The interaction with the Higgs field is responsible for the masses of the weak gauge bosons, the  $W^+$ ,  $W^-$  and  $Z^0$ , and of the elementary fermionic matter fields in the standard model. The verification of the Higgs mechanism would be the ultimate confirmation of the Standard Model describing successfully a large variety of experimental data in particle physics. A failure of the Standard Model prediction or slight deviations will be a strong indication of new physics beyond the common knowledge. A resonance compatible with the properties of the Standard Model Higgs boson has been discovered in several decay channels at the mass of 125 GeV/ $c^2$  by the ATLAS<sup>3</sup> and the CMS<sup>4</sup> collaborations in the combined data sets of 2011 and 2012 [6, 7].

In addition to the pp program, the LHC is able to accelerate heavy-ions with unprecedented energies. During the runs in 2010 and 2011, the collisions of lead ions (Pb-Pb collisions) at a center of mass energy per nucleon pair ( $\sqrt{s_{NN}}$ ) of 2.76 TeV were recorded by ALICE<sup>5</sup>, ATLAS and CMS. These measurements are in continuation of the heavy-ion collision programs at smaller collision energies<sup>6</sup>. The main goal of these research programs at

---

1. Large Hadron Collider

2. Centre Européen de la Recherche Nucléaire

3. A Toroidal LHC Apparatus

4. Compact Muon Solenoid

5. A Large Ion Collider Experiment

6. They were/are carried out at several accelerators: Bevalac at Lawrence Berkeley National Laboratory (LBNL), the Alternating Gradient Synchrotron (AGS) at the Brookhaven National Laboratory (BNL), the Super Proton Synchrotron at CERN and the Relativistic Heavy Ion Collider (RHIC) at BNL, the last-mentioned being the first heavy-ion collider.

the high beam energies at RHIC and at LHC is the creation and precise characterization of the Quark-Gluon Plasma (QGP), a deconfined and chirally restored state of strongly interacting matter at low baryochemical potential<sup>7</sup> and large temperature (see for a review [8]). The early universe is assumed to have evolved through this phase. Besides this interesting connection to cosmology, heavy-ion collisions for instance present the best available laboratory for the investigation of a non-abelian gauge theory, namely QCD, in a true many-body system.

The  $J/\psi$  plays a significant role for the research program in the pp as well as in the Pb-Pb collision system. Firstly, it is very important in the flavor sector measured in pp collisions and exploited by the LHCb<sup>8</sup>, but also by the ATLAS and CMS collaborations, where the full reconstruction of neutral B-meson is very important for B-oscillation studies and of B mesons in general for the investigation of rare decays. The importance of the  $J/\psi$  is based on its sizeable muonic decay width representing a clear signature and on its defined quantum numbers for parity P and charge parity C. It is therefore a true working horse for neutral B oscillation studies and the measurement of the CP violation in the weak interaction sector. The determination of the CP violating phase  $\phi_S$  in the decay  $B_S^0 \rightarrow J/\psi + \phi$  by LHCb [9] is just one important example for the use of  $J/\psi$  in flavor physics.

Beside the detection of  $J/\psi$  for investigations in the B physics sector, the  $J/\psi$ -production on its own is an active field of research. Especially, the creation pattern of  $J/\psi$  in heavy-ion collisions was early proposed as a spectacular signature of the Quark-Gluon Plasma. It is clearly among the most interesting and most controversially discussed probes of this new state of matter. Matsui and Satz argued in 1986 that the presence of the QGP medium leads to the 'melting' of  $J/\psi$  due to color screening [10]. The experimental effect is a reduced detection rate of  $J/\psi$ -mesons in heavy-ion (AA) collisions compared to pp collision results scaled by the number of binary collisions. This applies more generally also to other charmonia and bottomonia states[11], when the 'melting' temperature for the specific state in the created medium is reached for a given collision energy and system. Since the  $J/\psi$  yield has significant contributions from other charmonium states, the  $\chi_c$  states and the  $\psi(2S)$ , the melting of the different charmonia states at different temperatures would lead to a sequential suppression behaviour of  $J/\psi$  as a function of temperature. Therefore, the observed suppression pattern could be used as a thermometer for the system[11] (see for a review [12]). However, the situation is complicated by effects, which come into play not due to the presence of a medium, but due to fact that there are additional differences between the pp and the nucleus-nucleus (AA) collision system

---

7. The baryochemical potential quantifies the energy, which is necessary to add a baryon to the ensemble of particles, either hadrons or quarks and gluons.

8. LHCbeauty

among them most prominently the possible absorption of charmonia caused by the presence of cold nuclear matter and the difference in the parton distribution functions of nuclei compared to the parton distribution functions of the proton. These phenomena lead to a suppression of the  $J/\psi$  compared to the pp results, but also exhibit dependencies on the collision energy. Their impact is investigated in proton-nucleus (pA) collisions, which are therefore an indispensable reference system especially for the investigation of heavy quarkonia in AA collisions.

Today, the suppression of heavy quarkonium states as a thermometer of the created medium, is in the charmonium sector in high energy heavy-ion collisions at RHIC and LHC questioned by models assuming that the charmonium production is significantly altered by recombination of initially produced  $c(\bar{c})$ -quarks to charmonium. The models can be divided in two principal classes, depending whether they assume a non-primordial production during the whole time evolution of the plasma [13, 14] or only during hadronization at the phase boundary [15, 16]. Both assumptions lead experimentally to a less pronounced suppression or even a striking enhancement of  $J/\psi$ -production in Pb-Pb compared to the scaled pp production at LHC energies due to the large amount of produced  $c\bar{c}$ -pairs. Despite the similarity of the  $J/\psi$ -prediction, both model types might be disentangled by differences in the  $\psi(2S)$ - and  $\chi_c$ -production[17]. Measurements of these charmonium states will be therefore crucial ingredients for a complete picture. The arising questions, which can be answered at LHC, are therefore: *Is the proposed colour screening picture in the medium created at the LHC not sufficient to describe the data? Are charm quarks thermalized and charmonia described by statistical hadronization or is charmonium described in the framework of kinetic theory inside the QGP?*

A confirmation of the enhancement scenario would be a strong evidence for deconfinement in heavy-ion collisions, since any hadronic picture is hardly accounting for a combination of  $D$ -mesons to  $J/\psi$ [18] and due to the fact that charm quarks are presumably only produced in the initial hard scattering processes of the heavy-ion collision. The experimental mission can be primarily tackled by ALICE being the only detector at the LHC exploiting the low- $p_T$  sector of charmonium production in Pb-Pb collisions, where low- $p_T$  refers to values not exceeding approximately 4-5 GeV/ $c$ . This region in phase space is most sensitive to the proposed phenomena of recombination due to the thermalization (or at least features of thermal behaviour) of the recombining charm quarks within the bulk particle production. First results of low- $p_T$   $J/\psi$ -production by ALICE at forward rapidities support the conjecture of a significant non-primordial  $J/\psi$  production [19]. Since the largest energy densities, indicated by the largest track densities, are reached and the strongest effects of collective behaviour are observed at midrapidity in heavy-ion collisions, medium effects on particle chemistry like the  $J/\psi$ -behavior are expected to be strongest at midrapidity. Therefore, the

measurement of low- $p_T$   $J/\psi$  at midrapidity will be most crucial to consolidate the emergent picture. The behavior observed by ALICE is compatible within the experimental errors with the different recombination pictures, although the present uncertainties still prevent quantitative comparisons [20]. More precise data on charmonium in the AA, the pA collision system and in addition the measurement of the total charm cross section in pp and in AA, which are important ingredients for the quantification of non-primordial charmonium production, are necessary for final conclusions.

In the case of pp collisions, the understanding of  $J/\psi$  production is of main importance as the baseline for the production in heavy ion collisions. Moreover, the charmonium production mechanism in pp collisions is under close investigation, since the theoretical description is very tough due to the intrinsic interplay between perturbative and non-perturbative QCD in the case of heavy quark bound states. The latter point is based on the assumption that perturbative QCD (pQCD) provides a reliable tool for the calculation of hard parton scattering processes in a pp collision. Due to the considerable  $J/\psi$  mass of 3.1 GeV/ $c$ , the production of the  $c\bar{c}$ -pair state should be accessible within this framework. Nevertheless, non-perturbative processes come into play, when the  $c\bar{c}$ -pair evolves in the  $J/\psi$ -resonance state. In this context, it has to be settled, whether the central assumption of factorization between the non-perturbative and the perturbative processes in QCD can be applied by making use of the whole theoretical inventory including effective field theory derived from QCD[21]. Therefore, charmonium production in pp collisions plays a major role for the basic understanding of the strong interaction.

ALICE has the opportunity to contribute significantly to the investigation of charmonium in pp collisions, because it can measure  $J/\psi$  down to  $p_T = 0$  and therefore the total cross section at midrapidity like in Pb-Pb collisions, which is unique at the LHC[22]. Furthermore, ALICE can exploit its tracking and particle identification capabilities down to very low- $p_T$  in order to characterize the event topologies and the particles associated with a  $J/\psi$  at midrapidity very accurately. The latter capabilities give access to observables constraining further the production mechanism beyond the total  $J/\psi$  cross section, the  $p_T$  differential cross section and the polarization being the standard measurements in the field. In this respect, the measurement of correlations of  $J/\psi$  with particles produced in the same event is one possible approach towards a better understanding of charmonium production in pp collisions.

This master thesis aims at a comprehensive introduction of the methodology and a first analysis of the correlation of charged tracks associated with  $J/\psi$  in pp collisions at  $\sqrt{s} = 7$  TeV with the ALICE detector setup at the LHC. The first chapter provides the theoretical and experimental context. In the following, the LHC and the ALICE detector are presented with emphasis on the details relevant for this analysis. The third chapter

explains the selection criteria for events, dielectron pairs and charged tracks. It follows the explanation of the analysis method. Finally, the results are presented and discussed. The last chapter consists of a short conclusion and an outlook concerning the future opportunities for  $J/\psi$ -hadron correlations within ALICE.



## – Chapter I –

# The $J/\psi$ and its Hadronic Production

### I.A The Role of the $J/\psi$ in High-Energy Physics

The discovery of the  $J/\psi$  particle in 1974 was an important step in the foundation of the standard model of particle physics: Two different experiments, an  $e^+e^-$  collider experiment at SLAC<sup>1</sup> [23] and a fixed target experiment at BNL<sup>2</sup> (a proton beam on a Beryllium target) [24], observed a narrow resonance at a mass of  $3.1 \text{ GeV}/c^2$ . The state was soon interpreted as a bound state of a charm and anticharm quark ( $c\bar{c}$ ) pair [25]. This experimental achievement called the 'November Revolution of Particle Physics' represents the first striking experimental evidence for the charm quark being the partner of the strange quark in the second generation of quarks. The effort of both experiments was awarded by the Nobel prize for S. Ting and B. Richter in 1976.

The  $J/\psi$  is a vector state with odd C-parity ( $J^{PC} = 1^{--}$ ) and has a total width of  $(92.9 \pm 2.8) \text{ keV}$  including a sizeable branching fraction (B.R.) in electron positron ( $e^-e^+$ ) pairs ( $(5.94 \pm 0.06)\%$ ) and in muon-antimuon ( $\mu^-\mu^+$ ) pairs ( $(5.93 \pm 0.06)\%$ ) [26]. Its narrowness for a hadronic state in this mass range is related to its charm content. Firstly, the decay into open charm mesons is kinematically forbidden (see Figure I.1): The  $J/\psi$  is lighter than a pair of  $D^0/\bar{D}^0$ , which are the lightest particles containing single charm quarks. Therefore, the decay has to proceed diagrammatically via gluon lines and is not possible via  $c$ -quark lines. Due to the conservation of color,  $J/\psi$  is a color singlet state, the decay via a single gluon is not allowed. In addition, the odd charge parity forbids the decay of the  $J/\psi$  vector state into an even number of gluons in analogy to the corresponding positronium

---

1. Stanford Linear Accelerator Center  
2. Brookhaven National Laboratory

to photons decay in QED [27]. Hence, the strong decay of the  $J/\psi$  has to involve at least three gluons. This leads to a strong partial decay width proportional to  $\alpha_S^3$ ,  $\alpha_S$  being the coupling constant of the strong interaction, since every gluon-quark vertex introduces another factor of  $\alpha_S$  in the matrix element squared. The scale for the momentum transfer in the decay process is set by the  $J/\psi$ -mass, which implies for the running coupling  $\alpha_S$  a value of approximately 0.26 [28]. Therefore the purely gluon induced decay width amounts to roughly 64% of the total decay width [26]<sup>1</sup>. In contrast to this, the electromagnetic decay can proceed via a single virtual photon. The respective decay width is therefore proportional to the fine structure constant  $\alpha_{QED}$ , the coupling constant of QED<sup>3</sup>, which can be taken as approximately 1/137 for the process scale of 3 GeV/ $c^2$ <sup>4</sup>. Therefore, the electromagnetic decay and the strong decay contribute within the same order of magnitude to the total decay width despite the by far smaller electromagnetic coupling strength. Naturally, not only the difference of the coupling constants and their powers have to be taken into account. In addition, the color factors for the involved QCD graphs and their possibly different structure compared to QED have to be considered. Other differences as for example the available phase space for the decay products play a crucial role, too ( e.g. one has to count only the lepton and quark pairs which are actually kinematically allowed). The argumentation using the coupling strengths gives therefore just a very rough estimate, what is to be expected. Finally, it has to be verified by more rigorous calculations, see e.g. [29], where also non-perturbative effects within an effective field theory approach are considered. The latter approach will be discussed in more detail later on regarding the production of  $J/\psi$ . Nevertheless, the only qualitatively derived picture is confirmed by the sizeable branching fraction of the  $J/\psi$  into  $\mu^-\mu^+$  and  $e^-e^+$  which involve only a part of the electromagnetic decay width (the virtual photon can also couple to quarks).

The  $J/\psi$  was just the starting point for the discovery of a whole family of bound states associated with the quark content of a  $c\bar{c}$ -pair below and above the open charm threshold, which corresponds to the lowest invariant mass necessary to produce a pair of two D-mesons. The mass hierarchy and the respective quantum numbers of the different states shown in Fig. I.1 can be understood by regarding the  $c\bar{c}$ -pair as the QCD analogue of the positronium in QED. Neglecting relativistic effects<sup>5</sup>, it is possible to describe the quarkonium system by a Schroedinger equation as in case of the positronium. As

---

1. There is also a non-negligible partial decay width from  $\gamma gg$  of 8.8%.

3. Quantum ElectroDynamics

4.  $\alpha_{QED}$  is only slightly scale dependent in the momentum scale ranges accessible at high energy physics experiments.  $\alpha_{QED} = 1/137$  correspond to its Rutherford limit (momentum transfer  $\rightarrow 0$ ).

5. The velocity squared of the relative motion of the two charm quarks in the charmonium system is roughly 0.23 [27] in units of speed of light squared [27].

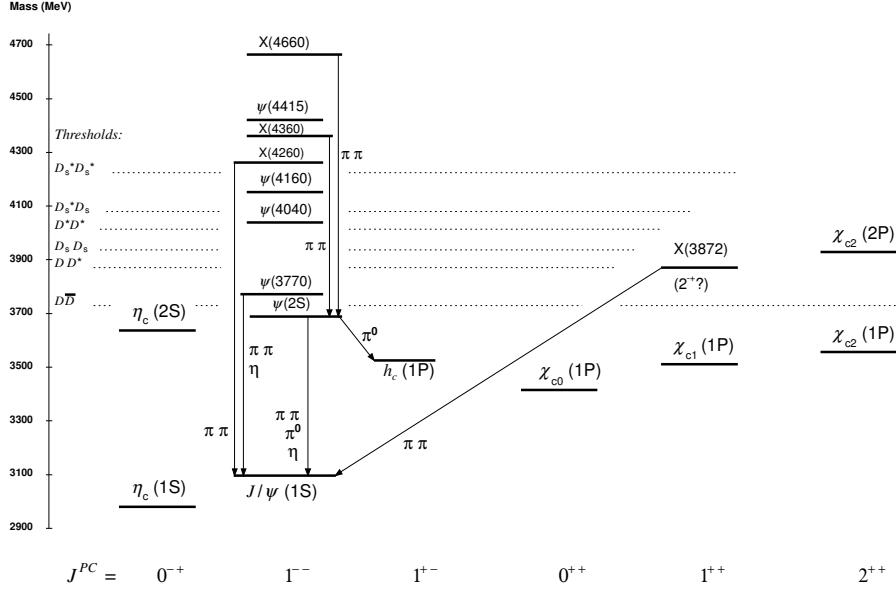


Figure I.1: Mass spectrum of charmonium states according to [26].

in case of QED, the eigenstates of the Hamiltonian represent the different states in the spectrum and the corresponding eigenvalues of the operator the different masses. In addition to a different reduced mass  $\mu = \frac{m_c \cdot m_{\bar{c}}}{m_c + m_{\bar{c}}} = m_c/2$  of the quarks compared to the reduced mass of the electron-positron pair, one has to modify the potential to account for the different behaviour of the strong interaction compared to the electromagnetic interaction. The least complicated, but most efficient parametrization is the so-called Cornell potential (see for a first review of this approach [30])<sup>6</sup>:

$$V(r) = -\frac{4}{3} \frac{\alpha_S(r)}{r} + k \cdot r \quad (\text{I.1})$$

Where the equation is given in natural units ( $\hbar = c = 1$ ) and the used variables are defined as:

- $r$ : distance between the two quarks
- $\alpha_S(r)$ : the strong coupling constant, a typical value is  $\frac{3}{4}\alpha_S = \pi/12$  by omitting the distance dependence for the different charmonium states for simplicity
- $k$ : so-called string tension (typical value:  $\sqrt{k} = 0.445$  GeV).

The charm quark mass in this effective model is typically taken to be  $1.25 \text{ GeV}/c^2$ . The numerical values are taken from [12].

6. In its original version, the coupling in the Coulomb-like term is a parameter of the model. The used parameter turns out to be roughly of the same size than what one is expecting from QCD.

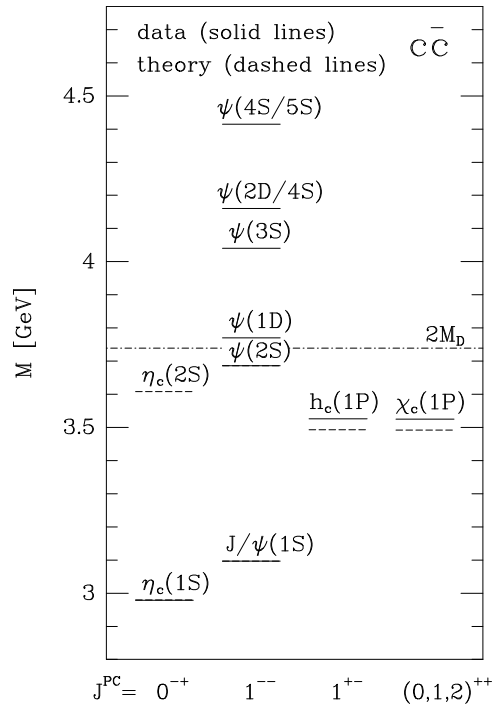


Figure I.2: Mass spectrum of charmonium states from experiment compared with a non-relativistic potential model with slightly modified functional shape of the potential taken from [27]. Models with the simple parametrization described in the text give also results very close to the experimental data, see e.g. in [12].

Equation I.1 encodes the phenomenologically most important property of QCD: Confinement. The impossibility to observe free color charges<sup>7</sup> in vacuum is reflected by the phenomenologically motivated term  $k \cdot r$  (see [27] for a short overview and further references), which is absent in QED and which dominates the large distance behaviour.

The small distance behavior is expressed by the single gluon exchange term  $-\frac{4}{3} \frac{\alpha_S(r)}{r}$  in complete analogy to QED. This implies already that the described state is at least for small radii in a weak coupling regime. In addition, the strong running of the coupling appears implicitly by the mentioned  $r$ -dependence of  $\alpha_S$ , which is dictated by the asymptotic freedom behaviour of QCD. The non-abelian structure of QCD with its SU(3) gauge symmetry group has to be taken explicitly into account by the numerical factor 4/3, which is absent in QED with the abelian gauge symmetry group U(1).

The description of the charmonium spectrum within the effective potential model is very successful in describing the observed spectrum of charmonia states. A model calculation is depicted in Fig. I.2.

<sup>7</sup>. represented by the charm quarks

It might seem, that from this conclusive picture based on the look at the mass spectrum, charmonium is a well understood system, at least in vacuum, if one neglects the controversial role of some resonances in the charmonium mass range [26]. In fact, the precise theoretical description of the charmonium decays and even more of the charmonium production remains difficult. In particular, the production of  $J/\psi$  in hadronic collisions although discovered at the BNL nearly 40 years ago is still not settled in pp ( $p\bar{p}$ ) collisions.

## I.B Hadroproduction of Charmonium in Theory

Although the  $J/\psi$  was also discovered in pA collisions, the theoretical description of hadroproduction already in pp ( $p\bar{p}$ ) remains very challenging [21]. We will focus the following discussion on the production in the latter collision system. In contrast to the production of hadrons composed of a heavy and a light quark,  $J/\psi$  -production does not only involve the quark mass of the heavy quark and  $\Lambda_{QCD}$  as relevant intrinsic scales, but several intrinsic scales [21]:

1. charm quark mass  $m_c$
2. the typical momentum of the charm quarks in the restframe of  $J/\psi$   
 $m_c v$
3. the binding energy of the charm quarks at the scale of  $m_c v^2$

The quantity  $v$ <sup>8</sup> denotes the relative velocity of the charm quarks in units of the speed of light. The occurrence of these scales and the ordering  $m_c > m_c v > m_c v^2$  is due to approximate non-relativistic nature of the system. In addition, one has to consider the extrinsic production scale, which is taken to be  $m_T = \sqrt{(2m_c)^2 + p_T^2}$  in pp ( $p\bar{p}$ ), where  $p_T$  denotes the transverse momentum of the detected charmonium state. Although the final creation of the quarkonium involves therefore softer processes<sup>9</sup>, the production scale  $m_T$  should give access to a perturbative treatment of the hard production of the  $c\bar{c}$ -pair<sup>10</sup>. But this is only the case, if the hard part of the production cross section is factorizing with respect to the non-perturbative part. In addition, the latter are assumed to show a universal behavior independent

---

8. Here and in the following theory chapter, natural units are adopted ( $\hbar = c = 1$ ).

9. Whether the momentum or/and the binding energy scale can be still perturbatively treated depends on the specific quarkonium state, which is considered. For the low lying bottomium state  $\Upsilon$ , this is usually assumed to be the case, whereas already for the light charmonium state  $J/\psi$ , the applicability of perturbation theory for this specific purpose is not clear [21].

10.  $m_T$  is strictly larger than the mass of the  $c\bar{c}$ -pair  $m_{c\bar{c}} \approx 3 \text{ GeV}/c$ .  $m_T$  is therefore a scale where the running coupling constant  $\alpha_S$  should be already small enough for a perturbative approach.

of the collision system and energy. Finally, it is not evident that the factorization assumption holds in the context of charmonium production, which is indispensable for the applicability of perturbative QCD.

In this light, it is useful to comment briefly more generally on the aspects of the theoretical picture of heavy quarkonia relevant for the hadronic production.

Naturally, the consideration of the charmonium system as a non-relativistic QCD pendant to the positronium in QED is simplifying, since the relevant scales for the  $J/\psi$  are already at the lower edge of scales treatable in perturbative QCD and of the modelling in a pure Schroedinger equation picture of two colour charges interacting with single gluon exchange for small distances. In addition, the momentum scales of the individual quarks are not a truly non-relativistic system with  $v^2 = 0.3$ . Finally, the *ad-hoc* introduction of an effective confinement potential is from a theoretical point of view unsatisfying.

It is therefore desirable to derive the wave function of the quarkonium and the interactions of quarkonium states from the QCD Lagrangian<sup>11</sup>:

$$L_{QCD} = -\frac{1}{4}F_{\alpha\beta}^A F_A^{\alpha\beta} + \sum_{flavours} \bar{q}_a (i\gamma_\mu D^\mu - m)_{ab} q_b \quad (\text{I.2})$$

where  $F_{\alpha\beta}^A$  corresponds to the Yang-Mills field tensor with the colour index  $A$ , including the pure gluon interactions,  $q_a$  is the spinor field for the quarks of flavor  $a$  and  $m$  the corresponding mass. The covariant derivative  $D^\mu$  incorporates the coupling between the quark field and the Yang-Mills field. More details and explanations can be found in [27].

The description of the spectroscopy and the decay of charmonium has seen large progress by relating the properties of charmonium to fundamental QCD by the use of QCD sum rules, effective field theory and also the combination of the latter approach with numerical calculations on the lattice (see for a review [21]). For the purpose of this work focusing on the hadronic production, we will only sketch the aspects of charmonia in the approaches, which are used in the context of production and are at the moment most widely considered.

The most common approach to describe quarkonium in a rigorous scheme is the use of non-relativistic QCD (NRQCD). NRQCD represents an effective field theory derived from QCD by introducing a ultraviolet cut-off  $\Lambda$  at the scale  $m_c$  for the part of the QCD Lagrangian encoding the dynamics of the heavy quark-antiquark system [29]. Interactions of the bound system at the scale  $\Lambda$  or above, which are excluded by this approach originally, are

---

11. The notation is adapted from the introductory chapter of [27], the P and CP violating term allowed by the gauge symmetry is omitted due to its irrelevance for the purpose of this work and due to the absence in nature within the accuracy of experiments sensitive to these effects. The gauge-fixing term needed for perturbation theory as well as the ghost terms are omitted for simplicity. More details and references can be found in [27].

incorporated by local four-fermion operators. In a second step, it is possible to separate the heavy-quark and antiquark degrees of freedom, which finally allows to derive a Schroedinger-like system including systematic relativistic correction terms.

The resulting representation of the  $J/\psi$  wave function is a Fockstate decomposition, which is organized as a series in the typical relative quark velocity  $v$ , which reflects the non-relativistic effects (see in [27] or [29]):

$$|\psi_{J/\psi}\rangle = O(1)|Q\bar{Q}[{}^3S_1^{(1)}]\rangle \quad (\text{I.3})$$

$$+ O(v)|Q\bar{Q}[{}^3P_J^{(8)}]g\rangle \quad (\text{I.4})$$

$$+ O(v^2)|Q\bar{Q}[{}^1S_0^{(8)}]g\rangle \quad (\text{I.5})$$

$$+ O(v^2)|Q\bar{Q}[{}^3S_1^{(1,8)}]gg\rangle + O(v^2)|Q\bar{Q}[{}^3D_J^{(1,8)}]gg\rangle + \dots \quad (\text{I.6})$$

where  $O(v)$  denotes the order in powers of the quark relative velocity  $v$  of the contribution to the  $J/\psi$  wave function and  $Q\bar{Q}[{}^{2S+1}L_J]$  the spectroscopic notation for the  $c\bar{c}$ -pair in a state with total Spin  $S$ , orbital angular momentum  $L$  and total angular momentum  $J$ . The superscripts  $(1)$  or  $(8)$  specify whether the  $c\bar{c}$  pair is in color singlet or color octet state and  $g$  represents the presence of a dynamical gluon.

In the approximation of a completely non-relativistic picture, the expression reduces to the contribution with the lowest order in  $v$ . Naturally, although the  $c\bar{c}$  is not necessarily in the right quantum number state, every contribution to the wave function shows the right quantum numbers due to the explicit involvement of one or several additional gluon(s). The amplitudes of each contribution might be only non-perturbatively accessible within the effective field theory, but they satisfy scaling rules due to their  $v$ -dependence.

This decomposition is used for the investigation of the decay and the production of charmonium states, although there are in principle an infinite numbers of terms contributing. The justification to cut at a specific order in  $v$  is the expected suppression of higher order terms in powers of  $v$ . Therefore, any theory based on this wave function expansion is only valid, if  $v$  is significantly smaller than 1.

After these more general remarks on the theoretical description of the  $J/\psi$  wave function, we turn to the different models of  $J/\psi$ -production in  $pp(\bar{p}\bar{p})$  collisions.

In case of hadroproduction of  $J/\psi$  at RHIC, TEVATRON and LHC, it is clear that the most prominent and by far dominating contribution to the  $J/\psi$  production comes from gluon fusion. This may happen directly or via feed-down from the heavier charmonia states (For this theoretical discussion, we don't consider the feed-down to charmonia from beauty mesons). Beyond this consensus, it is by now not yet settled, what is the dominant mechanism of the production of color-neutral charmonium states in high-

energy pp  $p\bar{p}$  collisions. The only common feature is that all theoretical calculations of (differential) cross sections and polarizations rely in some way on the factorization of the initial state parton distribution function, the hard production of the  $c\bar{c}$  and the soft binding of the  $J/\psi$  particle in order to apply perturbative QCD for the hard part.

The least parameter consuming way to try to compute  $J/\psi$ -production cross sections is to neglect all higher terms in the  $v$  expansion of equation I.6 and to assume that the relative velocity of the on-mass-shell-produced charm and anticharm quarks is zero in order to allow the production of charmonium. The only needed non-perturbative input in case of the  $J/\psi$  is the square of the radial wave function at the origin, which can be inferred from the leptonic decay width and is therefore fixed experimentally<sup>12</sup>. This approach called Color Singlet Model (CSM) in the static approximation (The latter denoting the vanishing relative momentum of the on-shell quarks). In case of the hadronic production, this ansatz failed in his Leading Order (LO) variant to describe first data on  $p_T$ -differential cross section from TEVATRON in 1992 [31] (The discrepancy of theory and experiment was actually most prominent and least ambiguous for the  $\psi(2S)$  with up to a factor 30 at large  $p_T$ ). Complete Next-to-Leading Order (NLO) order calculations (and attempts to mimic the NNLO behavior even to a larger extent) describe better the differential cross section in pp ( $p\bar{p}$ ) [32, 33]. Nevertheless, the slope of the measured  $p_T$ -differential cross section are still not compatible with these new CSM results, although also here the agreement is improved<sup>13</sup>.

The failure of the CSM at TEVATRON brought up the idea to allow so-called Colour Octet (CO) contributions in the framework of non-relativistic QCD, which effectively leads to a double expansion in  $v$  and  $\alpha_S$  for the cross sections[29]:

$$\sigma(J/\psi) = \sum_n \frac{F_n(\Lambda)}{m_c^{d_n-4}} \langle 0 | O_n^{J/\psi}(\Lambda) | 0 \rangle \quad (\text{I.7})$$

The variable  $n$  denotes the different Fock state configurations of the produced  $c\bar{c}$  and  $\Lambda$ , the cut-off taken to be equal to  $m_c$ .

The short distance factors  $F_n(\Lambda)$ , which are independent of the actually produced charmonium state, can be related to hard matrix elements calculated in perturbative QCD for the  $c\bar{c}$ -pair production in the corresponding angular momentum and colour state  $n$ <sup>14</sup>.

12. In case of P-wave states like the  $\chi_c$ , one needs the first derivative of the wave function evaluated at the origin.

13. It is a well-known phenomenon that higher-order  $\alpha_S$  contributions, which are kinematically enhanced at higher  $p_T$  due to a lower number of hard propagators in the amplitude, dominate over lower order  $\alpha_S$  contributions at higher  $p_T$ .

14. The mass factors are just chosen in a way that the coefficients  $F_n$  are dimensionless.  $d_n$  is the mass scaling of the  $O_n$ -operator, which are also called long-distance matrix elements (LDME).

The state-of-the-art approach to retrieve the LDME  $\langle O_n^{J/\psi}(\Lambda) \rangle$ <sup>15</sup>, is to fit the  $p_T$ -differential cross section and/or to the polarization measurements. There are also attempts to describe mainly high- $p_T$  charmonium production at hadron colliders within an ansatz, which introduces universal fragmentation functions for transitions of off-shell partons and for on-shell  $c\bar{c}$ -pairs in a charmonium state. This method might give a better handle on potential higher order effects, since it is organized in powers of  $m_c/p_T$ , which can be used for the summation large logarithms of  $p_T/m_c$  [21]. The fragmentation functions can be further constrained by exploiting the knowledge of the LDME behaviour, which are themselves encoded in the fragmentation function provided that NRQCD can be applied. We will therefore not further comment on this approach, because it is in its common implementation a specific realization of the NRQCD approach.

So far, there is no proof of the factorization between the hard matrix elements and the LDME beyond two loop corrections [21]. Since arbitrarily soft gluons can be involved in these higher order corrections, it is not clear, if they invalidate this factorization scheme. In addition, the effects of other heavy quarks comoving with the evolving quarkonium state cannot be treated properly by construction [21].

With the first LHC results, complete NLO calculations fitted to a variety of results from different collision systems [34] or more focused on high  $p_T$  data [35], give reasonable agreement with  $p_T$ -differential cross sections at CDF and LHC. A remaining caveat is that the polarization at TEVATRON, the second standard measurement besides the cross section, is at least in [34] not well reproduced. Additionally, these overall compelling results are only achieved for LDME fits to cross section measurements at transverse momenta larger than 3-5 GeV/c for hadronic collisions. Otherwise, they don't show a stable behavior. Consequently, the theoretical results are only shown at transverse momenta above this range. This restriction is possibly connected to the influence of soft gluons, which could invalidate a fixed order approach at low  $p_T$  according to the authors of [34]. The approach therefore does not treat a large fraction of the total  $J/\psi$  cross section at LHC. Hence, the model is not able to reproduce the bulk of the total cross section appropriately.

Most recently, a publication is applying soft gluon resummation [36] for NRQCD calculations in the limit  $P_T/M_{quarkonium} \ll 1$  for hadronic production. Further comparisons and the consistency of the used LDME parametrizations will have to confirm, whether this approach is able to describe quantitatively the full set of available data in the low transverse momentum range and can be combined with the descriptions at high  $p_T$ .

---

15. They are assumed to be universal and therefore identical to the ones, which have to be considered for other collision systems as the  $p\bar{p}$ -case. In principle, they could be also calculated via numerical calculations of NRQCD on the lattice.

In addition to the CSM and NRQCD fits including CO-contributions, there exists the so-called Colour Evaporation Model (CEM), which distributes the whole sub-open-charm threshold  $c\bar{c}$  cross section among the different charmonium states, assuming universal constant factors for every collision system and independent of energy and momentum, i.e. there is only one free parameter for the production of a specific charmonium state e.g. the  $J/\psi$  :

$$\sigma(J/\psi) = A_{J/\psi} \int_{2m_c}^{2M_D} dm_{c\bar{c}} \frac{d\sigma_{c\bar{c}}}{dm_{c\bar{c}}} \quad (\text{I.8})$$

The mass  $m_c$  refers to the charm quark mass,  $2M_D$  to the open charm threshold.  $A_{J/\psi}$  is the universal constant, which represents the non-perturbative input. Naturally, the feed-down processes have to be also taken into account in this approach. Therefore, the given formulae only applies to the production of  $J/\psi$  excluding contributions from  $\chi_c$  and  $\psi(2S)$  decays. Although this model is successful to describe the rough production features measured at various energies, it fails to model the charmonium production at TEVATRON on the same level of accuracy as the NRQCD calculations [21]. Moreover, the CEM is hard to motivate from first principles.

It is important to note that the LO production in the CEM is a fusion of two hard gluons to a  $J/\psi$  ( $2 \rightarrow 1$  process). Clearly, additional gluonic degrees of freedom have to be involved, but they are implicitly assumed to be soft and are not explicitly accounted for in the power counting of the strong coupling constant  $\alpha_S$ . On the contrary,  $J/\psi$ -production<sup>16</sup> in the CSM proceeds at LO via gluonfusion to a  $J/\psi$  and a hard gluon ( $2 \rightarrow 2$  process). Since the LO CSM predicts appropriately the total cross section for hadronic collisions according to [33], the LO  $2 \rightarrow 2$  process should be responsible for the bulk of the  $J/\psi$  production within the CSM. The LO CSM cross section is therefore of the order  $\alpha_S^3$ , whereas the leading order term of the colour evaporation model is  $\alpha_S^2$  and the underlying physical pictures are quite different ( $2 \rightarrow 2$  vs.  $2 \rightarrow 1$ ).

Finally, there are applications of  $k_T$ -factorization instead of the usual collinear factorization formalism for the parton distribution functions [37, 38]<sup>17</sup>. One of the reasons to consider this approach is the fact that, for the intermediate and low- $p_T$  part of the spectrum, charmonium is originating from gluons with low  $x$ . For the production of  $J/\psi$  created at rest in the lab-frame at the LHC ( $\sqrt{s} = 7\text{TeV}$ )  $x = \frac{m_{J/\psi}}{\sqrt{s}} = 4.4 \cdot 10^{-4}$ .<sup>18</sup> Therefore, the parton

16. The production of  $\chi_{c0,c2}$  (and therefore of  $J/\psi$  via  $\chi_{c0,c2} \rightarrow J/\psi + \gamma$ ) is also allowed in the CSM by a two to one process due to the different quantum numbers compared to  $J/\psi$ .

17.  $k_T$  denotes in this context the transverse momentum of the incoming partons.

18. Naturally, one of the two tested  $x$ -values can be even much smaller for forward rapidities and can be even in a regime, where non-linear effects in the evolution equations could become relevant.

distribution functions assuming collinearity of the partons should be less accurate. Despite these conceptual arguments in favor of this approach, the calculations using  $k_T$ -dependent parton distribution functions suffer from large uncertainties because they are not well constrained from data. In addition, theoretical uncertainties are not investigated to the same level of accuracy as in the case of the collinear parton distribution functions.

Generally, but especially at low- $p_T$ , there are lots of open questions. They are also of main interest for the measurement of  $J/\psi$  in heavy-ion collisions, since at low- $p_T$  medium induced non-primordial  $J/\psi$  production plays the role of a key observable for deconfinement as explained in the introduction. It is therefore important to understand the underlying mechanisms in pp ( $p\bar{p}$ ) collisions in the same kinematic regime, since they are used as a baseline. In this context, it is even not settled, whether the dominating contribution to the bulk  $J/\psi$  production is a  $2 \rightarrow 2$  or a  $2 \rightarrow 1$  process.

In addition to the controversial situation of  $J/\psi$  cross section and polarization, the multiplicity dependence of  $J/\psi$  production measured by the ALICE collaboration [39] is not well reproduced at all with the standard event generator PYTHIA 6.4 (see Fig. 1.3)<sup>19</sup>. This is very interesting, since the multiplicity dependence of  $J/\psi$ -production could be sensitive to multi-parton interactions[40]. Furthermore, the observed multiplicity behavior might be related to the geometry of proton-proton collisions, i.e. that hard processes like  $J/\psi$ -production preferentially occur at small impact parameters of the colliding protons as pointed out in [41]; these events might be in turn also connected to higher multiplicities. In addition, gluon distribution fluctuations could also play a role according to [41]. Hence, a better understanding of the  $J/\psi$ -multiplicity observable may improve the knowledge of the interplay of soft and hard interactions in pp collisions in general.

In summary, the production mechanisms of charmonium states are still not well understood theoretically in hadronic collisions in terms of cross section and polarization, although large efforts have been made from the theory side in recent years. In this context, the understanding of charmonium will profit with the already present wealth of results from LHC and future measurements. The next section is devoted to a short introduction to  $J/\psi$  measurements at pp ( $p\bar{p}$ ) colliders in order to put the  $J/\psi$ -hadron correlations in a context.

---

<sup>19</sup>. The event generator description of  $J/\psi$ -production will be discussed in more details with respect to the results obtained in this thesis VI.C.

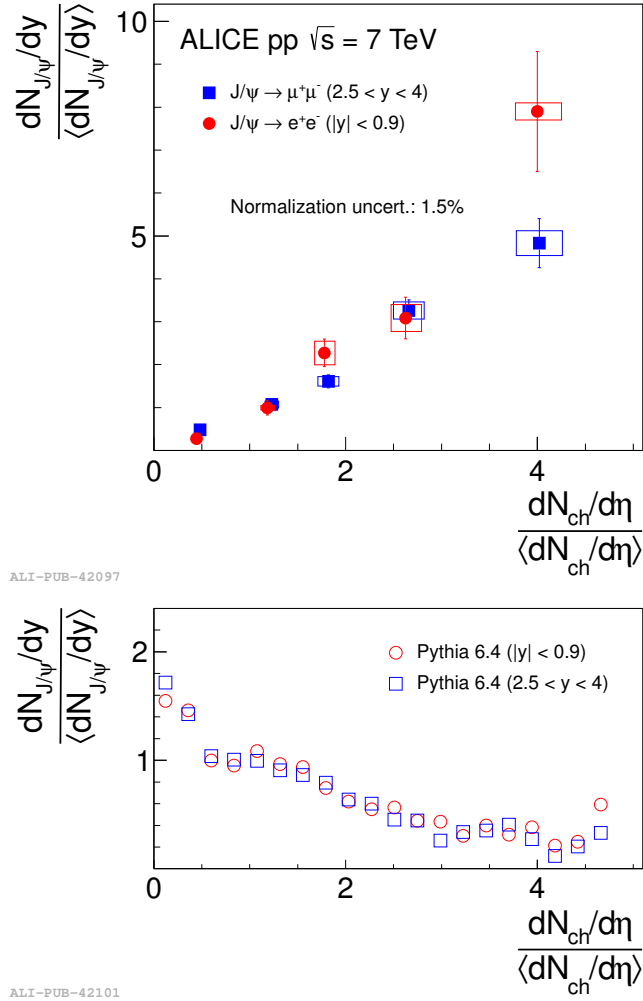


Figure I.3: The  $J/\psi$ -production as a function of multiplicity as measured by ALICE and as implemented in PYTHIA 6.4.25 (Perugia 2011 tune). The figures are taken from [39].

## I.C The $J/\psi$ at $pp(p\bar{p})$ Colliders

The detection of heavy quarkonia states in the crowded environment of non-diffractive hadronic interactions is mostly realized by the detection dilepton pairs, since specific hadronic channels suffer from more particles in the detected final state, no clear trigger signatures and from larger backgrounds (even in case of good PID capabilities in the hadronic sector). In addition, the branching ratios for a specific decay channel are typically small. Therefore, the investigation of charmonium and bottomonium at hadron colliders is mostly restricted to the investigation of states, which decay to  $e^+e^-$  and  $\mu^+\mu^-$  pairs. This is the case for the  $J/\psi$  and the  $\psi(2S)$  in the charmonium and the  $\Upsilon(1S)$ ,  $\Upsilon(2S)$  and  $\Upsilon(3S)$  in the bottomonium sector. Furthermore, states, which decay under emission of a photon to the latter, are accessible, namely the  $\chi_c$  states in the charmonium and the  $\chi_b$  states in the bottomonium system.

Among these states, the  $J/\psi$ -resonance is the first candidate for the investigation of heavy quarkonia in hadronic collisions from an experimental perspective. It has the largest inclusive cross section and the largest branching fraction in  $e^+e^-$  and  $\mu^+\mu^-$  of all mentioned states. Therefore,  $J/\psi$  cross sections were measured in the last two decades intensively at the TEVATRON [31, 42, 43], at RHIC [44–46] and now at LHC [22, 47–49]. In the following, we shortly discuss a few important experimental details about  $J/\psi$ -production at these hadron colliders.

As already mentioned, the production of  $J/\psi$  does not involve only direct production at hadron colliders, but it consists of different feed-down contributions, which should be disentangled for easier comparisons with theory. Experimentally, one first distinguishes between two contributions:

*non-prompt  $J/\psi$*  : originating directly or indirectly from B-hadron decays

*prompt  $J/\psi$*  : originating not from B-hadron decays

Today, the use of high granular semiconductor vertex detectors close to the interaction region made possible to resolve the secondary decay vertex of B-hadrons ( $c\tau \approx 400 - 500\mu\text{m}$ ) on a statistical basis by track extrapolation of the tracks from dilepton pairs toward the primary vertex. This is the standard approach, which is pursued by the LHC experiments ALICE [50], ATLAS [47], CMS [48] and LHCb [49] and also by CDF [42] and DØ [43] at TEVATRON. The contribution from B-hadrons is strongly dependent on  $p_T$  starting from around 10% at vanishing transverse momentum of the  $J/\psi$  up to 65% at 50 GeV/c at the LHC. A compilation of results at midrapidity is shown in Fig. 1.4.

The fractions of the prompt  $J/\psi$  cross section can be further separated in:

- *prompt direct* production
- *prompt non-direct* production

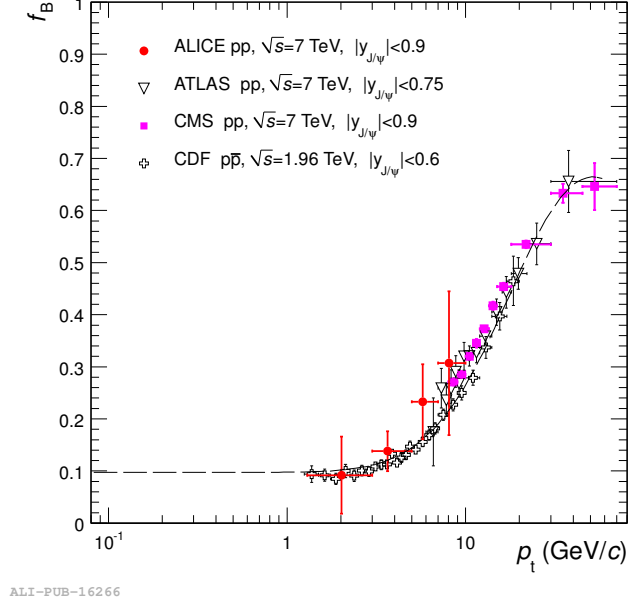


Figure I.4: The fraction of non-prompt  $J/\psi$ -production as a function of transverse momentum measured at central rapidity at LHC and TEVATRON. In addition a phenomenological curve is depicted, which is used for extrapolation purposes. The figure is taken from [50].

Prompt direct  $J/\psi$ -particles are not produced via feed-down, whereas non-direct prompt production refers to  $J/\psi$  from promptly decaying mother particles. The latter fraction is attributed to decays from heavier charmonium states: The  $\chi_c$ -states and the  $\psi(2S)$ <sup>20</sup>.

The fraction of prompt  $J/\psi$  coming from the  $\chi_c$  states was measured at TEVATRON via the radiative  $\chi_c$  decays for  $p_{T,J/\psi} > 4$  GeV/c at midrapidity for  $\sqrt{s} = 1.8$  TeV[51]. Within the exploited  $p_T$ -range and measurement precision, a  $p_T$  independent value of about 30% has been found. The contribution of  $\psi(2S)$  to the prompt  $J/\psi$  cross section can be inferred by the direct measurement of  $\psi(2S)$  in its dilepton decay channel, its branching to  $J/\psi$  and slight acceptance corrections. This fraction amounts to roughly 10% between  $p_T = 5$  and  $p_T = 18$  GeV/c slightly increasing as a function of  $p_T$  according to [51]. In absence of a precise measurement, the direct part of the  $J/\psi$ -production cross section is usually expected to be very similar at LHC compared to TEVATRON.

Besides total and differential cross sections and the ratio of  $\chi_{c1}$  and  $\chi_{c2}$

<sup>20</sup>. The  $\chi_{c0}$  has only a small partial decay width to  $J/\psi$  of 1.16% and also only a spin degeneracy of 1 and does not contribute in large amounts to the prompt  $J/\psi$  yield like the  $\chi_{c1}$  (BR = 34.4%) and the  $\chi_{c2}$  (BR = 19.5%).

yields measured by LHCb and CMS [52, 53]<sup>21</sup>, the measurement of the polarisation of vector state decays is the most important measurement in the field of charmonium, since it exhibits different behavior depending on the production mechanism[54]. The polarization is in this context the angular distribution of the daughter electrons respectively positrons in the rest-frame of the mother particle with respect to a specific quantization axis<sup>22</sup>. In case of the  $J/\psi$ , there are two measurements by CDF[55, 56] at TEVATRON, one by PHENIX at RHIC[57] and one at LHC by ALICE [58].

In addition, ALICE at LHC pioneered the measurement of  $J/\psi$ -production as a function of multiplicity[39], which was already shortly reviewed in the previous chapter.

Finally, a complete discussion of results at RHIC, TEVATRON and LHC in view of the large variety of models is beyond the scope of this introduction.

However, none of the models is firmly ruled out or really confirmed by a comprehensive explanation of all results at the present stage. Therefore, the measurement of additional observables will be crucial to understand the  $J/\psi$ -production mechanism in  $pp$  ( $p\bar{p}$ ) collisions. One possibility is the study of  $J/\psi$ -hadron correlations as discussed in the following section.

## I.D $J/\psi$ -Hadron Correlations in $pp(p\bar{p})$ Collisions

Historically,  $J/\psi$ -hadron correlations or, to be more precise from an experimental point of view, the correlations between the reconstructed dilepton pair from a  $J/\psi$  and charged tracks in the same event have been used by UA1 [59] and STAR [45] to separate the contributions from non-prompt and prompt  $J/\psi$  at transverse momenta of  $J/\psi$  larger than  $5 \text{ GeV}/c$ .

This method is motivated by the production mechanism expected for prompt  $J/\psi$ . In case of direct  $J/\psi$  production at leading order of CSM or  $J/\psi$  production from feed-down from  $\chi_c$ -states or  $\psi(2S)$  at leading order, there are no gluons and therefore no primary charged tracks associated in the direction of the charmonium on top of the underlying event activity. In fact, there should be only hadrons in the opposite direction in azimuth, originating from gluon-induced parton showers balancing the non-zero  $p_T$  of the charmonium. On the contrary, the  $J/\psi$ -production from B-hadron is accompanied by a non-negligible hadronic activity in the  $J/\psi$  direction due to the other decay products.

The described approach is conceptually not unproblematic, since a large fraction of  $J/\psi$  at high  $p_T$  is expected to come from gluon fragmentation according to the results of NLO CSM and NRQCD calculations incorporat-

---

21. The latter measurement is experimentally attractive due to the partial cancellation of systematic errors.

22. The standard choices for the reference axis are the momentum of the mother particle or the beam axis. An introduction is given in [54].

ing Color Octet components (see for a comprehensive theoretical introduction [60]). These prompt production processes are also accompanied with hadronic activity in the direction of the  $J/\psi$ . Therefore, this method cannot be very reliably used for the extraction of  $J/\psi$  from B-hadron decays. Furthermore, it is in any case strongly relying on the modelling of the correlation for both sources of prompt and non-prompt  $J/\psi$  production, which is usually done with Monte Carlo generators, which are not tuned for this special purpose and represent therefore a source of systematic errors difficult to estimate.

Today, modern silicon vertex detectors open a direct way to measure the fraction of  $J/\psi$  production from B-hadron decays as explained in the previous section. The use of  $J/\psi$ -hadron correlation is therefore clearly not the method of choice for this purpose.

Nevertheless, correlations with hadrons provide very interesting information on the production mechanism of  $J/\psi$ . Instead of disentangling prompt and non-prompt production via correlations, the correlation of prompt  $J/\psi$  is accessible by exploiting the information from the secondary vertexing. If it can be properly done by getting the hadron correlation of B-hadrons either from Monte Carlo generator information or even from data using the correlation as a function of the secondary vertex displacement of the dilepton, then one has in fact the opportunity to study the hadronic activity around the prompt  $J/\psi$  and not only of inclusive  $J/\psi$  in order to constrain the contributions from different production mechanisms by exploiting the event topology.

However, any quantitative interpretation of  $J/\psi$ -hadron correlations necessitates theoretical guidance. In this context, it is important to note that exclusive and semi-exclusive observables in general require a complete picture of the whole pp collision. The standard approach is the use of event generators. Broadly speaking, the modelling of heavy quarkonia is not very advanced in current implementations of event generators as we will discuss at the example of PYTHIA in VI.C. The main difficulty, but at the same time the main interest in the case of quarkonia-hadron correlations is the exact modelling of the potential colour neutralization of quarkonia necessary in case of CO production, i.e. the processes taking place between the hard  $c\bar{c}$ -creation and the final establishment of the quarkonium wavefunction. These processes during the preresonant stage of the  $c\bar{c}$ -pair, are encoded in the LDME elements of NRQCD factorization. The constants themselves only provide information about the quantum numbers of the states, which are connected by these matrix elements, but do not provide exact information, how a possible hadronic activity associated with  $J/\psi$  or other quarkonia states could look like. In this respect, the measurement of  $J/\psi$ -hadron correlations beyond underlying event activity and B-hadron fragmentation could be very interesting in order to understand, how two color charges bind together and how actually color neutralization really works. Therefore, the

$J/\psi$ -hadron correlations could be the input for improvements in the event modelling, which in turn could give valuable input about the underlying physics.

For high- $p_T$   $J/\psi$  ( $p_T > 20$  GeV/c), there was an intensive investigation to use the hadronic activity around prompt  $J/\psi$  in order to separate between the CO and CS contributions[61]. For this purpose, the possible parton showers associated with  $J/\psi$  assuming similar parton splitting kernels known from light quarks and gluons were examined in an event generator<sup>23</sup>. A certain sensitivity could be identified, although the background from  $J/\psi$  from B seemed to be quite problematic, since non-prompt  $J/\psi$  becomes equally important as prompt  $J/\psi$  at these values of  $p_T$ . Naturally, it is unclear, whether the color neutralization of a  $c\bar{c}$ -pair preresonant state necessary for CO contributions should be comparable to the behavior of quarks radiating off gluons. A comprehensive measurement, which could enhance the sensitivity, should be as differential as possible and requires a very good modelling of the underlying event. Especially, an investigation of the transverse momentum of the tracks in the cone around the  $J/\psi$ , but also the study of the transverse momentum of the considered tracks in the cone relative to the  $J/\psi$  could improve the sensitivity. The investigation of Jet- $J/\psi$  correlations for high  $J/\psi$ - $p_T$  could be also considered, since it could give potentially a more straightforward access to the different contributing Feynman diagrams.

At low  $p_T$  values exploited in this work, it is not clear that there is a sensitivity to disentangle CO and CS contributions using  $J/\psi$ -hadron correlations, since the significant underlying event could hide these presumably small effects from the not very hard charmonium production. In addition, standard calculations for CO contributions do not extend to low  $p_T$  as explained in the previous section and the precise Monte Carlo modelling of these events are at the moment at a premature level. Nevertheless, the observation of the strong dependence of  $J/\psi$ -production on multiplicity depicted in Fig. I.3 and the relevance for heavy-ion physics on its own motivates further investigations of  $J/\psi$ -production at low transverse momenta. The analysis of correlations can be crucial to establish a more precise picture of  $J/\psi$ -production in pp collisions and can provide important input for Monte Carlo generator descriptions of pp events. The question is whether one can identify a strong correlation of the large number of associated tracks with the  $J/\psi$ . Therefore, a precise measurement of  $J/\psi$ -hadron correlations should be sensitive to multi-parton interactions, and will be even more interesting as a function of multiplicity. Furthermore, the developed techniques can be also applied on future studies of  $J/\psi$  at  $p_T > 5$  GeV/c measured

---

23. In this study, a cone around the  $J/\psi$  was defined; the transverse momentum of the  $J/\psi$  and of the hadrons within different cone radii were considered as observables. The cone radius is defined in analogy to the one used in jet measurements  $R = \sqrt{(\Delta\phi)^2 + (\Delta\eta)^2}$ .

with ALICE, where correlations might be a tool to understand better the principal nature of  $J/\psi$ -production in pp collisions.

## – Chapter II –

# A Large Ion Collider Experiment at the LHC

## II.A The Large Hadron Collider

The Large Hadron Collider at CERN near Geneva is the highest energy particle accelerator ever built with a design center-of-mass energy ( $\sqrt{s}$ ) of 14 TeV in pp collisions. Between late 2009 and late 2012, the accelerator already delivered pp collisions to the experiments at  $\sqrt{s} = 0.9, 2.36, 2.76, 7$  and  $\sqrt{s} = 8$  TeV, Pb-Pb collisions at a center of mass energy per nucleon pair of  $\sqrt{s_{NN}} = 2.76$  TeV and proton-lead (Pb-p) collisions at  $\sqrt{s_{NN}} = 5.02$  TeV. The tunnel of the accelerator, with a circumference of 27 km, is inherited from the previous Large Electron-Positron (LEP) collider. Despite the large bending radius, superconducting dipole magnets operated at a temperature of 1.8 K allowing a magnetic field strength of 8.33 T are required to constrain the two proton beams in their orbits at the top beam energy of 7 TeV [62]. There are four major experiments placed at the four interaction points, where the two beams collide:

- A Large Ion Collider Experiment (ALICE)[63]
- A Toroidal Apparatus (ATLAS)[64]
- Compact Muon Solenoid (CMS)[65]
- LHCbeauty (LHCb)

The LHC itself is the last step in a whole chain of accelerators [62]. In case of the protons, the acceleration starts in the LINAC 2 and proceeds subsequently via the booster, the PS and SPS. Finally, the protons are injected in the LHC with a beam energy of 450 GeV. In the LHC, the protons are accelerated to their final beam energy, which amounts to 3.5 TeV for the collisions considered in this work.

The physics programme in pp collisions does not only require highest energies to produce large invariant mass states, but includes the search of very rare processes. Among them, the production of the Standard Model Higgs

Particle is the most prominent one. Assuming a mass of  $125\text{GeV}/c^2$ , the cross section times branching fraction in the  $ZZ^{(*)}$  decay channel amounts to  $2.2(2.8)$  fm at  $\sqrt{s} = 7(8)$  TeV [6]. The LHC is therefore designed to deliver<sup>1</sup> instantaneous luminosities up to  $L = 10^{34}\text{cm}^{-2}\text{s}^{-1}$ <sup>2</sup>.

In Pb-Pb collisions, the luminosity is physically limited by the large electromagnetic cross section of 506 barn [62]<sup>3</sup>. The latter is responsible for the removal of Pb-ions from the beam and potentially causing the quenching of the supraconducting magnets of the accelerator. In practice, the injector chain also significantly limits the possible performance at the present stage. Nevertheless, the LHC ran in 2011 at peak luminosities of  $5 \cdot 10^{-26}\text{cm}^{-2}\text{s}^{-1}$  at  $\sqrt{s_{NN}} = 2.76$  TeV [66] close to the design goal  $L = 1.0 \cdot 10^{-27}\text{cm}^{-2}\text{s}^{-1}$  [62] at  $\sqrt{s_{NN}} = 5.5$  TeV, despite the lower collision energy.

## II.B A Large Ion Collider Experiment

A Large Ion Collider Experiment (ALICE) is the dedicated heavy-ion experiment at the LHC. In addition to its capabilities in heavy-ion collisions, it is also able to perform measurements in pp collisions that are unique at LHC.

Although ALICE is not able to trigger on pp events at comparable interaction rates than the multipurpose experiments ATLAS and CMS and the single arm forward spectrometer LHCb, ALICE can perform measurements down to very low  $p_T$  also at midrapidity and involving Particle IDentification (PID) from the lowest (100 MeV/c [67]) to the highest recorded transverse momenta.

In the charmonium sector exploited in this work, ALICE is the only experiment at the LHC able to perform measurements at midrapidity down to zero  $p_T$ . This is possible using the dielectron decay channel relying on particle identification in the tracking detectors via specific energy loss and optionally Transition Radiation and the Time Of Flight (TOF) information. The other two experiments performing measurements at midrapidity, ATLAS and CMS, have to rely on their muon systems behind their extended calorimetry and a much stronger solenoidal magnetic field compared to ALICE<sup>4</sup>. They could also use tracks from the inner tracker systems matched with electromagnetic showers compatible with the electron assumption. For this purpose, the ratio of momentum and energy deposit and the shower shape can be exploited. However, the latter method is only getting efficient at comparable energy scales like the muon system. ATLAS and CMS are

---

1. to the multipurpose detectors ATLAS and CMS  
 2. The instantaneous luminosity reached in the current operations amounts to  $7.73 \cdot 10^{-33}\text{cm}^{-2}\text{s}^{-1}$  [66] never achieved before in hadron colliders.  
 3. out of a total cross section of 514 barn  
 4. The solenoidal magnetic field in ALICE amounts to 0.5 T, whereas the ATLAS and CMS systems have solenoidal fields around the beam pipe of 2 T and 3.8 T.

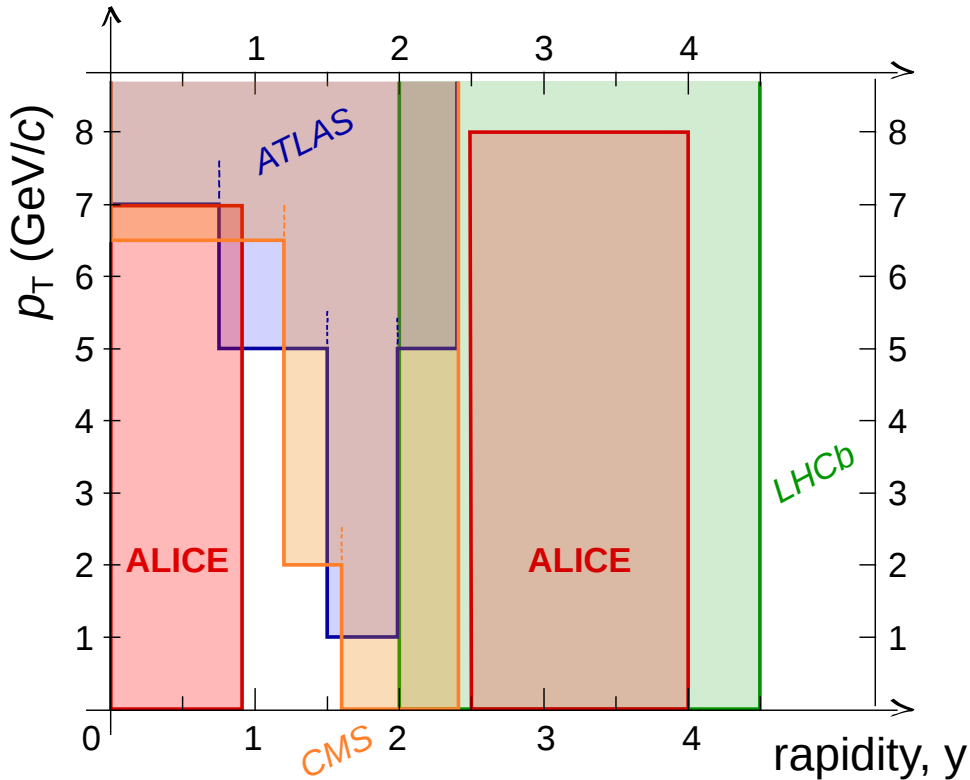


Figure II.1: Acceptance of the LHC experiments in published  $J/\psi$ -measurements according to [22, 47–49](courtesy of A. Maire).

therefore restricted to measurements of  $J/\psi$  with a  $p_T$  larger than 6–7 GeV/ $c$  at midrapidity, where they can trigger very efficiently and extend the measurement up to very high  $p_T$  of up to 70 GeV/ $c$  [47]. Since the mean- $p_T$  of inclusive  $J/\psi$  produced at the LHC is around 2–3 GeV/ $c$  [22], ALICE is in contrast to ATLAS, CMS and LHCb able to measure the total  $J/\psi$  cross section with limited need of extrapolation for the rapidity and the transverse momentum dependence. Fig. II.1 shows the acceptance of the four main LHC detectors in rapidity and transverse momentum in pp collisions.

In the following, a short introduction of the different detector systems of ALICE is given with emphasis on the relevant ones for the  $J/\psi$ -measurements at midrapidity.

### II.B-1 Overview

ALICE is divided into two subdetector systems: the forward muon spectrometer and the central barrel detectors (see Fig. II.2). In addition to the central barrel and the forward spectrometer, several detector systems can be used for triggering and/or event characterization: the ZDC, the VZERO,

the FMD, PMD and T0 detector<sup>5</sup> [63]. The ACORDE detector provides trigger signals for cosmic data taking.

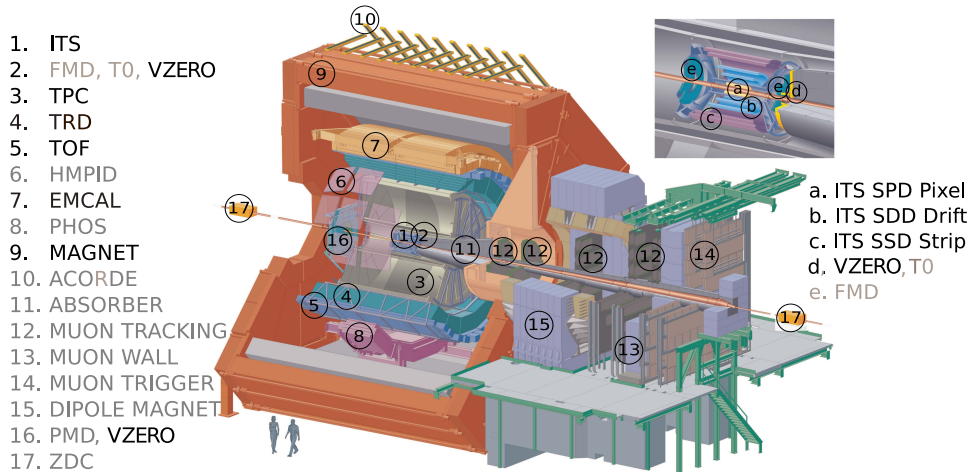


Figure II.2: Overview of all ALICE subsystems, figure adapted from [63]. The names of all detectors relevant for the dielectron analysis and the L3 magnet are highlighted.

The single arm spectrometer equipped with a 1.5 Tm dipole magnet aims at measuring muons in the pseudorapidity range  $2.5 < \eta < 4.0$  in pp, in Pb-Pb and in p-Pb and Pb-p collisions. It is especially designed for the record of charmonia and bottomia states decaying in dimuons. Since this part of ALICE is not used in the present analysis, we will concentrate in the following on the relevant central barrel detectors and the V0 detector involved in the minimum bias trigger.

The central barrel detectors are covering the midrapidity range in pp and Pb-Pb collisions. All central subdetectors are placed inside the normal conducting L3 magnet, which provides a solenoidal magnetic field with a strength of 0.5 T and which is inherited from the corresponding LEP experiment. Within the central barrel, the Inner Tracking System (ITS), a six-layer silicon tracker, the Time Projection Chamber (TPC) and the Transition Radiation Detector (TRD)<sup>1</sup> provide tracking of charged particles in a pseudorapidity range from  $[-0.9; 0.9]$  over full azimuth.

Besides the excellent and robust tracking capabilities of the central barrel also in ultra-high multiplicity events, the ITS, TPC, TRD, TOF, HMPID, PHOS and EMCaL are able to provide PID in different transverse momentum regimes and for different particle species. ITS, TPC and TOF are covering the full azimuth and the pseudorapidity range  $\eta \in [-0.9, 0.9]$  and the TRD will provide PID information over full azimuth, whereas HMPID,

5. the T0 detector can also provide a start signal for the Time-Of-Flight measurements.

1. In case of the TRD, the detector is not yet fully installed.

PHOS and EMCal provide PID information in smaller regions in  $\eta$  and azimuthal angle.

In the following, the discussion will be restricted to a more detailed description of the detector systems actually used for the present  $J/\psi$ -hadron correlation analysis or which will contribute to the  $J/\psi$ -measurements in future.

### II.B-2 The Inner Tracking System

The Inner Tracking System (ITS) consists of three different detector types: The Silicon Pixel detector (SPD), the Silicon Drift Detector (SDD) and the Silicon Strip Detector (SSD), each being composed out of two layers. The radial distance of the innermost layer with respect to the beam axis is 3.9 cm and of the outermost layer 43 cm. Especially the two innermost layers are responsible for the good vertex resolution due to their close distance to the beam axis (3.9 cm and 7.6 cm) and their high granularity in the  $r\phi$  direction of  $50\mu\text{m}$  [63]. Furthermore, the precise tracking enables to measure the distance of closest approach to the vertex for tracks very precisely and to perform secondary vertexing. Therefore, the ITS is an indispensable ingredient for open heavy flavour measurements in ALICE and for the  $J/\psi$  from B-hadron measurement. Hence, the figure of merit of the ITS is the resolution of the distance of closest approach (DCA) in the transverse plane, which is depicted as a function of transverse momentum in Fig.II.3.

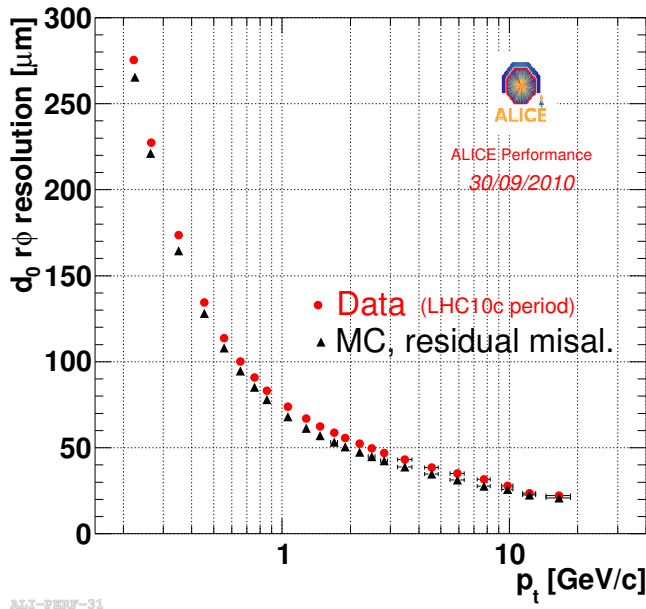


Figure II.3: Transverse DCA-resolution with ALICE ITS-TPC tracking in pp collisions at  $\sqrt{s} = 7$  TeV.

Furthermore, the inclusion of the ITS information in addition to the track information of the TPC improves the tracking capabilities in terms of transverse momentum resolution significantly due to the longer lever arm with high granular information. More details about the precise role of the ITS for the tracking in ALICE can be found in [63].

The 4 outer layers have in contrast to the SPD also an analog readout and are therefore capable to deliver particle identification (PID) information using the specific energy deposit of charged particles, which is caused by energy loss  $dE/dx$  described by the Bethe-Bloch formulae[26]. This PID information is of importance for low transverse momentum tracks.

### II.B-3 The Time Projection Chamber

The Time Projection Chamber (TPC) is the main tracking detector of the central barrel and serves as the main source of PID in the vast majority of the ALICE measurements at midrapidity. It is the largest of its type ever built [68].

It is a cylindrical detector placed around the beam pipe and the ITS with a inner radius of the active detector volume of 85 cm and a outer radius of 250 cm and a total length of 500 cm. Its electric drift field is parallel to the magnetic field of the solenoidal L3-magnet. In the center of the TPC, the central electrode is spanned to provide a field gradient of 400 V/cm to both end caps of the field cage cylinder. The electrons from the ionisation initiated from the passage of charged particles through the gas volume are transported by the drift field to one of the two the read-out planes. The latter consist of 18 sectors on each end of the cylinder. Each sector is equipped with two multi-wire proportional chambers<sup>6</sup>. In total, the read-out chambers provide 557568 read-out channels. The two dimensional projection of the track on the read-out plane and the arrival time of the signal from a ionization cluster together with the drift velocity and the collision time information provide a truly three-dimensional picture of every recorded track.

The dimensions and the high granularity are chosen such that robust tracking is possible in events with a charged track multiplicity per unit of pseudorapidity of up to  $\frac{dN}{d\eta} = 8000$  and to provide precise  $dE/dx$  for particle identification.

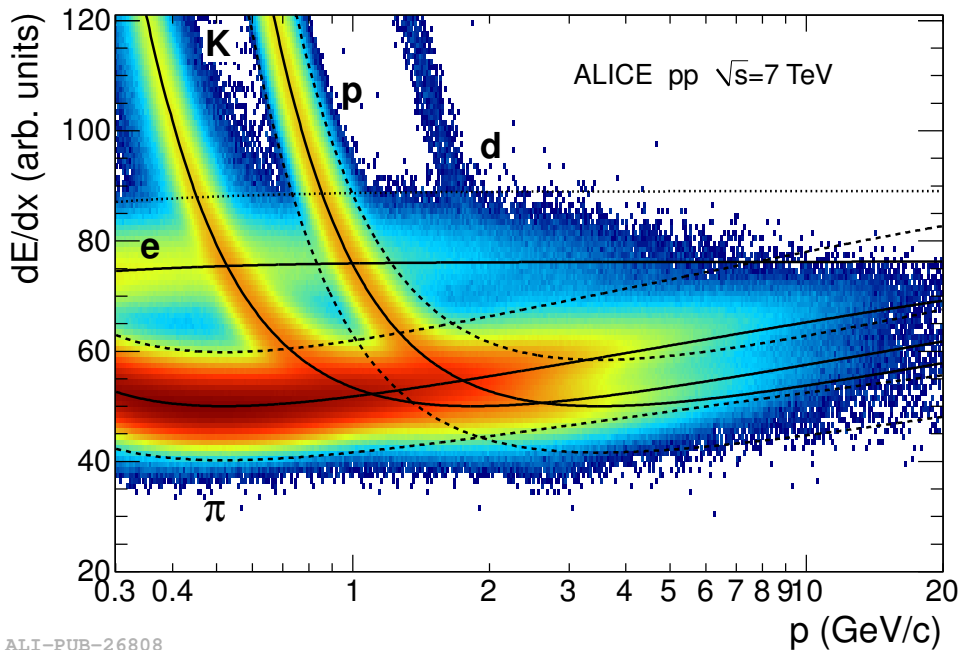
The TPC-ITS combined tracking provides precise  $p_T$ -information over a wide range of transverse momentum. Furthermore, the large number of up to 159 pad rows crossed by a charged particle enables a very precise determination of the particle specific energy deposit  $dE/dx$  in the drift volume.

---

6. The borders of the outer and inner read-out chambers are aligned. The TPC is therefore optimized for the best possible single track measurements and not for the best available azimuthal coverage. For completely straight tracks, i.e. for  $p_T \rightarrow \infty$ , the efficiency is reduced by roughly 10% by this purely geometrical effect.

A truncated mean of the measured energy deposits from the pad rows is used to extract information for particle identification in combination with information of the rigidity  $p/z$  of every track. Fig. II.4 demonstrates the capabilities of this technique in pp collisions. Details concerning the calibration and operation of the particle identification provided by the TPC can be found in [69].

The relative  $dE/dx$ -resolution reached in pp collisions relevant for this work is 5.5% [49], which enables the separation of electrons with respect to the most abundant pions at moderate values of transverse momentum. This is very crucial for the  $J/\psi$ -measurement at midrapidity, which relies on the  $e^+e^-$ -decay channel.



ALI-PUB-26808

Figure II.4:  $dE/dx$  vs. momentum  $p$  measured with the ALICE TPC in the phase space region relevant for the  $J/\psi$ -measurement including the lines for the expected energy deposit for different particle species, the figure is taken from [22].

#### II.B-4 The Transition Radiation Detector

The Transition Radiation detector of ALICE is a gaseous detector especially designed for electron identification above 1 GeV/ $c$  and for triggering on electrons and jets in pp, Pb-p as well as in Pb-Pb. It is placed at a radius from 370 up to 399 cm and covers the pseudorapidity range  $|\eta| < 0.84$ .

The detector is subdivided into 18 supermodules, following the same spatial segmentation as the TPC read-out sectors. Every supermodule consists

of five stacks arranged in z-direction. every stack consists of six read-out chambers in radial direction with respect to the beam axis.

The particle identification capabilities rely on transition radiation, which is emitted from highly relativistic particles with a relativistic  $\gamma$ -factor of 1000 or larger and which traverse the boundaries between different dielectrics (see for a short introduction [26]). The only particles, which exceed these  $\gamma$ -factors in high energy physics experiments, are electrons and positrons due to their small mass of  $511 \text{ keV}/c^2$ .

At the moment of data taking relevant for this analysis, seven supermodules out of eighteen were installed. Therefore, the TRD was not yet used for this analysis.

In future, the TRD will be an important ingredient for  $J/\psi$ -measurements in pp, pPb and in Pb-Pb with ALICE, especially the use of an electron trigger down to relatively low transverse momenta compared to the muon system capabilities of ATLAS and CMS will improve the available statistics for dielectron measurements in a phase space domain exclusively accessible to ALICE at the LHC.

### II.B-5 The Time of Flight Detector

The Time of Flight detector (TOF) of ALICE is placed at a radius of 3.7 cm around the LHC beam axis covering full azimuth and  $|\eta| < 0.9$  and is composed of multi-gap resistive plate chambers. It provides separation between different hadron species and between hadrons and electrons up to momenta of a few  $\text{GeV}/c$  depending on the specific particle species to be separated (see Fig.II.5 ). This particle identification method is completely independent of energy loss measurements and it is therefore complementary to these especially in the crossing regions between different energy loss bands.

Combining the measured track length  $l$ , the time difference between the occurrence of the event, the arrival time in the TOF wall and the momentum  $p = m\beta\gamma$  information from tracking, the particle type of the charged track can be identified via:

$$m = p \cdot \sqrt{\frac{t^2}{l^2} - 1} \quad (\text{II.1})$$

The intrinsic resolution of the 1628 individual chambers is approximately 80 ps [69]. The time resolution  $\sigma_{PID}$ , which is relevant for the particle identification has to include also the time resolution  $\sigma_{start}$  for the event itself:  $\sigma_{PID} = \sqrt{\sigma_{intrinsic}^2 + \sigma_{start}^2}$ . The value of  $\sigma_{PID}$  amounts to  $\approx 120$  ps in pp and  $\approx 86$  ps in PbPb collisions [69]. For the purpose of PID selection criteria, one looks at the distribution of the measured arrival time with respect to the one expected for a specific particle species.

For the  $J/\psi$ -analysis in the dielectron channel, the TOF can provide particle information in the crossing of the TPC  $dE/dx$  electron/positron band with other bands for moderate momenta. For instance, the crossing with the much more abundantly produced protons can be exploited using TOF information.

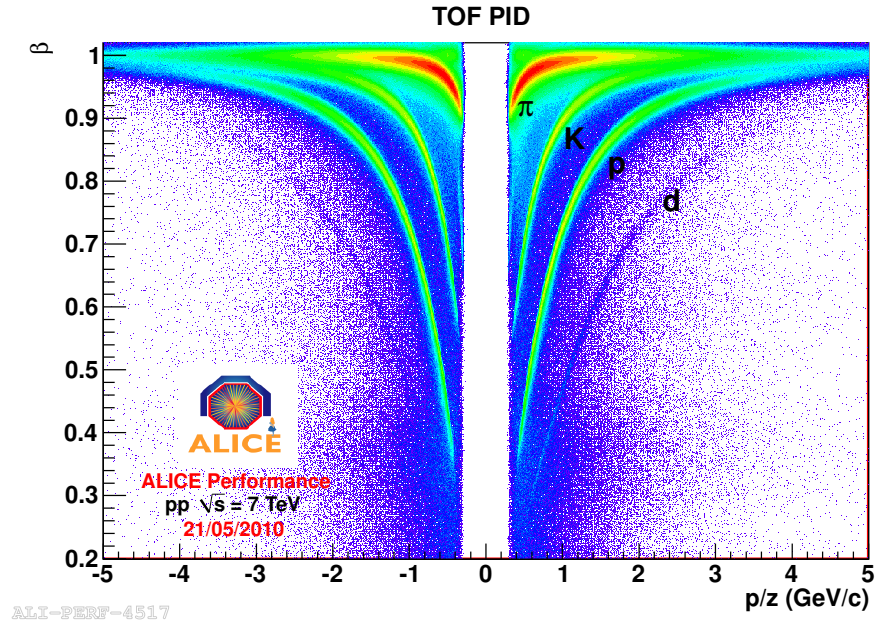


Figure II.5:  $\beta$  vs. rigidity  $p/z$  measured with the ALICE TOF in pp collisions. .

### II.B-6 The Electro-Magnetic Calorimeter

The electromagnetic Calorimeter is a Pb-scintillator sampling calorimeter with a depth of 20.1 radiation lengths placed behind the TOF detector seen from the interaction point at a radius of 4.5 m with an energy resolution of  $1.7 \oplus 11.1/\sqrt{E(\text{GeV})} \oplus 5.1/E(\text{GeV})$  [70]. It covers an angle of  $\Delta\phi = 107^\circ$  and a pseudorapidity range of  $|\eta| < 0.7$ . It enables to measure the energy deposit of charged tracks as well as of neutral particles and can be exploited as fast trigger detector.

Together with the momentum information from the tracking detectors ITS and TPC in front of the calorimeter, the energy deposit in the EMCal matched with the track enables also a good possibility of particle identification of electrons and positrons by exploiting the ratio energy over momentum, which is possible due to the very small electron mass. The shower shape can also be exploited as a discriminating observable.

### II.B-7 The VZERO Detector

The VZERO A and VZERO C detectors are both arrays of scintillator counters. VZERO A is placed at a pseudorapidity range from 2.8 to 5.1, VZERO C at -1.7 to -3.7. The asymmetric positions are due to the presence of the muon absorber at negative values of pseudorapidity. Both detectors are used in this analysis as minimum bias collision trigger detectors.

## – Chapter III –

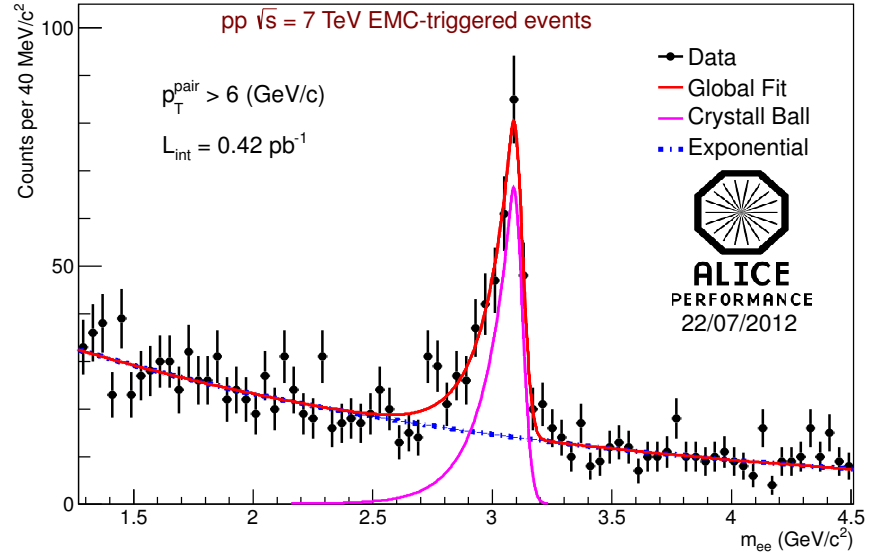
# Data Samples and Analysis Selection Criteria

The aim of this thesis is the measurement of azimuthal correlations between  $J/\psi$ -mesons and charged tracks in the same event. Especially in case of limited statistics, the selection of  $J/\psi$ -candidates and charged tracks has to be optimized for this purpose. The following chapter is devoted to an introduction of the available data samples, the explanation of the underlying criteria for the cut choices and the actual choices made in the investigated event sample.

### III.A EMCal-Triggered Data 2011

ALICE recorded during 2011 EMCal-triggered pp events at  $\sqrt{s} = 7$  TeV, which contain a significant number of  $J/\psi$  (see Fig.III.1) above a trigger threshold of roughly  $p_T = 6$  GeV/ $c$ . For the identification of the electrons, the  $E/p$ -ratio as explained in section II.B-6 can be exploited and leads, combined with the TPC PID, to a good separation of electrons from hadronic tracks. At these values of transverse momentum, the electron background is also reduced compared to  $J/\psi$ -candidates from dielectrons at lower transverse momenta.

During data taking in 2011, large instantaneous luminosities were delivered to the multipurpose experiments ATLAS and CMS. Due to the by far smaller interaction rates in ALICE compared to the other experiments, the beam induced background was non-negligible for ALICE. As a consequence, a fraction of the TPC multi-wire proportional chambers could not be operated at nominal gains, which had an impact on the tracking efficiency and their homogeneity as well as, most significantly, on the PID performance. In addition, the investigation of  $J/\psi$ -hadron correlations in this sample is complicated by the only partial EMCal coverage ( $107^\circ$ ) and possible trigger



ALI-PERF-27234

Figure III.1: Signal extraction in the integrated 2011 EMCal triggered data sample recorded by ALICE.

efficiency effects. All the raised points can affect the  $J/\psi$ -hadron correlation and make large corrections on the raw correlation necessary. Therefore, the EMCal data sample needs a better understanding for a correlation analysis. Consequently, this first investigation of the  $J/\psi$ -hadron correlation is focused on the  $J/\psi$  minimum bias sample recorded in 2010. Nevertheless, the 2011 sample can be very valuable for correlation studies, since the correlation effects of  $J/\psi$  in this momentum range are considerably larger. At least, this is suggested by the findings of the STAR collaboration at lower collision energies[45].

## III.B Minimum Bias Data 2010

In 2010, about  $4.1 \cdot 10^8$  minimum bias pp interactions were recorded by ALICE at  $\sqrt{s} = 7$  TeV. The applied selection scheme combines the trigger signals from VZERO A, B and the SPD in a logical disjunction<sup>1</sup>.

This sample was exploited by ALICE for measurements of the inclusive  $J/\psi$ -cross section at midrapidity via the  $e^+e^-$ -decay channel of  $J/\psi$ [22]. Furthermore, the multiplicity dependence of  $J/\psi$ -production at midrapidity [39] and the prompt and non-prompt fraction of the  $J/\psi$  cross section [50] could be determined. Therefore, it represents a well known sample and is well suited for a first investigation of  $J/\psi$ -hadron correlations with ALICE. It follows the explanation of the applied selection criteria.

### III.B-1 Event Selection

Firstly, the so-called physics selection is applied to remove events, which are associated with activity originating from beam-induced background by exploiting the timing information of VZERO. For the  $J/\psi$ -hadron analysis, good running conditions for TPC and TOF are required. Furthermore, the events processed in the dielectron analysis have to fulfill the following requirements:

- reconstructed vertex
- at least one reconstructed contribution to the vertex
- z-coordinate of the vertex within  $[-10.0, 10.0]$  cm with respect to the nominal position

The latter requirement guarantees a good and homogeneous coverage in pseudorapidity of the central barrel detectors.  $3.19 \cdot 10^8$  events pass all the mentioned quality criteria.

The effect of pile-up in this data sample is negligible in light of the achieved statistical precision of the measurement. The  $\mu$ -value specifies the expectation value of the underlying poisson distribution for the beam-beam interaction. It amounts on average over the whole sample to 0.06. Consequently, the average probability for a pile-up event among the triggered events is 3.0%. Pile-up effects are therefore not further considered. The presented event selection is in accordance with the inclusive  $J/\psi$ -measurements with ALICE in pp collisions.

### III.B-2 Dielectron Selection

The selection of  $J/\psi$ -candidates at low transverse momenta in the dielectron decay channel in pp collisions is a delicate analysis involving extended PID. It follows a short introduction of some specific features of the

---

1. A more detailed discussion of the minimum bias trigger and the full trigger scheme of ALICE can be found in [63].

$J/\psi \rightarrow e^+e^-$  measurement in ALICE, which enables a comprehensive understanding of the subsequent correlation-specific considerations and cut choices.

### III.B-2.i PID and Kinematic Basics of $J/\psi \rightarrow e^+e^-$

In the following, the general selection set-up is presented. The cuts used for the  $J/\psi$  analysis beyond the event selection can be subdivided in five principal categories:

1. quality of daughter tracks
2. kinematic restrictions on daughter tracks
3. electron and positron identification
4.  $e^+e^-$ -pair prefilter
5. kinematic restrictions on  $e^+e^-$ -pairs

The pair prefilter removes positron or electron tracks from the list of tracks used for the final pair combination. The prefilter is used in order to remove tracks, which are assumed to originate from  $\gamma$ -conversions. This leads to a reduction of the combinatorial background. A summary of all applied cuts in addition to the event selection for different reference choices are depicted in Table III.3. We will focus in the following on a few important details of the dielectron analysis. A description of all mentioned cut types can be found in [22].

Since electrons and positrons are much less abundant than pions, kaons and protons in hadronic collisions, a good signal extraction for the  $J/\psi$ -resonance requires an effective rejection of these species. The PID plays therefore the most crucial part of the  $J/\psi$ -analysis.

In this work, TPC and TOF were considered for PID purposes. The electron/positron identification is achieved by using the difference of the measured TPC  $dE/dx$ -signal or the measured TOF arrival time and the expected values for a given particle species and the measured momentum. By dividing these differences by the resolution at the measured momentum, a  $n\sigma$ -value for every measured track with respect to all considered particle species is defined. The  $n\sigma$  deviations can be used for inclusion and exclusion cuts. For the TPC, a detailed description can be found in [69].

Another important background detail is the amount of positron and electron tracks from  $\gamma$ -conversions. They are mainly created from neutral pions during the passage through the detector material at smaller radial distance to the beam pipe than the inner TPC wall. This background can be efficiently reduced by requiring an associated tracking point in the innermost ITS layer (referred as *SPDfirst*). Alternatively, an associated hit in one of the two or three innermost ITS layers (referred as *SPDany* or *ITS3any* in the following) can be used.

### III.B-2.ii Signal Distribution of $J/\psi \rightarrow e^+e^-$

Subsequently, the reasons for the special signal shape and its consequences are discussed. Finally, the signal extraction method, which is adapted for the  $J/\psi$ -yield determination, is explained. Firstly, It is important to explain the non-trivial signal shape, which is observed in Monte Carlo (see Fig. III.2) and confirmed in the data within the present statistical limitations. Since the intrinsic width is very small ( $92.8 \pm 2.8 \text{ keV}/c^2$ ), the width of the observed peak in the data –  $28.3 \pm 1.8 \text{ MeV}/c^2$  [22] – reflects the finite measurement precision, determined mainly by the  $p_T$ -resolution of the two daughter tracks.

Besides this instrumental effect causing a Gaussian line shape in absence of additional influences, the line shape is effected by bremsstrahlung from the electron and positron tracks. The emission of bremsstrahlung leads to the reduction of the observed invariant mass of a specific  $e^+e^-$ -pair. Hence, a large tail of the signal peak in the invariant mass is the result.

In addition, at Next to Leading Order (NLO) in QED, the decay  $J/\psi \rightarrow e^+e^-$  is only separable from to decay  $J/\psi \rightarrow e^+e^-\gamma$  [71] by defining a minimum energy of the emitted photon (For a photon energy larger than 100 MeV in the  $J/\psi$ -restframe, this process contributes with a branching ratio of 0.9 % to be compared with B.R. ( $J/\psi \rightarrow e^+e^-$ )  $\approx 6$  % [26] ). It turns out that there is therefore a non-negligible part of the total  $J/\psi \rightarrow e^+e^-$  decay amplitude, which does not appear in the peak of the  $J/\psi$  within the achieved mass resolution due to the emission of photons. The overall effect is an irreducible distortion of the Gaussian signal shape similar to the material induced bremsstrahlung also in case of negligible radiation length of the detector material. We refer to the photon emission by the  $J/\psi \rightarrow e^+e^-\gamma$  decay channel as 'internal' bremsstrahlung in contrast to the usual bremsstrahlung, which we call 'external' bremsstrahlung in case of ambiguities. In order to extract a large fraction of the  $J/\psi$  yield via bin counting in the invariant mass distribution, it is therefore necessary to choose an asymmetric range with respect to the sharp  $J/\psi$ -peak for the signal count summation. For all dielectron analysis in ALICE the range of  $[2.92 - 3.16] \text{ GeV}/c^2$  was selected. The precise fraction of the signal yield in this range depends slightly on the specific cut choice, especially on the allowed momenta of the daughter tracks and amounts roughly to 60 – 70 %. The same interval in the invariant mass distribution was adopted in this work.

In order to retain the number of signal counts, the background is estimated by the number of  $e^+e^+$ - and  $e^-e^-$ -pairs. They are scaled to the opposite charge sign (OS) spectrum in the invariant mass range of  $m \in [3.2, 5.0] \text{ GeV}/c^2$ . The number of signal counts is then retrieved via bin counting. The same method was used in [22]. The scaling factor accounts for the correlated background sources, which are not present in the Like Sign (LS) distribution, mainly due to semileptonic decays of  $D$ - and  $B$ -mesons. The

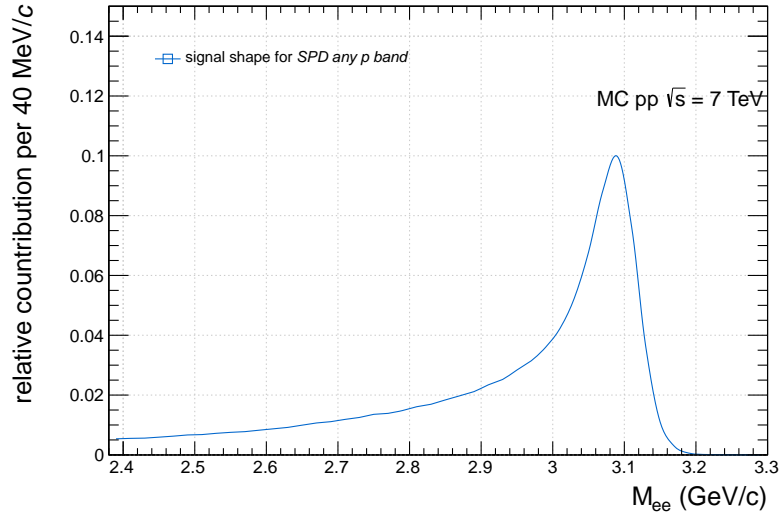


Figure III.2:  $J/\psi$  signal shape for *SPD any proton band* cut set from PYTHIA 6.4 perugia tune0 Monte Carlo combined with a full GEANT 3 simulation of ALICE for the data taking period d. The  $J/\psi$ -particles are injected on top of minimum bias events and decayed in their restframe isotropically. The underlying  $p_T$ -spectrum is based on the measurement by CDF at TEVATRON[72] at  $\sqrt{s} = 1.96$  TeV scaled to  $\sqrt{s} = 7$  TeV. The effect of external and internal bremsstrahlung is included in the plot.

background composition including the heavy flavor component is shown in Table III.2<sup>2</sup>. In addition, the explained LS-subtraction method assumes implicitly that the  $\psi(2S)$ -contribution is negligible, which is justified within the present sample and selection criteria<sup>3</sup>.

This signal extraction approach represents a conservative method with respect to the propagated statistical uncertainty of the signal counts, since the latter consists of the quadratic sum of the uncertainty of OS and scaled LS spectrum. It is therefore larger than the statistical uncertainty of mixed event, track rotation or background fit methods combined with a bin counting of the background subtracted yield<sup>4</sup>.

It is clear that the signal extraction in this work with a number of signal counts of around 250-500 and a non-Gaussian signal shape on a non-negligible background represents a considerable source of uncertainty. The related systematic uncertainties are discussed in chapter V.

2. In addition, there is also a contribution from Drell-Yan lepton pairs, but this is in this case a negligible contribution.

3. Due to the smaller branching fraction and smaller inclusive cross section, the expected  $\psi(2S)/J/\psi$ -yield ratio amounts to about 1-5% depending on  $p_T$ .

4. The latter methods are only limited by the statistical uncertainty of the  $S+B$  counts and provide smaller statistical uncertainties by up to a factor of  $\sqrt{2}$  in the limit  $S/B \rightarrow 0$ .

### III.B-2.iii Correlation Requirements

The  $J/\psi$ -hadron correlations necessitate different considerations for the selection criteria than, for example, a cross section determination. In the following, the conceptual key points are explained and the consequences for the subsequent cut optimization.

In order to improve the cut choice for the correlation measurement, it is necessary to know, which quantities have to be optimized. Firstly, there is no need for absolute efficiency corrections, but only for relative efficiencies, since the correlation observables are normalized per  $J/\psi$ -candidate. Therefore, also cut choices, which are more complicated to handle for an absolute efficiency determination, can be considered as long as the signal extraction works well and a reasonable background description for the final correlation observables is possible.

Furthermore, It is clear that a correlation measurement with less than 1000 signal events as in this analysis is statistically limited. Hence, a minimization of the statistical uncertainty is foremost important in order to allow a correlation measurement at all. In general, the quantity, which should be maximized for this purpose, is the significance  $S/\sqrt{S+B}$  of the  $J/\psi$ -peak in the invariant mass distribution of the  $e^+e^-$ -pairs.

In case of the correlation measurement between the  $J/\psi$  and associated charged tracks  $N_{assoc,S}$ , the situation is slightly different. One has to take into account the abundance of tracks associated with the signal  $N_{assoc,B}$  and associated with the background  $N_{assoc,S}$ , too. For this purpose, the maximization of  $N_{assoc,S}/\sqrt{N_{assoc,B} + N_{assoc,S}}$  is appropriate. In order to quantify this conveniently for an easier comparison with the usual significance, we define an 'effective' significance  $sig_{eff}$  for correlation measurements by normalizing  $N_{assoc,S}/\sqrt{N_{assoc,B} + N_{assoc,S}}$  by the square root of the  $J/\psi$  signal counts  $\sqrt{S/N_{assoc,S}}$ , which yields to :

$$sig_{eff} = \frac{S}{\sqrt{S + (N_{assoc,B} \cdot S/(N_{assoc,S}))}} \quad (III.1)$$

$$(III.2)$$

This quantity will be given in addition for the different signal extraction choices. Since the number of associated tracks is not necessarily the same for the background and for the signal, the quantity  $sig_{eff}$  leads not automatically to the same best choice as the ordinary significance. In the case of this analysis, the number of associated tracks only slightly varies between the considered cut choices for the dielectron selection. The number of associated tracks of the background is in all cases a factor 1.5 – 2 larger than the number of associated tracks for the  $J/\psi$  as we will see in the final distributions. Therefore a slightly larger value of  $S/B$  is favored compared to an optimization of the significance.

Furthermore, it is important to explain an analysis detail specific to the correlation measurements between tracks and particles decaying to more than one track.

Usually, most observables, like e.g. cross sections, are measured in intervals of rapidity  $y$ , since the rapidity is additive under Lorentz transformations along the beam axis and the use of this quantity is more suited for theoretical cross section calculations and also for comparisons between collider experiments with symmetric and asymmetric beam energies and fixed target experiments. All previous  $J/\psi$ -measurements of ALICE at midrapidity used therefore the interval  $y \in [-0.9, 0.9]$ . For the investigation of correlations, this choice is not optimal as we will explain in the following.

Since the mass of the  $J/\psi$  is not small compared to the regarded momenta, it is easily possible to detect  $J/\psi$ -particles, which have considerably larger pseudorapidities  $\eta$  than rapidities  $y$ . Therefore, the emission direction of  $J/\psi$ -mesons extends to values of  $\eta$ , where there is no tracking available. Hence, this can substantially reduce the observed correlation. Therefore, the absolute value of the  $J/\psi$  pseudorapidity is restricted to a value of smaller than 0.9, which corresponds to the same range considered for tracking. This is in accordance with the usual practice of dihadron studies, where the so-called 'trigger' particle is restricted to the same pseudorapidity range as the associated tracks (see e.g. in [73]). Unfortunately, this restriction of  $|\eta| < 0.9$  for the  $J/\psi$  leads to a reduction of the observed  $J/\psi$  raw yield of approximately 25 % compared to the restriction in rapidity  $|y| < 0.9$  and otherwise unchanged selection criteria.

Finally, due to the tight statistical limitations, there is no attempt so far to extract the correlation for a specific transverse momentum range of the  $e^+e^-$ -pairs. In particular, a minimum transverse momentum requirement will enhance the sensitivity of the measurement to observed some correlated behavior of the associated tracks, since it is not expected to see a strong correlation for very low transverse momentum  $J/\psi$ . The latter fact is caused by the absence of a large transverse momentum imbalance in the event by the  $J/\psi$ , which has to be counterbalanced by other particles. In addition, the restriction in transverse momentum would lead to better signal-over-background values for the extraction of the  $J/\psi$ -yield. But there is no strong argument, which exact cut on  $p_T$  should be chosen for this lower bound, and every further restriction of the phase space is difficult with the present statistical limitations. An analysis differential in the transverse momentum will be one of the next steps with a larger  $J/\psi$ -sample.

### *III.B-2.iv Cut Variations: PID and ITS Requirements*

In the following, the variation of selection criteria, which were adapted, are explained in more detail.

The starting point for the  $J/\psi$  selection of the  $J/\psi$ -hadron correla-

cut set	Signal counts	S/B	Significance $S/\sqrt{S+B}$	Effective significance
SPDfirst p band	$302.0 \pm 27.2$	$1.3 \pm 0.15$	$13.1 \pm 0.57$	10.6
SPDany p band	$437.2 \pm 40.8$	$0.7 \pm 0.07$	$13.5 \pm 0.54$	11.4
ITS3any p band	$529 \pm 53.0$	$0.5 \pm 0.05$	$13.0 \pm 0.49$	10.6
SPDfirst no p band	$207.4 \pm 20.2$	$2.0 \pm 0.27$	$11.7 \pm 0.58$	10.1
SPDany no p band	$296.0 \pm 29.4$	$1.1 \pm 0.13$	$12.4 \pm 0.56$	10.5
ITS3any no p band	$348.1 \pm 38.1$	$0.7 \pm 0.08$	$11.8 \pm 0.53$	10.1

Table III.1: Overview of different signal extractions. The expression effective efficiency takes into account the ratio between the associated tracks of the signal and of the background. This quantity is defined in equation III.2.

tion measurement is the cut choice for the cross section publication[22]. If not explicitly mentioned differently, these established selection criteria were adopted. Two different different variation possibilities were considered for a optimization of the selection criteria for the measurement of correlations. They concern the particle identification and the rejection of non-primary tracks:

1. ITS requirements for the  $J/\psi$ -daughter tracks
2. exploitation of TOF-PID

Firstly, the requirements on the tracking points of the electron/positron candidates in the ITS are investigated. For an optimal background suppression of electrons and positrons from  $\gamma$ -conversion, the requirement of a hit in the first layer of the ITS is the best choice in case of a 100 % efficient detector and track reconstruction. The claimed background reduction can be confirmed from the increase of S/B for *SPDfirst* (track point in first layer) with respect to *SPDany* (track point in one of the first two layers) and *ITS3any* (track point in one of the first three layers) depicted in Table III.1. In addition, the improvement of the signal purity can be traced back to the relative amount of  $\gamma$ -conversion related background according to a complete Monte Carlo detector simulation (see Table III.2). During data taking in 2010, the efficiency of the two innermost ITS layers was partially decreased due to cooling problems. Therefore, the efficiency to detect electron/positrons requiring a hit in the first or one of first two layers for the dielectron was significantly reduced. In order to determine the optimal choice for the correlation measurement, the ITS cut was varied from *SPDfirst*, *SPDany* to *ITS3any*.

Secondly, the PID potential of the TOF detector for the  $J/\psi$  analysis was exploited.

In the cross section analysis, only the TPC was considered for PID purposes. With this choice of PID-source, it is necessary to restrict the analysis to electron and positron tracks with momenta larger than roughly 1.0 - 1.5

GeV/ $c$  due to the crossing of the electron and the proton  $dE/dx$ -band. Fig. III.5 shows the precise contour of the applied  $3.0 \sigma_{proton,TPC}$ -exclusion. In addition, the default cut choice for the electron and positron selection includes the requirement of a  $p_T$  of 1 GeV/ $c$ . Furthermore a pion rejection of  $3.0 \sigma_{pion,TPC}$  was applied. We refer to this cut choice for the electron and positron PID and the corresponding kinematic restrictions as *no proton band* in the following.

Since the momentum distribution of the daughters from  $J/\psi$  dielectron decays has significant contributions from tracks with lower momenta, the *no proton band* cut choice reduces the detected part of the  $J/\psi$  phase space significantly<sup>5</sup>. It is possible to recover these  $J/\psi$  mesons by exploiting the PID potential of the TOF detector in the proton-electron crossing region. It can separate in this momentum region unambiguously between electrons and positrons and (anti)protons, although it is not fully efficient in this momentum range. Due to the latter fact, the TOF-PID is only required for tracks with  $n\sigma_{proton,TPC} < 3.0$ . In addition to the PID changes, the requirement of a minimal  $p_T$ -cut of 1 GeV/ $c$  is replaced by requiring a minimal total momentum of 0.7 GeV/ $c$ . This cut choice is chosen to select nearly all positron and electron candidates, which are still not affected by the  $dE/dx$  electron band crossing with the kaon band. In addition, a  $3.0 \sigma_{kaon,TPC}$  exclusion is applied. These PID criteria set is labelled subsequently *proton band* cuts. The full set of the applied cuts, is listed in Table III.3. In order to illustrate the PID-selection, the measured  $dE/dx$  versus the corresponding momentum for the electron/positron candidates is shown for the *no proton band* cuts in Fig. III.5 and for the *proton band* cuts in Fig. III.4. For a better orientation, Fig. III.3 shows the  $dE/dx$ -bands of the different relevant particle species.

It is clear that the *proton band* choice is accompanied at the same time with an increase of background and not only signal, since most background electrons are produced at low transverse momentum. This is caused by the shape of background electron  $p_T$ -spectra. Nevertheless, the observed significance is a bit larger than the one, which is achieved with the *no proton band* cuts and the  $p_T$  distribution of the candidates is closer to the  $p_T$  distribution of all measured  $J/\psi$ -mesons (see Fig. IV.5 and discussion in IV.E), which is a direct consequence of the fact that a larger part of the possible decay kinematics is included by this cut choice.

---

5. These small momenta for the daughter particles, which are not possible for  $J/\psi$ -decays at rest, are caused by the  $J/\psi$ -boosts.

Selection set → Sources ↓	<i>SPD</i> <sub>first</sub> proton band	<i>SPD</i> <sub>any</sub> proton band	<i>ITS</i> <sub>any</sub> proton band	<i>SPD</i> <sub>first</sub> no proton band	<i>SPD</i> <sub>any</sub> no proton band	<i>ITS</i> <sub>any</sub> no proton band
$\gamma$ -conversions	2.0%	10.9%	19.6%	3.8%	10.1%	18.6%
open charm + open charm	19.4%	15.4%	11.9%	18.9%	16.3%	13.4%
open beauty + open beauty	8.2%	4.9%	3.9%	13.2%	8.5%	7.0%
prim. $e^+$ + sec. $e^-$	10%	18.2%	21.1%	3.8%	14.7%	18.0%
mis. id. + true $e^\pm$	35.7%	34.8%	30.6%	32.0%	30.2%	26.1%
mis. id. + mis. id.	8.2%	4.9%	3.6%	7.5%	5.4%	4.0%

Table III.2: Main contributions to background for different cut sets in Monte Carlo minimum bias PYTHIA 6.4 perugia tune 0 and full GEANT 3 detector simulation.

Finally, it is necessary to comment on the different background contributions for the invariant mass range  $m \in [2.92, 3.16]$  GeV/ $c^2$  and different cut choices, which are depicted in Table III.2. In this table, the contribution from  $\gamma$ -conversions includes  $e^+e^-$ -combined together from different  $\gamma$ -conversions. For the other background sources, the label are always indicating both sources of electrons and positrons combining to an invariant mass in the vicinity of the  $J/\psi$ -peak. All contributions don't add up to 100%, since small fraction of true electron pairs, mainly with at least one electron from light flavored hadrons, are not listed. In the context of the different background sources, the hadronic contamination requires explanation. First of all, it is not expected that this Monte Carlo simulation with PYTHIA 6.4 and GEANT 3 simulating the detector conditions during the data taking period d<sup>6</sup> in 2010 gives a completely accurate description of the actual background. This is mainly caused by an imperfect description of the TPC PID in this Monte Carlo simulation. In addition, the D-meson  $p_T$ -spectra in this sample are harder than in data [74]. Nevertheless, it should give an approximate impression of the situation in real events. The non-negligible pair contamination of true electron/positrons combined with hadrons, predominantly pions (about 80 – 90%), could be further reduced by the a stronger pion rejection with TPC-PID. However, a  $3.5\text{-}n\sigma_{\text{pion,TPC}}$  in comparison to the default 3.0 choice lead to a slight decrease of the significance of 5%

6. The actual sample size of about  $10^8$  simulated events.

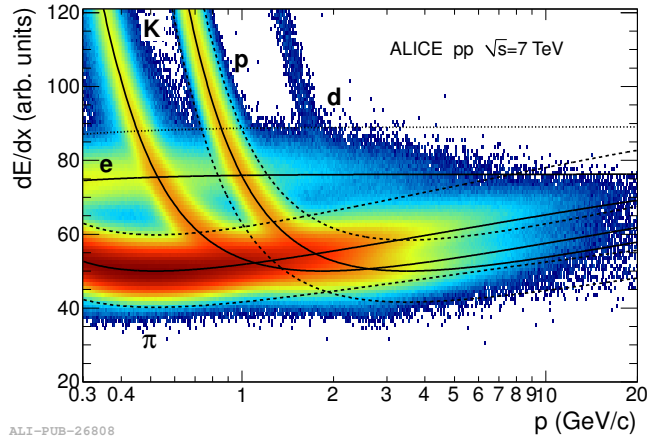


Figure III.3:  $dE/dx$  vs. momentum  $p$  measured with the ALICE TPC including the lines for the different particle species for orientation, figure taken from [22].

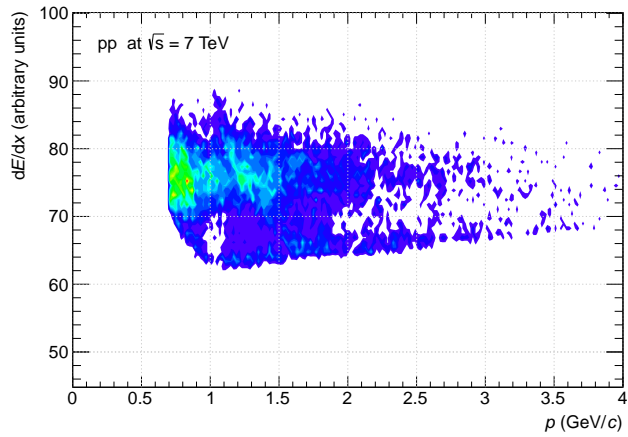


Figure III.4: TPC  $dE/dx$  vs. momentum for described cut choice *proton band SPDany* for all daughters of Opposite Sign (OS) dielectron pairs in the invariant mass range  $m \in [1.6 - 5.0]$   $\text{GeV}/c^2$ .

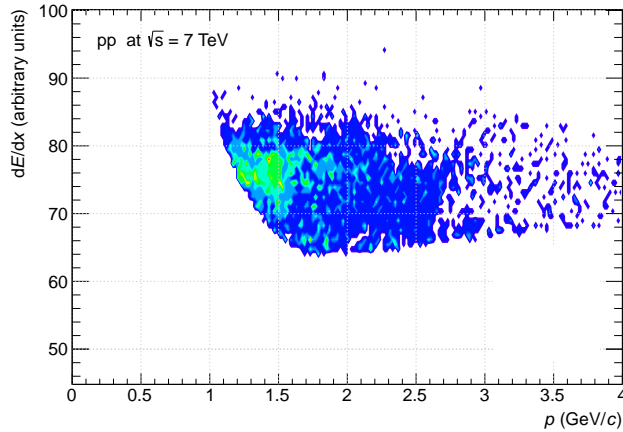


Figure III.5: TPC  $dE/dx$  vs. momentum for described cut choice *no proton band SPDany* for all daughters of Opposite Sign (OS) dielectron pairs in the invariant mass range  $m \in [1.6 - 5.0]$   $\text{GeV}/c^2$ .

for the cut choice *SPDany no proton band*. There were also attempts to vary the  $n\sigma_{\text{pion,TPC-rejection}}$  as a function of momentum, which lead not to significant improvements. Although, there might be some fine-tuning potential, it is not expected that a better hadronic background suppression, which is clearly accessible also by requiring more TPC-tracking points for the TPC-PID[69], can be achieved with a simultaneous preservation of the signal significance.

In summary, besides the additional pseudorapidity restriction, several changes for the cut choice were considered. The six signal extractions show significances between 11.8 and 13.5. Since the background shape is quite different for *no proton band* and *proton band* cuts, both PID alternatives were kept in order to cross check the reliability of the correlation background subtraction, which are described in the chapter IV.D-2. The *SPDany* type cut sets provide the best significances and best effective significance among the different ITS related cuts. The corresponding signal extraction for the *no proton band* (*proton band*) selection is depicted in Fig. III.6 (III.7). Nevertheless, all six cut choices are considered for the correlation study in order to judge the stability of the retained result, since the relative  $p_T$  abundances of the  $J/\psi$  or relative abundances of any other  $J/\psi$  specific variable influencing the correlation shape should within the ITS cut variation not be altered. But the background composition is changing for these different selection criteria, which can be also checked explicitly in Monte Carlo simulation (see in Table III.2). Naturally, these cut variations serve therefore as an estimate of the systematic uncertainty, which is related to the background subtraction and provide therefore valuable information.

Selection set	<i>SPDany no proton band</i>	<i>SPDany proton band</i>
<b><math>e^\pm</math> kinematics</b>	$p_T > 1 \text{ GeV}/c$ , $ \eta  < 0.9$	$p_T > 0.7 \text{ GeV}/c$ , $ \eta  < 0.9$
<b><math>e^\pm</math> track quality</b>	TPC, ITS refit, $n_{TPC,cluster} > 70$ , $\chi^2/n_{TPC,cluster} < 4$ , no kink daughters, $ dca _{xy} < 1.0 \text{ cm}$ , $ dca _z < 3.0 \text{ cm}$ , SPDany	TPC, ITS refit, $n_{TPC,cluster} > 70$ , $\chi^2/n_{TPC,cluster} < 4$ , no kink daughters, $ dca _{xy} < 1.0 \text{ cm}$ , $ dca _z < 3.0 \text{ cm}$ , SPDany
<b><math>e^\pm</math> PID</b>	$n\sigma_{e^\pm,TPC} < 3.0$ , $n\sigma_{proton,TPC} > 3.0$ , $n\sigma_{\pi^\pm,TPC} > 3.0$	$n\sigma_{e^\pm,TPC} < 3.0$ , ( $n\sigma_{proton,TPC} > 3.0$    ( $n\sigma_{proton,TPC} < 3.0$ && $n\sigma_{e^\pm,TOF} < 3.0$ )), $n\sigma_{K^\pm,TPC} > 3.0$ $n\sigma_{\pi^\pm,TPC} > 3.0$
<b>pair prefilter</b>	conversion-tagging, $m_{e^+e^-} > 50 \text{ MeV}/c^2$	conversion-tagging, $m_{e^+e^-} > 50 \text{ MeV}/c^2$
<b>pair kinematics</b>	$ \eta_{ee}  < 0.9$	$ \eta_{ee}  < 0.9$

Table III.3: Overview of applied cuts for the  $J/\psi$ -selection for SPDany cut choices.  $n_{TPC,cluster}$  refers to the number of tracking points. Explanations for the different criteria can be found in [22].

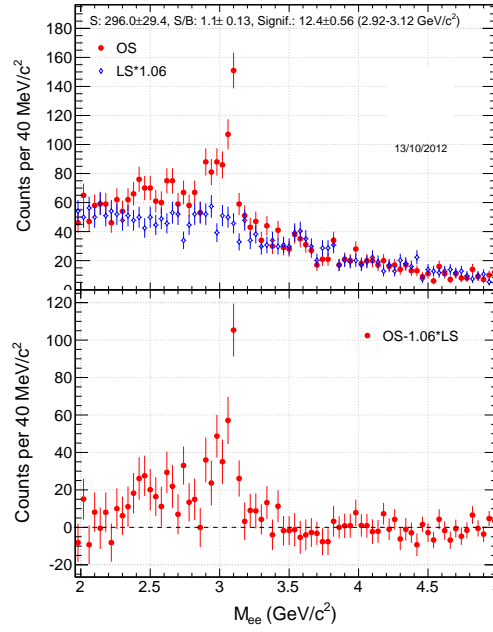


Figure III.6:  $J/\psi$  signal extraction for *SPDany no proton band* cut set in 2010 minimum bias data sample.

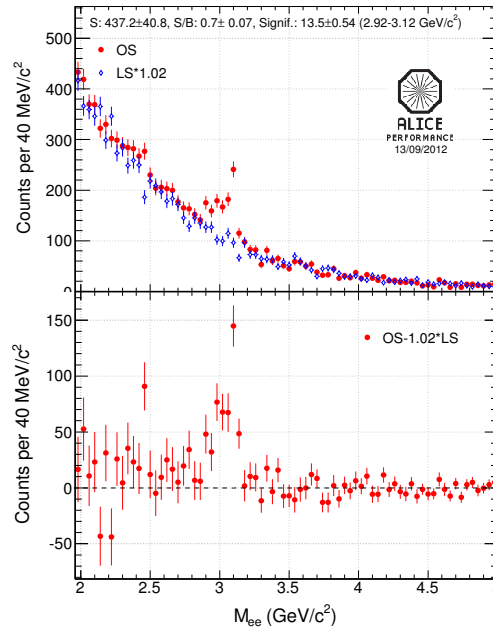


Figure III.7:  $J/\psi$  signal extraction for *SPDany proton band* cut set in 2010 minimum bias data sample.

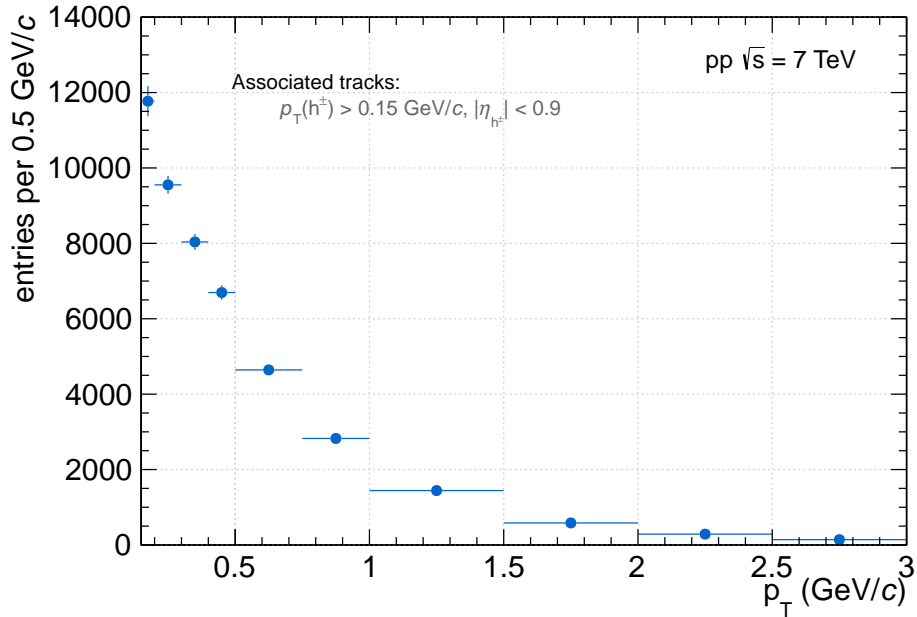


Figure III.8: Efficiency corrected transverse momentum distribution of charged tracks in events containing a dielectron pair with invariant mass within  $[2.92, 3.16]$   $\text{GeV}/c^2$  passing the cut set *SPD any proton band* in data taking period 10d.

### III.B-3 Associated Track Selection

In order to choose the best cut set for the primary tracks within an event containing a  $J/\psi$ -candidate, it is important to mention several aspects, which are important for this specific analysis.

Firstly, there is a strong  $\phi$ -dependence of the  $J/\psi$ -detection due to the already mentioned partial inefficiencies of the SPD detector during the 2010 data taking period. In consequence, the selection criteria of the tracks should exhibit the most homogeneous efficiency, which is achievable, since otherwise an interplay between the azimuthal  $J/\psi$ -efficiency variation and the azimuthal associated track efficiency variation can be imprinted in the raw correlation function. Naturally, these effects can be corrected. They are actually also corrected in this analysis, but every large correction factor is a potential source of systematic error or might be not straightforwardly retrievable.

Secondly, as demonstrated by Fig. III.8, the  $p_T$  of the tracks occurring in the regarded dielectron events are quite low. In addition, the transverse momentum information is only used for a proper  $p_T$ -differential efficiency correction at the present stage. Hence, the  $p_T$ -resolution of the TPC alone is already sufficient for this analysis and no additional folding of the  $p_T$ -

distribution is necessary. This was explicitly checked in case of the triggered dihadron analysis in Pb-Pb as well as in pp collisions [75], where the impact of the  $p_T$ -resolution on the azimuthal correlations amounts only to 0.2%.

In addition, the removal of tracks with sizeable distance to closest approach by using the tight cuts of the underlying event [73] and spectra studies [67] in ALICE, is a non-critical step in case of a  $J/\psi$ -hadron correlation analysis. This is due to the expected particle composition differences compared to minimum bias events as explained in more detail in the subsequent chapter.

Consequently, the use of the TPC as stand-alone tracking device using only the vertex information provided by the ITS is appropriate for a first study, since it exhibits a very good homogeneity in the 2010 data period and because the improvement for the  $p_T$ -position resolution for ITS-TPC combined tracks is not essential. Therefore, TPC only tracks were used for the associated tracks in accordance with the dihadron analysis [75]<sup>7</sup> fulfilling the following criteria:

- at least 70 out of 159 tracking points within the TPC
- $\chi^2/n_{TPC,cluster} < 4$
- kink daughter rejection
- $\left(\frac{dca_{xy}}{d_{xy}}\right)^2 + \left(\frac{dca_z}{d_z}\right)^2 < 1$  with  $d_{xy} = 2.4$  cm and  $d_z = 3.2$  cm
- $|\eta| < 0.9$
- $p_T > 0.15$  GeV/ $c$

---

7. except of the larger considered range in pseudorapidity in order to increase the available statistics



## – Chapter IV –

# Analysis Method

A proper measurement of  $J/\psi$ -hadron correlations requires several conceptual steps. In order to retain the correlation function, it is not only necessary to sort the number of charged tracks depending on their relative coordinates with respect to the  $e^+e^-$ -pair and to normalize them by the number of  $e^+e^-$ -pairs. In fact, the recorded quantity is subject to several corrections, which are sensitive to efficiency and acceptance effects. Furthermore, the retrieved  $e^+e^-$ -pair-hadron correlation has to be translated in a  $J/\psi$ -hadron correlation by an adequate background subtraction. In this chapter, we follow the track of the analysis from the raw distribution to the final  $J/\psi$ -hadron correlation.

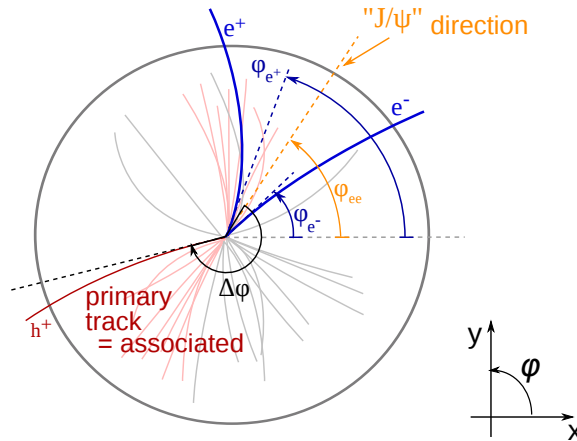


Figure IV.1: Schematic illustration of measurement variables in the azimuthal  $J/\psi$ -hadron correlation measurement. The z-axis perpendicular to the x-y-plane corresponds to the beam axis in the experiment. The reconstructed  $e^+e^-$ -pairs are only identifiable on a statistical basis as  $J/\psi$ -mesons.

## IV.A Terminology

The purpose of this analysis is the investigation of  $J/\psi$ -hadron correlations. More precisely, we intend to measure the spatial emission direction between charged particles with respect to the emission direction of the  $J/\psi$ -direction in pp collisions. In order to facilitate the following explanations, we summarize at this point the used definitions:

- $e^+e^-$ -pair: track pair passing the selection criteria for  $J/\psi$
- associated track: track passing the selection criteria in the same event as the  $e^+e^-$ -pair excluding the tracks of the  $e^+e^-$ -pair
- $p_{T,assoc.}$ : transverse momentum of a charged track at the Distance of Closest Approach (DCA) to the primary vertex
- $p_{T,e^+e^-}$ : transverse momentum of a dielectron pair at the production vertex
- $\phi_{assoc.}$ : azimuthal angle of the charged tracks at the DCA to the vertex
- $\phi_{e^+e^-}$ : azimuthal angle of the dielectron pair at its production vertex
- $\eta_{assoc.}$ : pseudorapidity of the charged track at the DCA to the primary vertex
- $\eta_{e^+e^-}$ : pseudorapidity of the  $e^+e^-$ -pair at the production vertex
- $\Delta\phi$ : differences between the respective quantities of the  $e^+e^-$ -pair and the associated track
- $\Delta\eta$ : differences between the respective quantities of the  $e^+e^-$ -pair and the associated track

The azimuthal angle  $\phi$  refers in this context to the angular coordinate in the x-y-plane perpendicular to the beam axis as depicted in Fig. IV.1.

## IV.B Raw Distributions

The starting point of the analysis is the raw  $\Delta\phi$ -distribution between the reconstructed  $e^+e^-$ -pairs in a restricted invariant mass range, e.g. the  $J/\psi$ -peak region and the reconstructed associated tracks in the same event without acceptance and efficiency corrections.

For the purpose of azimuthal correlation studies, the conventional  $\Delta\phi$ -range  $[-1/2\pi, 3/2\pi]$  is subdivided in several bins with the bin borders  $\Delta\phi_i$ . The raw  $\Delta\phi$ -distribution consists of a histogram subdivided in these  $\Delta\phi$ -bins. For every detected  $e^+e^-$ -pair, the content of the bin  $[\Delta\phi_i, \Delta\phi_{i+1}]$  is incremented by the number of detected associated tracks  $N_{assoc.,raw,SE}$  with  $\Delta\phi \in [\Delta\phi_i, \Delta\phi_{i+1}]$ <sup>1</sup>. In addition, the raw correlation is divided by the bin width in order to derive a 'differential' quantity. The relevant efficiency and

---

1. Principally, a single event can therefore contribute several times to the raw distribution.

acceptance uncorrected distribution is therefore:

$$\frac{dN_{assoc.,raw,SE}}{d(\Delta\phi)}(\Delta\phi \in [\Delta\phi_i, \Delta\phi_{i+1}]) = \frac{N_{assoc.,raw,SE}(\Delta\phi \in [\Delta\phi_i, \Delta\phi_{i+1}])}{(\Delta\phi_{i+1} - \Delta\phi_i)} \quad (IV.1)$$

Although the results of this thesis will be restricted to the one-dimensional correlation in  $\Delta\phi$  due to the limited statistics, it will be instructive to inspect also the two-dimensional case of  $\Delta\phi - \Delta\eta$ -distributions:

$$\frac{d^2 N_{assoc.,raw,SE}}{d(\Delta\phi)d(\Delta\eta)}(\Delta\phi \in [\Delta\phi_i, \Delta\phi_{i+1}], \Delta\eta \in [\Delta\eta_j, \Delta\eta_{j+1}]) = \frac{N_{assoc.,raw,SE}(\Delta\phi \in [\Delta\phi_i, \Delta\phi_{i+1}], \Delta\eta \in [\Delta\eta_j, \Delta\eta_{j+1}])}{(\Delta\phi_{i+1} - \Delta\phi_i)(\Delta\eta_{j+1} - \Delta\eta_j)} \quad (IV.2)$$

The pseudorapidity bin borders are denoted here by  $\eta_j$ .

In this work, the number of  $\Delta\phi$ -bins is restricted to sixteen due to limited statistics and due to the effect of bremsstrahlung on  $\phi_{e^+e^-}$ . The latter influence is discussed in more detail in Appendix B.

In order to retrieve the final result, the raw distributions are subject to two analysis steps:

1. Correction of acceptance and efficiency effects on the raw distributions
2. Background subtraction and normalization by the number of  $J/\psi$ -candidates

They are explained subsequently.

## IV.C Corrections on Raw Distributions

The acceptance and the efficiency for the  $e^+e^-$ -pairs and for the associated tracks are not constant over the measured phase space. They depend on  $p_{T,e^+e^-}, \phi_{e^+e^-}, \eta_{e^+e^-}$  concerning the  $e^+e^-$ -pairs and on  $p_{T,assoc.}, \phi_{assoc.}, \eta_{assoc.}$  concerning the associated tracks<sup>2</sup>. Since these effects can affect the shape of the measured correlation and the number of correlated tracks, differential corrections have to be applied on the raw distributions. They are similar in nature compared to the ones necessary in hadron-hadron correlation analyses. The latter have been carried out by the ALICE Collaboration in the pp as well as in the Pb-Pb collision system. This work is therefore relying partially on the developed strategies in this context [73, 75]. All corrections presented in the following are done separately for the data samples from the period e and d. The period b and c are treated together due to the small statistics in these samples. All three samples represent approximately one third of the whole data sample.

The correction procedure can be subdivided in two parts:

---

2. Theoretically, the efficiency of the  $e^+e^-$ -pair (associated tracks) might depend also on the parameters of the associated tracks ( $e^+e^-$ -pair).

1. application of weighting factors on the raw entries
2. mixed event distribution correction for  $\eta$  and  $\phi$ -dependent effects

They are discussed subsequently.

#### IV.C-1 Corrections via Weighting Factors

In order to correct for efficiencies differentially by weighting factors in other observables than  $\Delta\phi$  and  $\Delta\eta$ , it is necessary to keep the information on these variables. Therefore and for the signal extraction explained in IV.D-2, not a two dimensional, but a six dimensional histogram is filled in the present analysis. The information on  $p_{T,assoc.}$ ,  $p_{T,e^+e^-}$ , the z-coordinate of the event vertex and the mass of  $e^+e^-$ -pair are available in the present analysis scheme. Hence, it is possible to correct for efficiency effects by applying weighting factors in this six-dimensional structure.

In practice, this method is used for the correction of the tracking efficiency for the associated tracks as a function of transverse momentum. A similar strategy was followed in the underlying event analysis and the dihadron analysis by ALICE[73, 75] :

$$\begin{aligned} \frac{dN_{assoc.,pTcorr.,SE}}{d(\Delta\phi)}(\Delta\phi \in [\Delta\phi_i, \Delta\phi_{i+1}]) = \\ \sum_{p_T \text{ bins}} \frac{N_{assoc.,raw,SE}(\Delta\phi \in [\Delta\phi_i, \Delta\phi_{i+1}], p_{T,assoc.} \in [p_{T,assoc.,j}, p_{T,assoc.,j+1}])}{(\Delta\phi_{i+1} - \Delta\phi_i)} \\ \cdot \frac{1}{f(p_{T,assoc.})} \end{aligned} \quad (IV.3)$$

$N_{assoc.,raw}(\Delta\phi \in [\Delta\phi_i, \Delta\phi_{i+1}], p_{T,assoc.} \in [p_{T,assoc.,j}, p_{T,assoc.,j+1}])$  denotes a two-dimensional histogram in the dimensions  $\Delta\phi$  and  $p_{T,assoc.}$ .

$[p_{T,assoc.,j}, p_{T,assoc.,j+1}]$  represents a specific  $p_T$ -bin. The other dimensions of the actually used distributions are suppressed, since this specific correction factor applied does not dependent on these dimensions. The weighting factor is retrieved from the tracking efficiency  $f(p_{T,assoc.})$ , which is determined by a PYTHIA 6.4 Monte Carlo simulation of the detector conditions during the 2010 data taking used in this analysis. The tracking efficiency is depicted in Fig. IV.2 in the adopted binning choice. For high transverse momenta, it saturates at a slightly smaller value than for  $p_T \approx 1$  GeV/c. This behavior is caused by non-sensitive areas between the read-out chambers of the TPC, which reduce the acceptance for straight tracks. The achieved values are actually very close to the theoretical limit, which is plausible during the pp data taking in 2010 for TPC stand-alone tracking.

The inverse of this correction factor, which represents the tracking efficiency, is shown in Fig. IV.2.

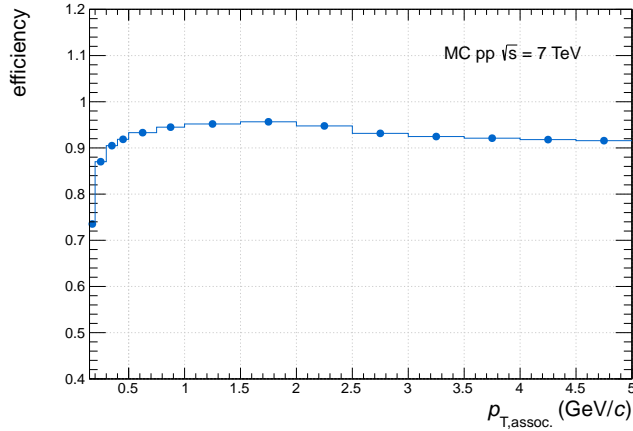


Figure IV.2: Tracking efficiency for used track cuts extracted from PYTHIA 6.4 and GEANT 3 Monte Carlo simulation for 2010 minimum bias data.

This approach allows also to correct for other effects, which have to be taken into account as well. Besides the  $\phi$ - and  $\eta$ -dependence of the efficiency discussed later, the correction of the contribution of non-primary particles is important. Usually considered sources of secondary tracks are decay products from strange particles ( e.g.  $K_S^0$ ,  $\Lambda(\bar{\Lambda})$ ),  $\gamma$ -conversions, hadronic interactions in the detector material and the decay products of charged pions. They are statistically subtracted as a function of  $p_T$  (and as a function of  $\eta$ ) in underlying event studies or spectra analyses, knowing the particle yields from other analyses or Monte Carlo simulations and the DCA distributions of the different track sources. Since the particle composition is different in  $J/\psi$ -candidate events due to the considerable occurrence of charm and beauty decays compared to minimum bias pp collisions, this correction is not directly adoptable from minimum bias events. Therefore, this correction was not yet applied in the current analysis. With increased statistics, a precise analysis of the contamination from secondaries has to be addressed, which would be by now only possible based strongly on Monte Carlo information and not from real data due to the limited statistics, which is in case of particle production in association with  $J/\psi$  and with the background  $e^+e^-$ -pairs not trustworthy.

The correction factors could be also used to correct for the full  $\phi$ - and  $\eta$ -dependence of the efficiency of both associated tracks and  $e^+e^-$ -pairs. In this work, this correction is done via the mixed event correction, which represents a proper data driven method. This approach is further explained in the following subchapter. All further effects related to the  $J/\psi$ -detection efficiency are discussed separately in chapter IV.E.

### IV.C-2 $\phi$ - and $\eta$ -dependent Corrections via Mixed Events

Now, we turn to the effects depending on the azimuthal angle  $\phi$  and the pseudorapidity  $\eta$ . Before we explain the actual correction, we discuss a few crucial aspects for correlation studies caused by efficiency inhomogeneities in the azimuthal angle  $\phi$  and the pseudorapidity  $\eta$ .

In principle, a relative correction of the  $\Delta\phi$ - as well as for the  $\Delta\phi - \Delta\eta$ -distributions for  $\phi$ -dependent effects is only needed, if none of the two  $\phi$ -efficiency distributions, i.e. the one for the tracks and the one for the  $e^+e^-$ -pairs, is not sufficiently homogeneous, where sufficiently means that the inefficiencies does not contribute significantly compared to the other measurement errors.

In case of a inhomogeneous  $e^+e^-$ -efficiency in the azimuthal angle  $\phi$ , but a completely homogeneous efficiency of the associated tracks in  $\phi$ , there is no need for a correction beyond the already applied weighting factors to get the absolute scale of the associated tracks per bin. This is due to the fact that all final results are normalized to the number of  $e^+e^-$ -pairs or to the number of  $J/\psi$ -mesons. In addition, the  $\phi$ -dependencies of the efficiencies enter only as a convolution in the resulting  $\Delta\phi$ -distribution. In case of a completely homogeneous  $e^+e^-$ -pair efficiency, there is also no need for a relative correction between the  $\Delta\phi$ -bins for the same reason. A detailed explanation follows from the formulae given in Appendix A.

The situation is different for  $\eta$ -dependent effects, since the pseudorapidity  $\eta$  is not a variable with periodic boundaries like the azimuthal angle  $\phi$  for the usual setup in collider experiments. We will first consider the effect on the  $\Delta\eta$ - $\Delta\phi$ -distribution: Also in case of a fully efficient detector, but with the same restricted pseudorapidity acceptance for the  $J/\psi$ -candidates and the associated tracks, the measured distribution will not reflect the one without acceptance restrictions. The typical triangular shape is caused by the different combinatorics at the boundary and in the center of the considered pseudorapidity range<sup>3</sup>. Naturally, a  $\eta$ -dependent variation of the detection efficiencies will further distort the  $\Delta\phi - \Delta\eta$ -distribution in absence of corrections.

In addition, if the detection efficiency for the associated tracks or the  $e^+e^-$ -pair is not constant as a function of the pseudorapidity  $\eta$ , this can also influence the  $\Delta\phi$ -distribution. The latter effect will be discussed in more detail for the specific case of this analysis later on.

In order to correct for  $\phi$ - and  $\eta$ -dependent acceptance and efficiency effects, a correction by Mixed Event (ME) distributions after the  $p_T$ -dependent tracking efficiency correction with weighting factors is the standard approach in correlation analyses. The ME distributions are constructed from associ-

---

3. Only if the pseudorapidity acceptance difference between the tracks or the  $e^+e^-$ -pair is equal or larger than the considered  $\Delta\eta$ -range, the measured raw  $\Delta\eta$ -correlation does not show this acceptance effect in case of a fully efficient detector with finite acceptance.

ated tracks and  $e^+e^-$ -pairs from different events. In order to be sensitive for efficiency variations for different event types, one has to introduce several event pool categories, within which the associated tracks and the  $e^+e^-$ -pairs are mixed. These mixed events in a given pool, are then only used for the correction of same event distributions from the same category. The choice of necessary mixed event pools in a given problem and the underlying principles of this method are explained in more detail in Appendix A.

The ME approach removes, since the mixed events are by definition completely uncorrelated between tracks and  $e^+e^-$ -pairs, the effects of efficiency and acceptance on a relative level. The division has to be done separately in the dimensions considered in the correlation and in the dimension of the event pools. If the shape is the only relevant quantity to be extracted, the normalization of both distributions by the number of entries before the bin-wise division in the two considered dimensions  $\Delta\phi$  and  $\Delta\eta$  is in the usual approach:

$$\frac{d^2 N_{SE,asso.,corr.}}{d(\Delta\phi)d(\Delta\eta)} \bigg/ \frac{d^2 N_{ME,asso.,corr.}}{d(\Delta\phi)d(\Delta\eta)} \cdot \frac{K_{int.ME}}{K_{int.SE}} \quad (IV.4)$$

$$= \frac{C_{SE}(\Delta\phi, \Delta\eta)}{C_{ME}(\Delta\phi, \Delta\eta)} = C(\Delta\phi, \Delta\eta) \quad (IV.5)$$

The constants  $K_{int.SE}$  and  $K_{int.ME}$  refer to the respective integrals of the distributions divided by the number of considered bins, the one-dimensional  $\Delta\phi$ -distributions are defined in complete analogy:

$$\frac{dN_{SE,asso.,corr.}}{d(\Delta\phi)} \bigg/ \frac{dN_{ME,asso.,corr.}}{d(\Delta\phi)} \cdot \frac{K_{int.ME}}{K_{int.SE}} \quad (IV.6)$$

$$= \frac{C_{SE}(\Delta\phi)}{C_{ME}(\Delta\phi)} = C(\Delta\phi) \quad (IV.7)$$

In correlation publications, the quantity  $C(\Delta\phi, \Delta\eta)$  is referred as correlation function [76]. The resulting distributions are centered around one by construction.

The procedure of mixed event correction relies on the assumption that the  $p_T$ -efficiency correction for the associated tracks or other possible applied multiplicative corrections in other than the dimensions considered in the correlation factorize with the efficiency correction applied by the weighting factors as a function of  $\Delta\eta$  and/or  $\Delta\phi$ . For small efficiency variations as a function  $\phi$  and  $\eta$  like in this analysis, this assumption should hold approximately.

For the one-dimensional correlation in azimuthal angle, it is important to note, that the  $\Delta\phi$ -distribution retrieved from the projection of the two dimensional distribution after the event mixing technique without a additional reweighting is not the same as the distribution obtained by an only one dimensional correction by a mixed event division. In the latter case

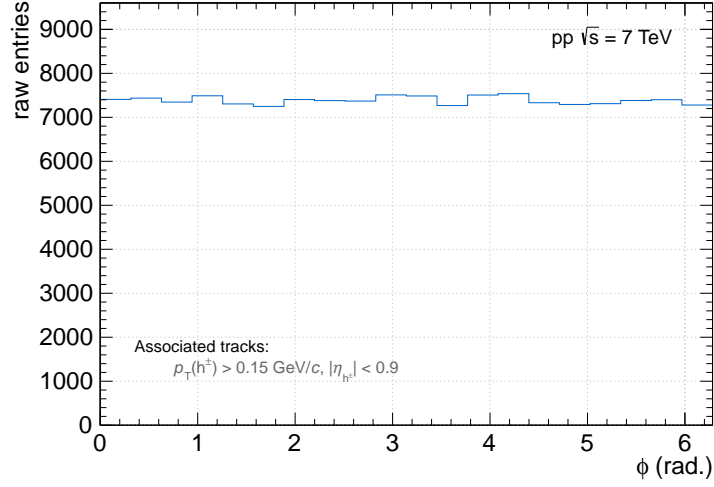


Figure IV.3: raw  $\phi$ -angle distribution of charged tracks in events containing a dielectron pair with invariant mass within  $[1.6, 5.0]$   $\text{GeV}/c^2$  passing the cut set *SPD any proton band* in data taking period 10d.

the sampling includes the relative abundances of  $\Delta\eta$ -distances between the  $e^+e^-$ -pair and the associated tracks observed in the experiment, whereas in the other case every  $\Delta\eta$  row contributes equally to the final  $\Delta\phi$ -distribution.

The purely one dimensional ME correction in IV.7 is the natural choice for azimuthal correlations assuming that the efficiencies in pseudorapidity are flat for both particles sorts to correlate with each other. Additionally, the projection of the two-dimensional distribution is only possible, if the statistics also for the bins with largest  $\Delta\eta$  has a still acceptable statistical error compared to the expected variation in the correlation, since this error will be equally weighted with the errors from other  $\Delta\eta$  values entering the projected  $\Delta\phi$  distribution. In the case of the available statistics of  $J/\psi$  in the analysis, the latter approach is not accessible. The ME correction in this analysis is therefore based on IV.7. The efficiency dependence on the pseudorapidity  $\eta$  is not corrected by the followed approach. The present statistical limitations in conjunction with the knowledge that the tracking efficiency variation as a function of  $\eta$  amounts maximally up to about 3% [77] for the 2010 data minimum bias sample lead to the conclusion that effect can be therefore fairly neglected. The impact of the pseudorapidity dependence of the  $e^+e^-$ -pair detection efficiency is discussed in the chapter on  $J/\psi$ -efficiency.

In the case of this analysis, the correction of the  $\Delta\phi$ -distribution for  $\phi$ -dependent effects is not imperatively necessary, since the tracking efficiency as a function of  $\phi$  for the associated tracks is nearly constant in the minimum bias data sample for the given kinematic restrictions. This can be already

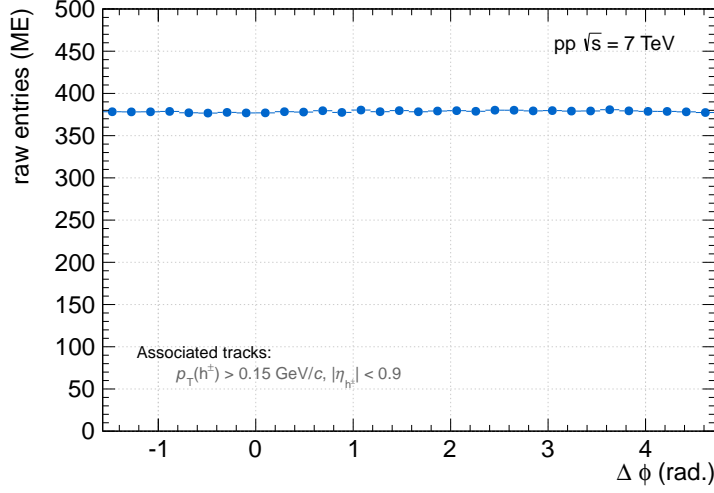


Figure IV.4: Raw ME  $\Delta\phi$ -distribution for  $e^+e^-$ -pairs with  $m \in [2.92, 3.16]$   $\text{GeV}/c^2$  and using *SPD any proton band* cut choice.

seen from the raw distribution in Fig. IV.3. But due to inhomogeneities in azimuth for the  $J/\psi$  candidates, which are a priori not uncorrelated with the efficiency for the associated tracks, a division with a mixed event distribution in case of the azimuthal correlations, is the method of choice in order to remove any possible remaining bias of correlated inefficiencies affecting the pairs and the primary tracks:

$$\begin{aligned} & \frac{dN_{assoc.}(\Delta\phi)}{d(\Delta\phi)} \\ &= \frac{dN_{assoc.,pTcorr.,SE}(\Delta\phi)}{d(\Delta\phi)} \cdot \frac{1}{\frac{1}{K} \frac{dN_{asso.,pTcorr.,ME}(\Delta\phi)}{d(\Delta\phi)}} \end{aligned} \quad (\text{IV.8})$$

where:

$$K = \sum_{\Delta\phi\text{-bins}} \frac{1}{\#bins} \frac{dN_{assoc.,pTcorr.,ME}(\Delta\phi)}{d(\Delta\phi)}$$

More details concerning the considered mixing pools can be found in the Appendix A. Fig. IV.4 shows the raw ME azimuthal distribution derived from all  $e^+e^-$ -pairs within the invariant mass range considered for the signal extraction ( $m \in [2.92, 3.16]$   $\text{GeV}/c^2$ ). This figure demonstrates the excellent homogeneity of the tracking efficiency on  $\phi$ . It illustrates also that the correction is not required for the 2010 minimum bias sample. Nevertheless, the implementation of this correction can be crucial for future applications.

In addition to the applied corrections, the entries of the bins of  $\frac{dN_{assoc.}(\Delta\phi)}{d(\Delta\phi)}$  with the same distance to  $\Delta\phi = 0$  for  $\Delta\phi \in [-\frac{1}{2}\pi, \frac{1}{2}\pi]$  are summed up and

divided by two. The same procedure is applied on the bins around  $\Delta\phi = \pi$ . This method is used in order to increase the statistics per bin for the best possible exploitation of the limited statistics. Naturally, this strategy reduces the number of independent bins, but preserves the finer segmentation in the  $\Delta\phi$ -dimension.

### IV.C-3 Statistical Uncertainties

Before turning to the background subtraction, it is important to consider the statistical uncertainty of the observables, since it requires more care in the case of a correlation analysis compared to a counting experiment. The formulae are given for the one-dimensional distribution  $\frac{dN_{assoc.}}{d(\Delta\phi)}(\Delta\phi)$ , but they generalize easily to the two-dimensional case.

Naively, the relative statistical uncertainty of the number of associated tracks  $N_{assoc.}(\Delta\phi_1, m_1)$  is equal to  $1/\sqrt{N_{assoc.}(\Delta\phi_1, m_1)}$ .  $N_{assoc.}(\Delta\phi_1, m_1)$  denotes here the counts of associated tracks for a sample of  $N_{e^+e^-}(m_1)$   $e^+e^-$ -pair occurrences with invariant mass  $m$  of the  $e^+e^-$ -pair within the mass range called  $m_1$ . The  $\Delta\phi$  value of the associated tracks is measured within the range of the  $\Delta\phi_1$ -bin.  $N_{assoc.}(\Delta\phi_1, m_1)$  is proportional to the central quantity of interest:  $\frac{N_{assoc.}(\Delta\phi_1, m_1)}{\Delta\phi_{1,end} - \Delta\phi_{1,start}} = \frac{dN_{assoc.}(\Delta\phi_1, m_1)}{d(\Delta\phi)}$ . The values  $\Delta\phi_{1,start}$  and  $\Delta\phi_{1,end}$  denote the borders of the bin  $\Delta\phi_1$ .

The quoted value for the statistical uncertainty turns out to be not a good description of the actual uncertainty of the measurement. This can be already seen by the fact that the fluctuations seen in the invariant mass distribution of the sheer  $e^+e^-$ -counts, which are compatible with a pure statistical nature, are still imprinted in the distribution of  $N(\Delta\phi_1, m)$  versus mass. But the relative naive statistical errors are smaller than the relative errors in the invariant mass distribution, since the average number of associated tracks per  $e^+e^-$ -pair in a  $\Delta\phi_1$ -specific bin is larger than one in this analysis and therefore the naive relative statistical  $1/\sqrt{N_{assoc.}(\Delta\phi_1, m_1)}$  for a specific bin is smaller than the relative statistical error in the invariant mass distribution of the  $e^+e^-$ -pairs, which is equal to  $1/\sqrt{N_{e^+e^-}(m_1)}$ . Hence, it appears intuitive, that the naive statistical uncertainty cannot be the true one for this distribution.

In order to explain the proper treatment of the statistical uncertainties, it is instructive to remind, what are the quantities of interest to be measured and how they are composed of. Actually, it is intended not to measure the sheer number  $N_{assoc.}(\Delta\phi_1, m_1)$ , but this number under the condition that we have observed an  $e^+e^-$ -pair with a mass  $m$  within the bin  $m_1$ . In order to explain the approach for the calculation of the statistical uncertainty, the following quantity should be looked at:

$$\langle N_{assoc. \text{ per } e^+e^-}(\Delta\phi_1, m_1) \rangle = \frac{N_{assoc.}(\Delta\phi_1, m_1)}{N(m_1)_{e^+e^-}}$$

The limit of  $\langle N_{assoc. \text{ per } e^+e^-}(\Delta\phi_1, m_1) \rangle$  for  $N_{e^+e^-}(m_1) \rightarrow \infty$  is the quan-

tity, which is estimated by  $N_{assoc.}(\Delta\phi_1, m_1)/N_{e^+e^-}(m_1)$  after  $N_{e^+e^-}(m_1)$  and is the quantity, which we intent to determine. We could assume that for every  $e^+e^-$ -pair that occurs in the mass window of  $m_1$ , that the number of tracks in the  $\Delta\phi_1$ -bin is completely determined, e.g. every  $e^+e^-$ -pair with a certain invariant mass is only accompanied with tracks pointing in pre-defined directions. In this case, there is no statistical uncertainty for the quantity  $N_{assoc.}(\Delta\phi_1, m_1)/N_{e^+e^-}(m_1)$ . This is clearly an unrealistic scenario. A reasonable assumption is that  $N_{assoc. \text{ per } e^+e^-}(\Delta\phi_1, m_1)$  is observed according to a statistical distribution  $P(m, \Delta\phi)$ <sup>4</sup>, which has a fixed mean value coinciding with the mean value for an infinite number of measured  $e^+e^-$ -pairs:

$$\langle P_{assoc.}(m_1, \Delta\phi_1) \rangle = \lim_{N_{e^+e^-}(m_1) \rightarrow \infty} \langle N_{assoc. \text{ per } e^+e^-}(\Delta\phi_1, m_1) \rangle \quad (\text{IV.9})$$

Assuming a Poisson distribution for  $P_{assoc.}(m_1, \Delta\phi_1)$ , the relative statistical uncertainty of  $\langle P_{assoc.}(m_1, \Delta\phi_1) \rangle$  using the estimator  $\langle N_{assoc. \text{ per } e^+e^-}(m_1, \Delta\phi_1) \rangle$  improves with the number of 'measurements' of  $N_{assoc. \text{ per } e^+e^-}(m_1, \Delta\phi_1)$ . This corresponds in our case to the number of  $e^+e^-$ -pairs within the invariant mass window  $m_1$ . We therefore assign for the relative statistical uncertainty of  $\frac{N_{assoc.}(\Delta\phi_1, m_1)}{N(m_1)_{e^+e^-}}$ :

$$\frac{\Delta_{stat} (N_{assoc., m_1, \Delta\phi_1} / N_{e^+e^-}(m_1))}{N_{assoc., m_1, \Delta\phi_1} / N_{e^+e^-}(m_1)} = \quad (\text{IV.10})$$

$$\frac{\Delta_{stat} \langle N_{assoc., m_1, \Delta\phi_1 \text{ per } e^+e^-} \rangle}{\langle N_{assoc., m_1, \Delta\phi_1 \text{ per } e^+e^-} \rangle} = \frac{1}{\sqrt{N_{e^+e^-}(m_1)}} \quad (\text{IV.11})$$

Since the measurement is not background free, it is necessary to consider also  $N_{assoc.}(\Delta\phi_1, m_1)$  after measuring  $N_{e^+e^-}(m_1)$  and not only normalized by  $N_{e^+e^-}(m_1)$ . This is due to the fact, that  $N_{assoc.}(\Delta\phi_1, m)$  is used as a function of mass for the background subtraction, which will be explained in detail in the subsequent section.

For the statistical uncertainty of  $N_{assoc.}(\Delta\phi_1, m_1)$ , we have not only to consider the uncertainty of  $\langle N_{assoc. \text{ per } e^+e^-}(\Delta\phi_1, m_1) \rangle$ , but also the uncertainty of  $N_{e^+e^-}(m_1)$ , since:

$$N_{assoc.}(\Delta\phi_1, m_1) = N_{e^+e^-}(m_1) \cdot \langle N_{assoc., \text{ per } e^+e^-}(\Delta\phi_1, m_1) \rangle \quad (\text{IV.12})$$

The relative statistical uncertainty of  $N_{e^+e^-}(m_1)$  amounts to  $1/\sqrt{N_{e^+e^-}(m_1)}$ . The latter enters also the invariant mass distribution of the  $e^+e^-$ -pairs. Since  $N_{e^+e^-}(m_1)$  and  $\langle N_{assoc. \text{ per } e^+e^-}(\Delta\phi_1, m_1) \rangle$  are independent in the sense that there is no residual functional dependence of  $\langle N_{assoc. \text{ per } e^+e^-}(\Delta\phi_1, m_1) \rangle$

---

4. This presumption can be contested. Albeit this fact, it should give a reasonable order of magnitude for the statistical uncertainty.

on  $N_{e^+e^-}(m_1)$ , the statistical uncertainty of  $N_{assoc.}(\Delta\phi_1, m_1)$  is the quadratic sum of both individual error contributions. Finally, we get therefore:

$$\frac{\Delta_{stat}N_{assoc.}(\Delta\phi_1, m_1)}{N_{assoc.}(\Delta\phi_1, m_1)} = \frac{\sqrt{2}}{\sqrt{N_{e^+e^-}(m_1)}} \quad (\text{IV.13})$$

Since the mean number of tracks in a specific bin for mass and  $\Delta\phi$  per  $e^+e^-$ -pair is larger than one in our binning choice as already mentioned,  $\sqrt{2}/\sqrt{N_{e^+e^-}(m_1)}$  is larger than  $1/\sqrt{N_{assoc.}(\Delta\phi_1, m_1)}$ . This fact leads to a larger statistical uncertainty of  $N_{assoc.}(\Delta\phi_1, m_1)$  in the given argumentation with respect to the naive approach.

## IV.D Background Subtraction

The background subtraction is the most delicate step of the analysis. In the following, the formalism is developed to extract the  $J/\psi$ -hadron correlation from the corrected  $e^+e^-$ -pair-hadron correlations.

In fact, the signal over background ratio in the invariant mass region considered for the signal extraction is roughly of order  $O(1)$  for the considered cut choices in case of the minimum bias data sample. The second crucial observation is that the  $e^+e^-$ -pairs with larger and smaller invariant mass than the  $J/\psi$ -peak show a non-negligible correlation. It is therefore necessary to get an appropriate estimate of the background correlation and subtract this properly from the measurement of the  $e^+e^-$ -pairs in the invariant mass region of the  $J/\psi$ .

### IV.D-1 General Considerations

The background subtraction takes place before the final division by the number of  $e^+e^-$ -pairs is done. Otherwise one has to determine the number of associated tracks for the signal and the background for every  $\Delta\phi$ -bin per  $e^+e^-$ -pair separately from the number of background and signal  $e^+e^-$ -pairs in order to scale the contributions to the associated track from the background  $e^+e^-$ -pairs in the  $J/\psi$  signal region. Only after the determination of  $\frac{dN_{assoc.,bkg}}{d(\Delta\phi)}$  the finally interesting quantities can be retrieved:

$$\frac{dN_{assoc.}}{d(\Delta\phi)} = \frac{dN_{assoc.,J/\psi}}{d(\Delta\phi)} + \frac{dN_{assoc.,bkg}}{d(\Delta\phi)} \quad (\text{IV.14})$$

$$\frac{dN_{assoc.,J/\psi}}{d(\Delta\phi)} = N_{J/\psi} \cdot \frac{1}{N_{J/\psi}} \frac{dN_{assoc.,J/\psi}}{d(\Delta\phi)} \quad (\text{IV.15})$$

The only information entering directly from the signal extraction in the invariant mass distribution in this approach is the absolute number of signal counts  $N_{J/\psi}$  in the regarded invariant mass window.

The determination of the background correlation can be event generator driven or data driven. First, we consider the Monte Carlo driven approach. Such an approach relies on a precise reproduction of the different background elements in Monte Carlo. The background  $e^+e^-$ -pairs do not originate from one dominant source as discussed in chapter III.B-2.i. Therefore, the description of the different  $e^+e^-$ -background pairs is already not an easy task, since it relies strongly on a very precise mapping of the particle identification and proper matching of all involved cross sections for electron producing processes. Furthermore, if this is achieved, one has still to face the problem that the Monte Carlo has to describe the hadronic particle production associated with the background cocktail accurately. Since

the particle production in association with these various background sources is not a standard observable, which is tuned in event generators, it is not expected that it provides a reliable description. In conclusion, a simulation driven approach for the background subtraction is not well suited.

There are in principle two different possible choices for a background description derived from real data: the correlation of  $e^+e^+$ - and  $e^-e^-$  (LS)-pairs in the invariant mass region of the signal and the use of the correlations from  $e^+e^-$  (OS)-pairs in the vicinity of the  $J/\psi$ -peak. The use of mixed-event distributions for the background subtraction is not reasonable, since the background shows a significant correlation.

Generally, both remaining methods have drawbacks: in case of the LS-method, one assumes implicitly that the composition of the sources contributing to the LS-pairs and the OS-pairs is the same. The significant contribution from two semileptonically decaying D-mesons to the  $e^+e^-$ -pair background invalidates this approach, since this source does not contribute to the LS-pairs<sup>5</sup>. The only remaining choice is the background estimation using the OS-pairs-hadron correlation with invariant masses close to the  $J/\psi$ -mass, although also this approach includes some caveats.

The first problem is the bremsstrahlung tail of the  $J/\psi$  toward the lower invariant mass region in case of the  $e^+e^-$ -decay channel, since a non-negligible fraction of  $e^+e^-$ -pairs from  $J/\psi$ -decays are entering the lower invariant mass region. Therefore, a significant distance to the  $J/\psi$ -peak for the mass ranges in the  $e^+e^-$ -spectrum used for the background estimation is necessary. At larger invariant masses, in principle the  $\psi(2S)$  also contributes to the background, but this effect is completely negligible due to the small abundance of  $\psi(2S)$  (discussed in chapter III.B-2.ii).

In summary, the use of the OS-spectrum neighboring the  $J/\psi$ -peak is the best available option for an adequate estimate of the background.

#### IV.D-2 Fit Approach for Assessing the Background Correlation

In this analysis, the background is retrieved by fitting the  $e^+e^-$ -pair-hadron correlation. The invariant mass ranges  $[1.6-2.6]$   $\text{GeV}/c^2$  and  $[3.24-4.0]$   $\text{GeV}/c^2$  were used simultaneously for these fits. The latter were carried out independently for every  $\Delta\phi$ -bin.

Since the background is monotonously falling for the cut choice *proton band*, a third order polynomial was used for the fit. In case of the cut choice *no proton band*, the background subtraction is more delicate, since the background correlation distributions for every  $\Delta\phi$ -bin are peaked near

---

5. The occurrence of D-meson mixing can also produce like sign pairs, but this mixing is a very rarely happening process in contrast to B-mixing. Also in case of B-meson pairs there remains a difference of the contribution of the like-sign and opposite-sign background, since the mixing only concerns the neutral B-pair production.

the  $J/\psi$ -mass region. Therefore, the ratio of two second order polynomials was used in order to fit the background distribution. The shape reproduces the features of the observed background distribution in the considered mass range from 1.6-4.0  $\text{GeV}/c^2$ . Example fits are shown in the section presenting the final results.

The resulting fit functions defined also in the signal region are used for the actual subtraction bin-by-bin for the invariant mass:

$$\frac{1}{N_{J/\psi}} \frac{dN_{ass,J/\psi}}{d(\Delta\phi)} = \frac{1}{S_{tot}} \sum_{m \in [2.92, 3.16] \text{GeV}/c^2} \frac{dN_{ass,e^+e^-}(m) - dN_{ass,bkg,fit}(m)}{d(\Delta\phi)} \quad (\text{IV.16})$$

It is important that the actual signal extraction in the  $e^+e^-$  invariant mass distribution only enters as an absolute normalization in this approach. Cross checks were done by using only the 40 MeV wide invariant mass bin from 3.08 – 3.14  $\text{GeV}/c^2$ , which contributes most prominently to the  $J/\psi$ -yield.

It is clear, that this first approach is still improvable. The use of unbinned distributions or at least an increase of the granularity in the invariant mass dimension is desirable. Furthermore, the presented approach can be also cross checked by the direct use of the appropriately scaled OS-pair-hadron correlations close to the  $J/\psi$ -peak without the use of a fit<sup>6</sup>. In addition, further investigations in Monte Carlo as well as in data for a better understanding of the background could bring also ideas for the improvement of the background description below the  $J/\psi$ -peak. These points will be crucial for a final validation of the presented approach and will be devoted to future studies with larger statistics.

### IV.D-3 Statistical Uncertainties

Finally, it is also necessary to have a closer look at the propagation of the statistical uncertainty for the signal extraction and the normalization by the signal counts. The statistical error, which was assigned to the  $dN_{ass,e^+e^-}(m)/d(\Delta\phi)$ -distribution contained an error for the number of  $e^+e^-$ -pairs and an uncertainty due to the statistical nature of the correlation distribution, which had both equal size (relative size of  $1/\sqrt{N_{e^+e^-}(m)}$ ) and were added in quadrature. This error is propagated in the background subtracted, but not yet normalized  $dN_{ass,J/\psi}/d(\Delta\phi)$  distribution. The error due to the counting of the  $e^+e^-$ -pairs is correlated bin-by-bin in the  $\Delta\phi$  correlation and is therefore an overall common error assuming that the background subtraction works properly<sup>7</sup>. In addition, this error is also strongly

6. At the present stage, the fit approach is expected to be more powerful due to the more efficient exploitation of the limited statistics.

7. The statistical uncertainty of the fit is neglected, since the corresponding error is very small, which was checked with a look at the fit parameter uncertainties. The error due to imperfect background subtraction is treated in the systematical error section.

correlated with the statistical error of  $N_{J/\psi}$  from the signal under the assumption that signal and background are properly separated. Nevertheless, in absence of a precise knowledge of the correlation, the bin-by-bin correlated statistical uncertainty from the signal extraction in invariant mass and of the bin-by-bin correlated error from signal extraction are handled, if they were independent quantities. The latter has to be understood as a conservative upper estimate for the overall correlated statistical uncertainty, although the statistical error of  $N_{J/\psi}$  and the overall scaling uncertainty of  $\frac{dN_{ass,J/\psi}}{d(\Delta\phi)}$  might cancel each other partially in reality.

Therefore the final bin-by-bin uncorrelated relative statistical error of  $\frac{1}{N_{J/\psi}} \frac{dN_{ass,J/\psi}}{d(\Delta\phi)}$  amounts to:

$$\Delta_{stat,uncorr} \left[ \frac{1}{N_{J/\psi}} \frac{dN_{ass,J/\psi}}{d(\Delta\phi)} \right] \left( \frac{1}{N_{J/\psi}} \frac{dN_{ass,J/\psi}}{d(\Delta\phi)} \right)^{-1} = \sqrt{\sum_{m \in [2.92, 3.16]} \left( \Delta_{stat} \left[ \frac{dN_{ass,e^+e^-}(m)}{d(\Delta\phi)} \right] \cdot \left( \frac{\sqrt{2} dN_{ass,e^+e^-}(m)}{d(\Delta\phi)} \right)^{-1} \right)^2} \quad (\text{IV.17})$$

And the overall bin-by-bin correlated statistical uncertainty is equal to:

$$\Delta_{stat,corr} \left[ \frac{1}{N_{J/\psi}} \frac{dN_{ass,J/\psi}}{d(\Delta\phi)} \right] \left( \frac{1}{N_{J/\psi}} \frac{dN_{ass,J/\psi}}{d(\Delta\phi)} \right)^{-1} = \sqrt{\sum_{m \in [2.92, 3.16]} \left( \Delta_{stat} \left[ \frac{dN_{ass,e^+e^-}(m)}{d(\Delta\phi)} \right] \cdot \left( \frac{\sqrt{2} dN_{ass,e^+e^-}(m)}{d(\Delta\phi)} \right)^{-1} \right)^2 + \left( \frac{\Delta_{stat} N_{J/\psi}}{N_{J/\psi}} \right)^2} \quad (\text{IV.18})$$

## IV.E $J/\psi$ -Efficiency

Albeit the knowledge of the absolute efficiency of the  $J/\psi$  in the restricted acceptance is not needed due to the normalization per  $J/\psi$ , it would be a priori necessary for a final result of  $J/\psi$ -hadron correlations to correct for the efficiency of the  $J/\psi$  at least on a relative level. The reason is the fact that the efficiency for detecting a  $J/\psi$  is not independent of its transverse momentum  $p_T$  and its pseudorapidity  $\eta$  and the  $J/\psi$ -hadron correlation might be a function of these variables. The remaining possibly necessary corrections reflect that the properly corrected correlation from the *detected*  $J/\psi$  sample is not identical to the correlation of *all*  $J/\psi$ s in the regarded kinematic regime, i.e. the selection of  $J/\psi$ -mesons is biased and can in turn influence the correlation with charged tracks.

First of all, measurements in subsets of the  $e^+e^-$ -pair sample in bins of the mentioned variables would be the best option to circumvent the problem, since in this case the influence of the variables could be seen and would not affect the correlation intensive in the number of  $e^+e^-$ -pairs considered for bin sizes with negligible  $J/\psi$  efficiency differences inside the bin. Since the measurement is limited by statistics, these differential measurements are not feasible. We will therefore discuss the possible impact on the correlation caused by the selection bias of the detected  $J/\psi$ .

The most important efficiency correction of the  $J/\psi$  is the correction of the  $p_T$ -dependence, since the shape of the correlation and also the number of associated tracks might be dependent on this variable. Furthermore, the efficiency is not constant as a function of transverse momentum due to the kinematic cuts on the electron and positron and the particle identification selection criteria.

Nevertheless, the effect on the correlation by weighting correlation entries of  $J/\psi$  from different  $p_T$  intervals will not be very strong for the *proton band* cut choices due to the large part of possible phase space for the daughter tracks and is still not very large for the *no proton band* cut choice. This claim can be verified by comparing the efficiency corrected  $p_T$  differential shape from the  $J/\psi$ -cross section publication of ALICE with the sequential signal extraction in the same  $p_T$  bins<sup>8</sup>. Fig. IV.5 shows this comparison<sup>9</sup>. The *SPDany* cut choices are displayed. The corresponding signal extractions

---

8. In fact, it is ignored for this comparison that the overall  $p_T$ -shape is also effected non-trivially by the cut in pseudorapidity for the correlation selection instead of the rapidity cut in the cross section reference. The  $J/\psi$  selection in this work will have a slightly higher  $p_T$ , but the effect depends on the  $p_T$ - and rapidity shape of the detected  $J/\psi$  and is not of major importance in view of the statistical uncertainties.

9. The bin-by-bin uncorrelated systematic uncertainty, which is also relevant for these relative quantities, is dominated by the signal extraction systematics and is of similar size or slightly smaller than the statistical uncertainty for the cross section publication. This systematical uncertainty and the possible error caused by the polarization dependence of the efficiency calculation, which changes strongly as a function of  $p_T$ , are not displayed.

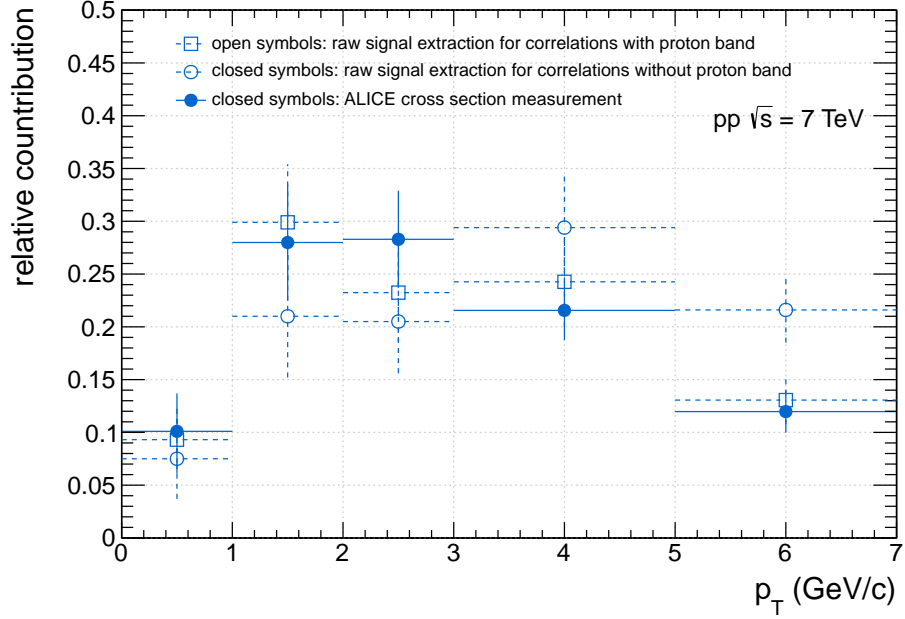


Figure IV.5: Normalized  $p_T$ -sequential signal extraction for *SPDany proton band* and *SPDany no proton band* compared with properly normalized and efficiency corrected cross section measured by ALICE at midrapidity [22]. The error bars represent the statistical uncertainties.

with *SPDfirst* and *ITS3any* cut sets are compatible within the uncertainties with the *SPDany*-result.

Secondly, we address the effect caused by a pseudorapidity dependence of the  $J/\psi$ -efficiency. We don't consider effects, by changes of the true correlation as function of pseudorapidity, since there is no change in the production mechanism expected within the considered pseudorapidity range of inspected  $J/\psi$  in  $\eta \in [-0.9, 0.9]$ . Nevertheless, a pseudorapidity dependent efficiency to detect a  $J/\psi$  can introduce a bias in the azimuthal  $J/\psi$ -hadron correlation: If one does not assume an azimuthal  $J/\psi$ -hadron correlation independent of the possible  $\Delta\eta$  within the acceptance range or in case that the correlated peaks don't extend in the pseudorapidity dimension. In both extreme cases, there is no deviation of the correlation shape caused by the  $J/\psi$ -efficiency. In all other cases, a pseudorapidity dependence of the latter can cause a difference to the correlation observed with completely homogeneous efficiencies. Nevertheless, the present measurement is not sensitive to these subtle distortion effects, since a correlation is not firmly established for the  $J/\psi$ .

There is also a bias introduced by the fact, that the acceptance does not allow to inspect all possible  $J/\psi$ -polarisation states with the same probabil-

ity. In case of any change of the  $J/\psi$ -hadron correlation as a function of the polarization, it would hence lead to a bias of the  $J/\psi$ -selection compared to a measurement without the experimentally given phase space restrictions. A possible correction could be applied by the weighting of the extracted  $J/\psi$ -hadron correlations according to a specific polarization assumption, which would originate ideally from a measurement of the polarization. The impact is also hard to quantify, but it is only adressable with larger statistics.

In summary, for this first study, there is no significant impact expected by the non-correction of the  $J/\psi$ -efficiency as a function of transverse momentum, pseudorapidity and polarization.



## – Chapter V –

# Systematic Uncertainties

Any physical measurement requires the quantification of the systematic uncertainties as an indispensable prerequisite for a reasonable interpretation of the result. Presently, an extended investigation of the systematic uncertainties for the  $J/\psi$ -hadron analysis is not yet undertaken. Nevertheless, the expected main sources of uncertainties can be identified. Furthermore, the size of the related systematic uncertainties can be, at least partially, estimated from the already performed cross checks or from other physics analysis.

The systematic uncertainties can be separated in three principle categories:

- uncertainties of the  $e^+e^-$ -pair-hadron correlation
- uncertainties of the signal extraction in the invariant mass distribution and within the correlation distributions
- uncertainties due to the bremsstrahlung

These different sources will be discussed subsequently.

## V.A Uncertainties of the Dielectron-Hadron Correlations

We will address in the following the systematic errors, which are already present in the not yet background subtracted dielectron-hadron correlations.

In this context, it is not expected that the effects related to the associated tracks and their efficiency correction contribute significantly to the systematic uncertainties due to the very good homogeneity of the TPC tracking in the analyzed sample.

It is just important to note, that the track definition involved in this study also includes non-primary tracks as explained in IV.C-1. In subsequent studies, the correction for non-primary tracks will be certainly important in order to really extract a  $J/\psi$ -*primary*-hadron correlation. However,

the precise quantification of this effect depends on the precise tracking cuts and on the particle composition in the exploited event sample and is at the present stage not yet estimated.

The effects connected to the detection efficiency of the dielectron pair are discussed in IV.E. They are also not expected to dominate the systematic uncertainty, albeit more precise investigations will be needed in future.

## V.B Signal Extraction Uncertainties

Finally, the signal extractions in the invariant mass distribution and in the associated track histograms is the major source of systematic error for this correlation measurement. This is mainly due to the fact the the  $J/\psi$  in the dielectron decay channel exhibits a long bremsstrahlung tail and the limited statistics, which complicate to judge the background description quality with a certain method.

The chosen Like-Sign (LS) subtraction for the invariant mass distribution has to be checked in future by other signal extraction methods. Since the dielectron sample is at least for the *proton band* cut choices nearly congruent with the sample used in the ALICE cross section publication[22], a similar systematic error for the signal extraction is realistic. In the publication, the relative systematic error of the signal extraction amounts to 8% for the inclusive yield, which is close to the relative statistical error of 9%. A systematic error of equal size than the statistical error seems therefore appropriate in the presented work. Certainly, a further investigation of the line shape with larger data samples and suitable comparisons with simulation will reduce this uncertainty significantly. This error is a strongly correlated one between the bins in the extracted  $\Delta\phi$  correlation and should not affect the derived shape of the correlation.

The systematic error on the signal extraction in the  $\Delta\phi$ -bins of the dielectron-hadron correlation is difficult to estimate. At the same time, it represents presumably the most important one.

In this context, it might be considered unnatural to choose a different approach for the signal extraction in the invariant mass distribution and for the background subtraction for the associated track distributions. The LS-distributions were not used for the background description in the latter case, since they don't represent a good model due to the correlated OS-background, which is not present in the LS background as explained in the analysis method section. The approach to fit, as every signal extraction method, which relies on information at lower mass of the OS-dielectron mass spectrum, suffers from the bremsstrahlung tail. For the correlation study, it was therefore decided that the fits only include the invariant mass region below  $2.6 \text{ GeV}/c^2$  (and above  $3.24 \text{ GeV}/c$ ) and not closer to the

peak region<sup>1</sup>. In view of the overall small dielectron statistics, the effect of  $J/\psi$ -contamination should be therefore negligible.

The fit approach was also applied for the signal extraction in the invariant mass distribution in order to estimate its reliability for the background assessment in the associated track distributions. It was observed that the signal extraction via the fit leads consistently to a smaller number of extracted signal counts in case of the *proton band* cut choices. Nevertheless, the results of both methods are compatible within their uncertainties. The consistently smaller yield for the fit approach in this case could be an effect of the Bremsstrahlungstail. However, it is important to note that the background has a approximately two times larger number of associated tracks. Therefore, the fit to the lower invariant mass is less critical for the  $\Delta\phi$  bins than for the dielectron invariant mass distribution, since the contamination of  $J/\psi$  does not contribute as strong as in the invariant mass distribution to the lower masses. For the signal extraction with the fit approach for the *no proton band* cut choice, the discrepancy between the fit approach and the LS signal extraction was negligible compared with the statistical uncertainties. These results seem to validate the approach within the present limitations.

In summary, due to the similar nature of the problem, it seems realistic to assign a systematic error of similar size for the signal extraction in the  $\Delta\phi$ -distributions than for the signal extraction than in the invariant mass distribution. Furthermore, it is difficult to judge, whether this systematical error is completely uncorrelated between the different bins and uncorrelated with the signal extraction in the invariant mass, although the latter is extracted with a different method. For the quantification of the bin-by-bin uncorrelated uncertainty, it is certainly necessary to accumulate a larger sample and vary the fits for finer binning choices.

Finally, the results of all ITS cut requirements *SPDany*, *SPDfirst* and *ITS3any* and also the results between the *no pband* and *pband* cut choice despite the slightly different  $p_T$  spectrum in the latter case show results for the total number of associated tracks derived with the  $J/\psi$ -hadron correlation, which are compatible with each other within the statistical uncertainty despite the strongly changing amount of background. In addition, the extraction of the  $J/\psi$ -correlation in a smaller invariant mass range ( $[3.04, 3.16]$  GeV/ $c^2$ ) is also consistent within the statistical uncertainties. These results validate that the method is not effected by systematics related with the background description, at least within the accuracy, which is accessible within the given statistical limitations. A more precise quantification of the systematic uncertainty within the signal extraction is difficult at the present

---

1. This is justified by the estimated contribution of the  $J/\psi$ -mesons to the total number of dielectron pairs in the mass range  $[2.4, 2.6]$  GeV/ $c^2$ . This contamination with  $J/\psi$  can be estimated to be about 5% for the cut choice *SPDany proton band*. This estimate relies on the signal shape from Monte Carlo simulation and the absolute scale set by the extracted  $J/\psi$ -signal counts within  $[2.92, 3.16]$  GeV/ $c^2$ .

stage and will be a major part of future investigations.

### V.C Uncertainty due to Bremsstrahlung

Finally, it is important to consider an effect, which is specific to a dielectron analysis.

The emission of photons either from the internal or external bremsstrahlung described in chapter III.B-2.ii has not only an impact on the invariant mass distribution, but also on the reconstructed  $\phi$ -angle and the pseudorapidity  $\eta$  of the  $J/\psi$ , which are measured by the corresponding quantities of the dielectron pair. The effect is estimated in Appendix B for different kinematic constellations, which maximize the effect for the azimuthal angle. It is the dominant uncertainty on the  $\Delta\phi$  angle, since the azimuthal angle of primary tracks is typically measured with a precision in the order of mrad within the ALICE setup[78]. For the used binning choice of  $22.5^\circ$ - $\Delta\phi$  intervals, the effect should not affect the observed distributions significantly according to the considerations in Appendix B. For future measurements, especially for narrower binning intervals in  $\Delta\phi$ , further investigations via simulation have to be done. Finally, a restriction to a smaller invariant mass window for  $J/\psi$ - $p_T$  of a few GeV/ $c$  is probably necessary to avoid the influence by the photon emission.

## – Chapter VI –

# Results and Discussion

The following chapter is devoted to the presentation of the results obtained within the  $J/\psi$ -hadron correlation analysis. Since the measurement is not background free, the distributions used for the background assessment and for the not yet background subtracted signal region are reviewed. Subsequently, the background is subtracted and the resulting signal correlations are discussed. Finally, an insight in the implementation of charmonia production and in its implications for the studied observable in the common event generator PYTHIA [79, 80] is given.

## VI.A Azimuthal Dielectron-Hadron Correlations

In order to understand the background behavior, it is important to look at the efficiency corrected azimuthal correlation for  $e^+e^-$ -pairs in certain invariant mass ranges. Therefore, the  $e^+e^-$ -pair-hadron correlation in the invariant mass regions  $[2.4, 2.6]$   $\text{GeV}/c^2$  and  $[3.24, 3.4]$   $\text{GeV}/c^2$  are depicted for the cut choices *SPDany proton band* and *SPDany no proton band* are shown in the Fig. VI.1, VI.2, VI.3 and VI.4. They show the  $\Delta\phi$ -differential number of associated tracks as a function of the azimuthal angle difference with respect to the azimuthal angle of the dielectron. The distributions are normalized to the number of dielectron pairs. The expected azimuthal symmetry of the distributions was exploited as described in the analysis method by doubling the entries per bin. Naturally, the number of independent bins is reduced by a factor two. The entries in the independent bins are nevertheless reflected according to the assumed symmetry in order to guide the eye. The displayed errors only account for the statistical error. The kinematic restrictions for the dielectron pairs and the charged tracks are displayed on the figures.

The total number of associated tracks, which are corrected for tracking efficiency, but not for contamination from non-primary tracks, amounts to about 30-35 tracks per dielectron for both invariant mass regions and for

both cut choices. A correlation in these background regions is visible on a relative level of 10 %, although the statistical uncertainties prevent from a precise characterization.

The observed behavior in these two invariant mass ranges illustrates that the background shows a non-negligible correlation. This correlation in the background can be caused by a multitude of sources, due to variety of background sources. Since the background includes a fraction of particle pairs from open charm and open beauty semileptonic decay electrons and positrons combined with other electrons and positrons from  $\gamma$ -conversions and combined with misidentified hadrons (the most important background contribution according to Monte Carlo simulation are shown in Table III.2), it is plausible to see a significant correlation in the background caused by decay or fragmentation processes.

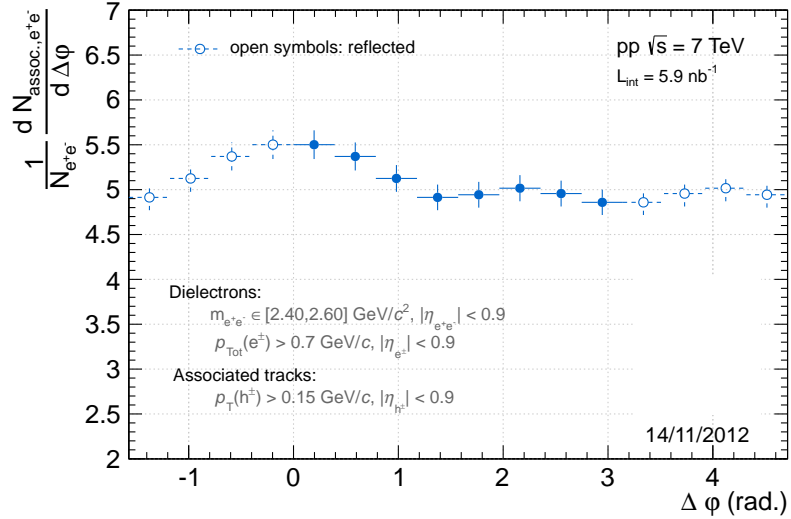


Figure VI.1: Azimuthal dielectron-hadron correlation for *proton band SP-Dany* cut choice,  $m_{e^+e^-} \in [2.4 - 2.6]$  GeV/ $c^2$ .

Furthermore, the number of tracks associated with the dielectron candidates is quite large for the sidebands. This can be deduced from the comparison of the observed number of associated tracks per unit of pseudorapidity  $\frac{1}{N_{e^+e^-}} \frac{dN_{ass}}{d\eta} = 15-20$  with the measured pseudorapidity track density in minimum bias events  $\frac{dN_{ch}}{d\eta} = 6.01 \pm 0.01(stat.)_{-0.12}^{+0.20}(syst.)$  measured at midrapidity within  $|\eta| < 1.0$  [81]. Although this comparison is only of qualitative nature due to the slightly different pseudorapidity ranges ( $|\eta| < 0.9$  for this study and  $|\eta| < 1.0$  for the charged track density measurement) and the low- $p_T$  threshold of  $p_T = 0.15$  GeV/ $c$  for the associated tracks in the correlation study.

The Fig. VI.5 for the cut choice *proton band SPDany* and Fig. VI.6

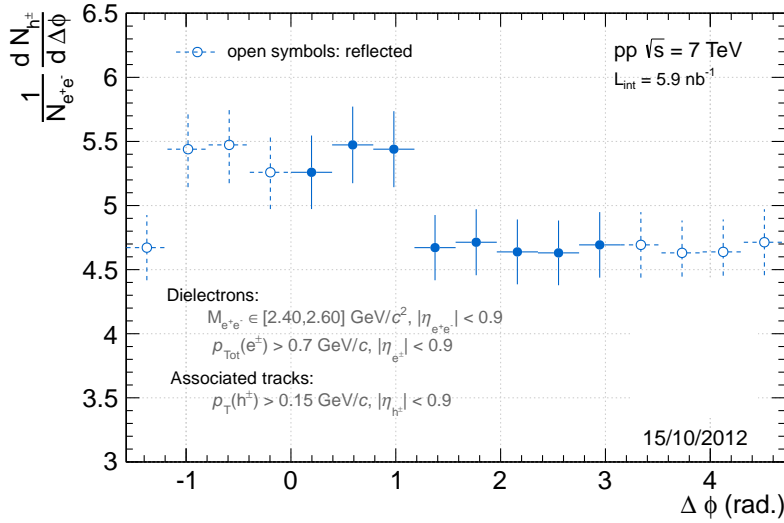


Figure VI.2: Azimuthal dielectron-hadron correlation for *no proton band SPDany* cut choice,  $m_{e^+e^-} \in [2.4 - 2.6]$  GeV/ $c^2$ .

for the cut choice *no proton SPDany* show the azimuthal correlation of the associated tracks for the dielectron pairs in the signal region  $m \in [2.92, 3.16]$  GeV/ $c^2$ , which are subject to the background subtraction. The associated tracks are efficiency corrected, but non corrected for contamination of secondary tracks as in the case of the distributions of the neighboring invariant mass regions of the  $J/\psi$ -peak. The error bars are representing the statistical uncertainty.

In order to put these results in a context, it is important to remark that the S/B-ratio amounts to 0.7 (1.1) in case of *proton band SPDany* (*no proton SPDany*) in this invariant mass range. In case of the choice *SPDany proton band*, a correlation can be observed, which seems to be slightly smaller than the one observed in the neighboring invariant mass regions, although the statistical uncertainty prevent from a firm statement. in case of the *SPDany no proton band*, a significant correlation can be hardly observed within the statistical uncertainties. In addition, the total number of associated tracks is significantly reduced compared to the one, which is observed in the neighboring invariant mass regions. It can be therefore retrieved from the dielectron correlation that the background is associated with a larger number of associated tracks. This fact leads in principle to a less unambiguous signal extraction although the effect of the bremsstrahlung tail below the signal extraction invariant mass range is therefore not equally problematic in the correlation distributions compared to the sheer invariant mass distribution as explained in the chapter treating the systematic uncertainties.

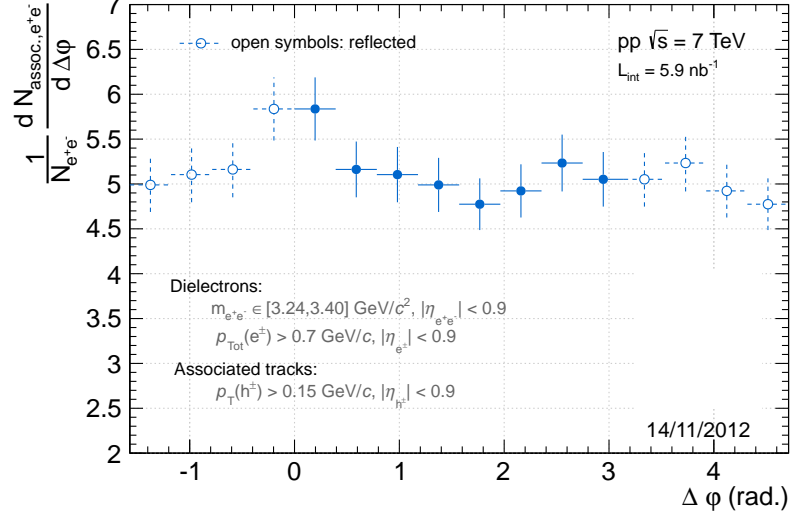


Figure VI.3: Azimuthal dielectron-hadron correlation for *proton band SPDany* cut choice,  $m_{e^+e^-} \in [3.24 - 3.4] \text{ GeV}/c^2$  used for background estimate.

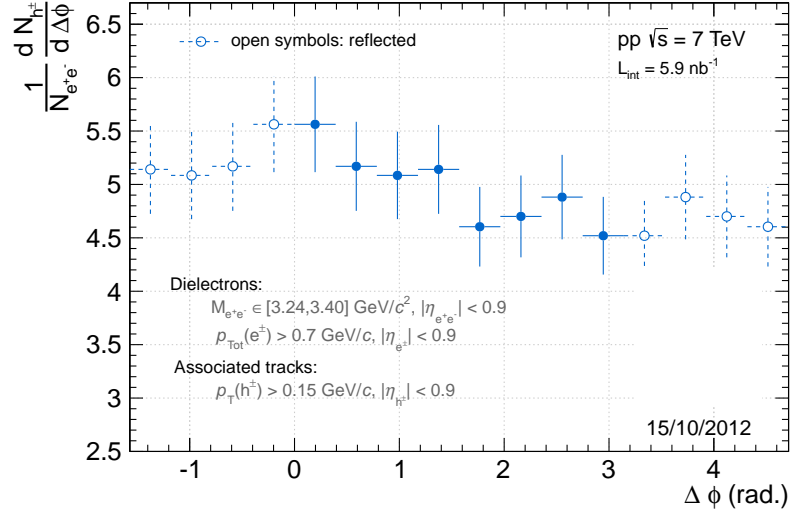


Figure VI.4: Azimuthal dielectron-hadron correlation for *no proton band SPDany* cut choice,  $m_{e^+e^-} \in [3.24 - 3.4] \text{ GeV}/c^2$  used for background estimate.

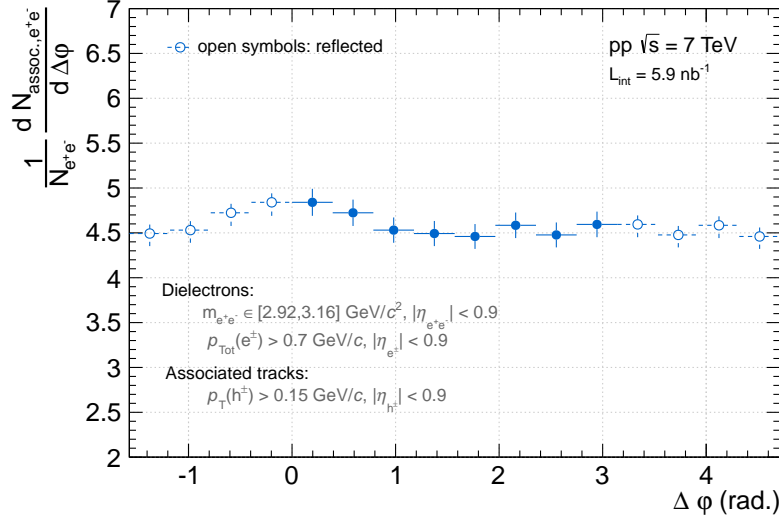


Figure VI.5: Azimuthal dielectron-hadron correlation for *proton band SP-Dany* cut choice in the **signal region**,  $m_{e^+e^-} \in [2.92 - 3.16] \text{ GeV}/c^2$ .

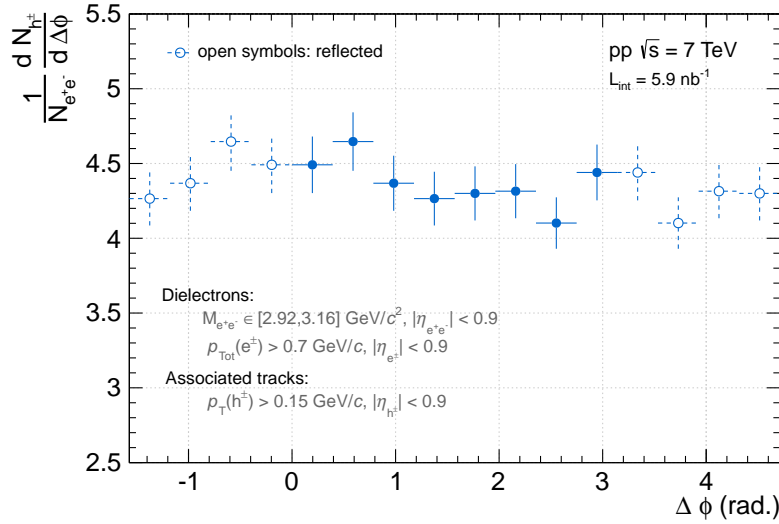


Figure VI.6: Azimuthal dielectron-hadron correlation for *no proton band SP-Dany* cut choice in the **signal region**,  $m_{e^+e^-} \in [2.92 - 3.16] \text{ GeV}/c^2$ .

## VI.B Azimuthal $J/\psi$ -Hadron Correlations

For the extraction of the azimuthal  $J/\psi$ -hadron correlation, the  $N_{assoc.}(\Delta\phi)$ -distributions are fitted as explained in IV.D-2. The corresponding distributions are depicted for the eight independent  $\Delta\phi$ -bins for the cut choices *SPDany proton band* in Fig. VI.7 and in Fig. VI.8. For the *SPDany no proton band* selection, they are shown in Fig. VI.9 and in Fig. VI.10. The fluctuations in the depicted distributions are strong, although they are still compatible with a statistical origin due to the sizeable statistical errors. The observed variations coincide partially with the ones observed in the invariant mass distributions (see Fig. III.7 for *SPDany proton band* and Fig. III.6 for *SPDany no proton band*). This is expected, since the correlation in every  $\Delta\phi$ -histogram are extensive in the number of dielectron pairs. It will be crucial to exclude any non-statistical origin of these fluctuations with larger statistics within the real data in future.

The fit functions evaluated in the signal region are then used for the quantification of the background shape, which is shown in Fig. VI.11 for *SPDany proton band* and in Fig. VI.12 for *SPDany no proton band*. The figures already divided by the number of background counts according to the LS signal extraction explained in III.B-2.ii. No uncertainty is depicted on the plots. The error of the systematic errors can be found in V. Fig. VI.11 shows qualitatively a shape, which is typical for a dihadron analysis is observed. This 'dijet-behavior' is compatible with the expectation that electrons (and also non-electronic contamination) from different sources combining accidentally to an invariant mass in the peak region of the  $J/\psi$ , is originating from a parton fragmentation process or from decay kinematics, which show this behaviour. However, the observed correlation is on top of a large uncorrelated pedestal. The observed behavior of the background description in Fig. VI.12 in the *SPDany no proton band* cut choice is less regular. Nevertheless, it is important to stress that the observed deviation of the bin near  $\Delta\phi = \pi$  with respect to the other bins has a similar size than the statistical uncertainty of the histogram, which enter in the fit determination.

Finally, one can retrieve the azimuthal  $J/\psi$ -hadron correlation, which are depicted in Fig. VI.14 for the cut choices *no proton band* and in Fig. VI.13 for *SPDany proton band*. The errors, which are shown only correspond to the bin-by-bin independent statistical errors. One has to take into account also the overall correlated statistical uncertainty and the systematic uncertainty, which is related to the signal extractions. The corresponding conservatively estimated relative statistical errors amount to about 20% (25%) for the cut choice *SPDany proton band* (*SPDany no proton band*). A trustworthy quantification of the systematic error is difficult at the present stage with the given statistical limitations. Nevertheless, it is expected that the statistical error is dominating in the case of this analysis as far as the

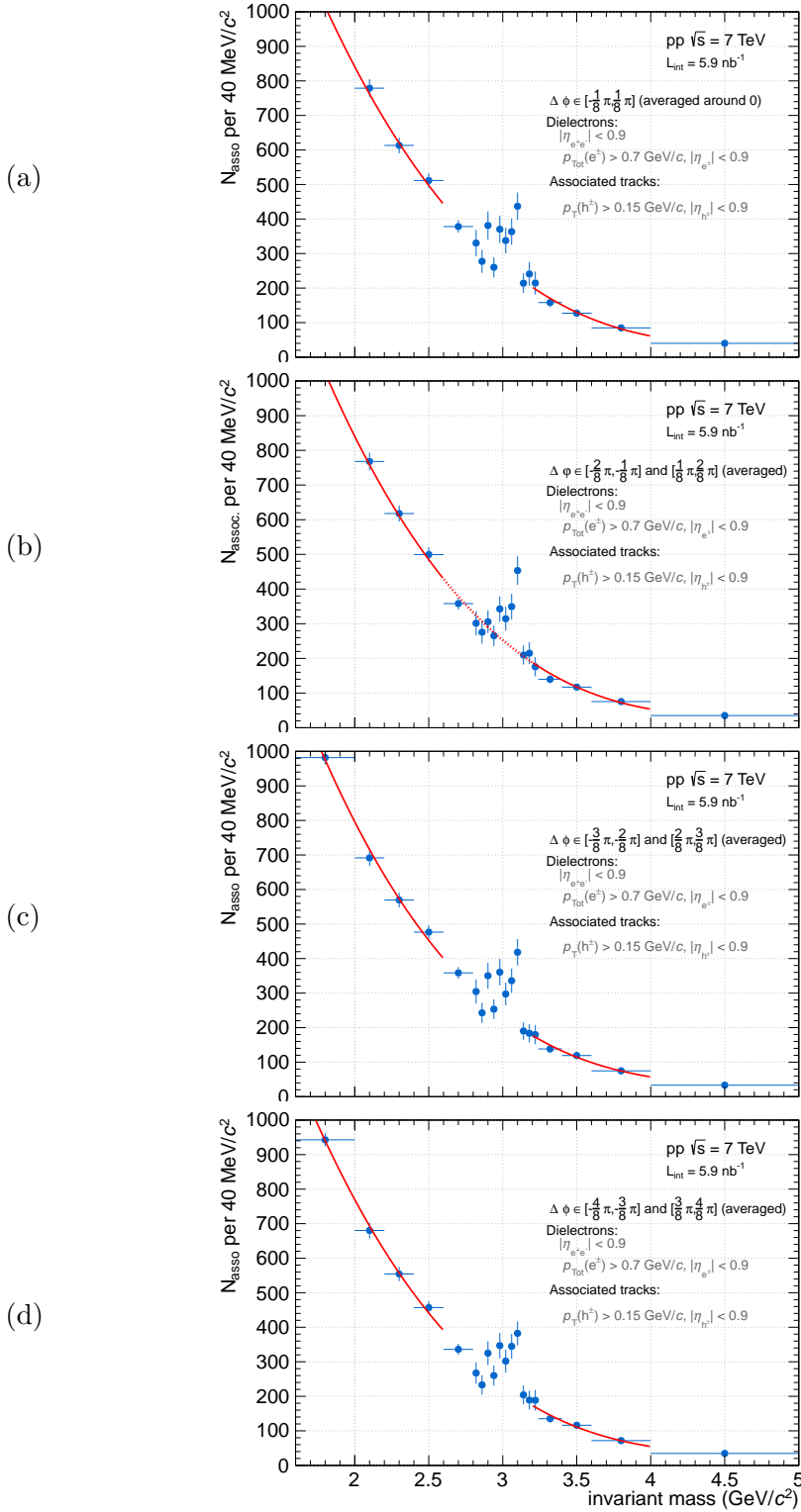


Figure VI.7: Azimuthal dielectron-hadron correlation as a function of invariant mass for  $\Delta\phi$ -bins around 0 (*proton band SPDany cut choice*). The fits for the background determination are also depicted.

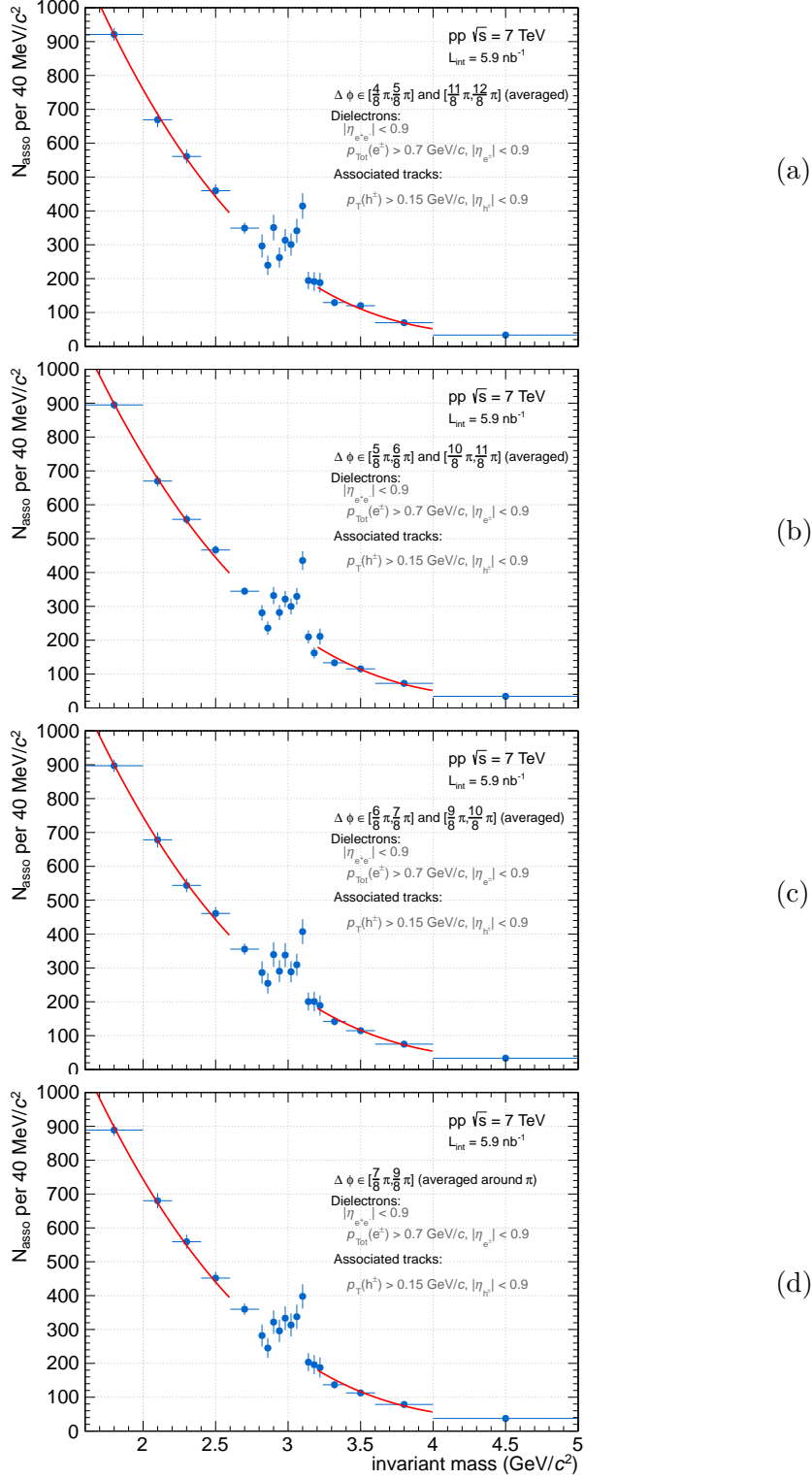


Figure VI.8: Azimuthal dielectron-hadron correlation as a function of invariant mass for  $\Delta\phi$ -bins around  $\pi$  (*proton band SPDany* cut choice). The fits for the background determination are also depicted.

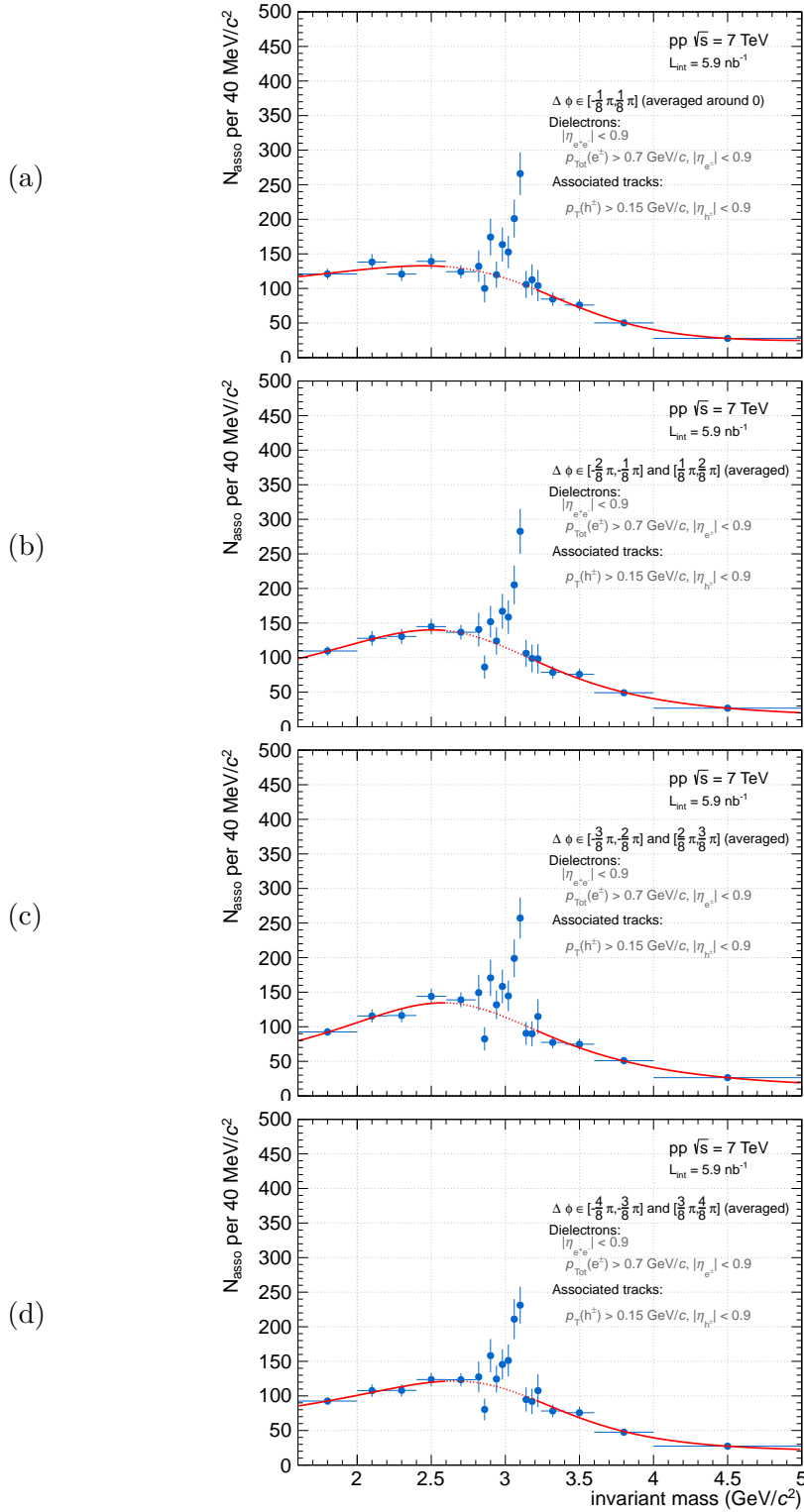


Figure VI.9: Azimuthal dielectron-hadron correlation as a function of invariant mass for  $\Delta\phi$ -bins around 0 ( *no proton band SPDany cut choice*). The fits for the background determination are also depicted.

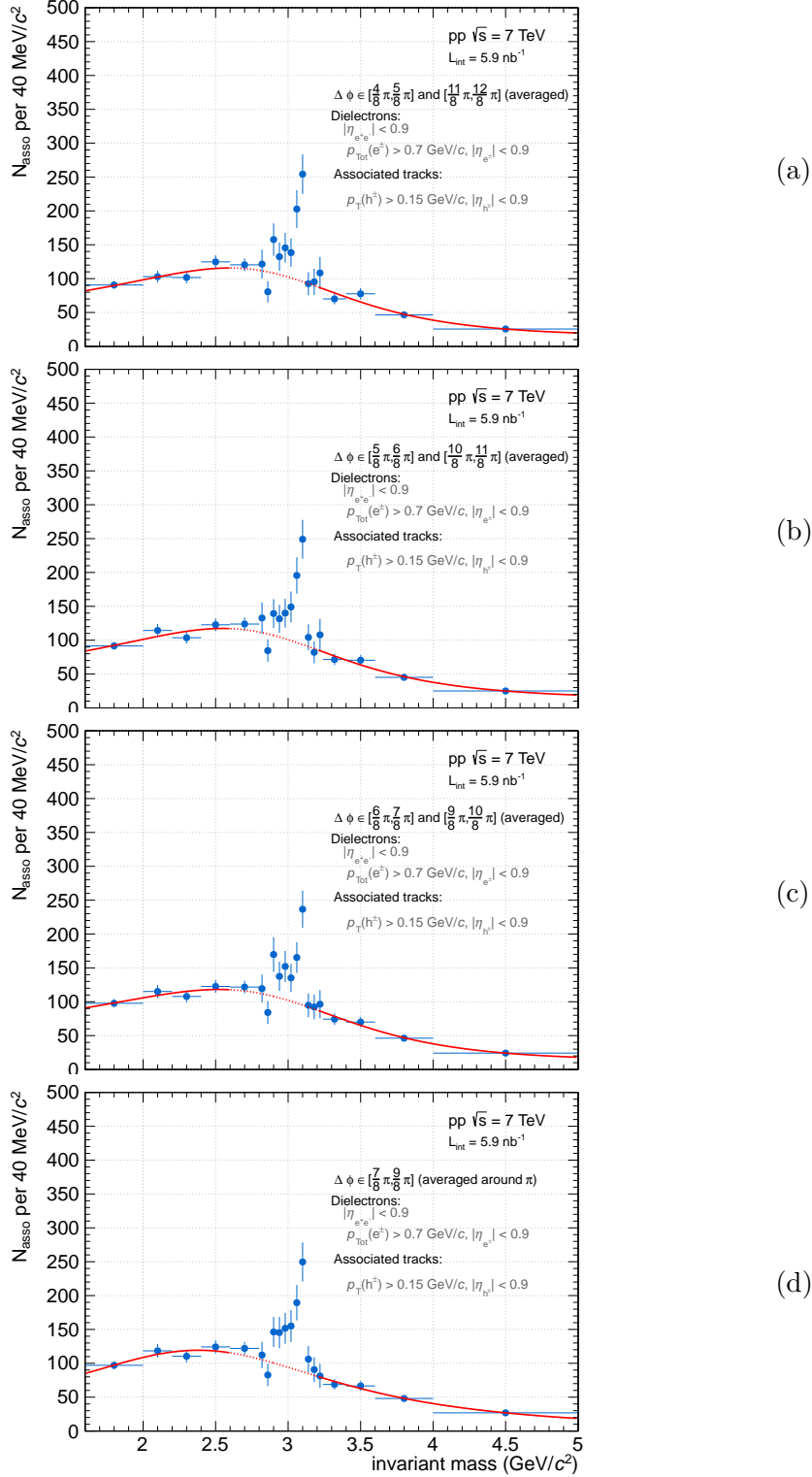


Figure VI.10: Azimuthal dielectron-hadron correlation as a function of invariant mass for  $\Delta\phi$ -bins around  $\pi$  (no proton band SPD any cut choice). The fits for the background determination are also depicted.

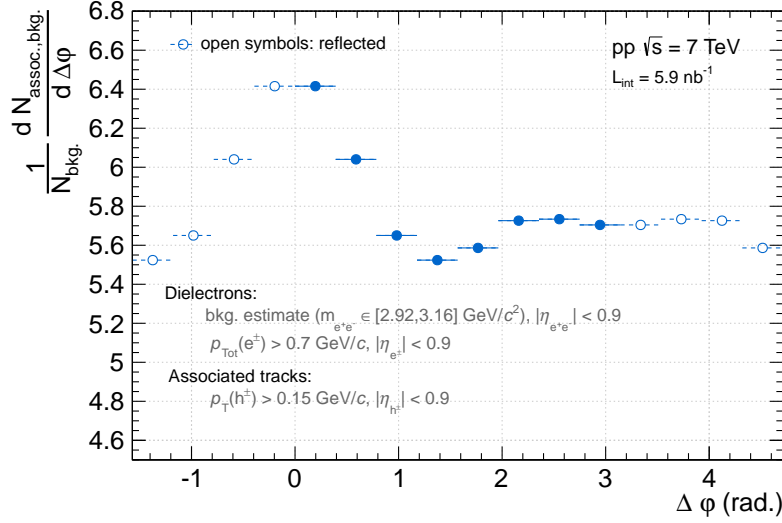


Figure VI.11: Extracted azimuthal dielectron-hadron **background** correlation estimate for *proton band SPDany* cut choice in the signal region,  $m_{e^+e^-} \in [2.92 - 3.16] \text{ GeV}/c^2$ .

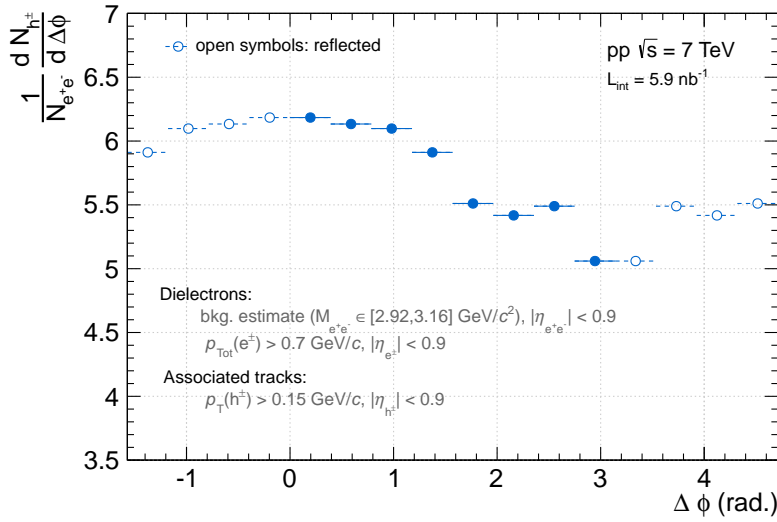


Figure VI.12: Extracted azimuthal dielectron-hadron **background** correlation estimate for *no proton band SPDany* cut choice in the signal region,  $m_{e^+e^-} \in [2.92 - 3.16] \text{ GeV}/c^2$ .

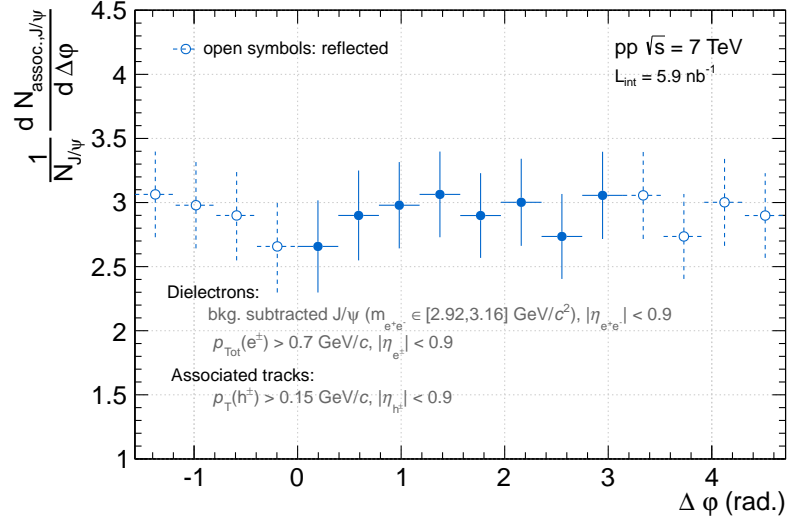


Figure VI.13: Extracted azimuthal  $J/\psi$ -hadron correlation for *proton band SPDany* cut choice.

derived shape of the correlation is concerned. For a more detailed discussion, see V. Within the present large statistical uncertainties, it is not possible to claim a significant correlation of the  $J/\psi$  with charged tracks. The result is also confirmed by the use of only a part of the invariant mass range, which yields completely compatible results. This is a reasonable cross check despite the even lower statistics, since the signal over background is strongly increased and, hence, the dependence on the background description and the influence of bremsstrahlung described in Appendix B is strongly reduced.

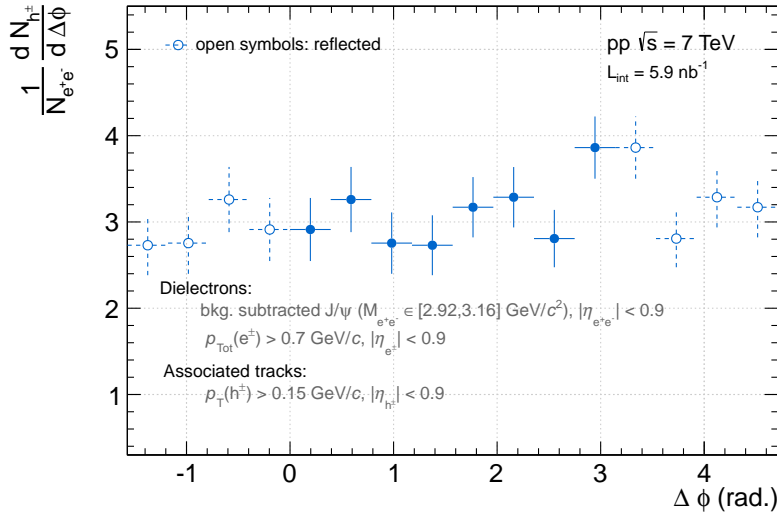


Figure VI.14: Extracted azimuthal  $J/\psi$ -hadron correlation for *no proton band SPDany* cut choice.

## VI.C Event Generator Description of $J/\psi$ -Hadron Observables

For an interpretation of the results or future analysis, it is necessary to consider possible theory expectations. The natural references are event generators, which try to provide a full description of charmonia in minimum bias proton-proton collision physics. For the event class analyzed in this study, it is important that the low  $p_T$  part of the  $J/\psi$  production is properly reproduced. Due to fact that it is not yet settled, which production mechanism model is most suited, Colour Octet (CO) or Colour Singlet (CS) amplitude dominance (see for more details in I.B), the issue is difficult to access. A large fraction of event generators, among them HERWIG[82] and Epos[83], does not provide a comprehensive attempt to model charmonium production[84].

One of the commonly used event generators in this context is PYTHIA. In PYTHIA 6.4[79], the production of prompt heavy charmonia is implemented via the CS Model and also NRQCD inspired hard matrix elements. It is important to note that only hard parton degrees of freedom are explicitly taken into account. Therefore, any hadronic activity, which might be connected to color neutralization of a color octet state evolving in a  $J/\psi$ , is intrinsically not incorporated in this event generator. In addition, the hard charmonium production is technically only allowed in the hardest scattering process in the event. Hence, there is no charmonium production from Multi-Parton Interactions, which might contribute significantly at low  $p_T$

to the total  $J/\psi$  cross section. Interestingly, there is also another source of charmonium in PYTHIA 6.4, which is the production via  $c\bar{c}$ -pair from initial and final state radiation [84]. These charmonia are created, since the charm quarks are typically close in phase space to each other. During the process of color reconnection, PYTHIA 6.4 simply forms charmonia states from these pairs. It is not clear, if this rather accidental production has any physical equivalent in nature. In summary, the PYTHIA 6.4 charmonium production is not expected to provide a reasonable description of the physical reality. In addition, it is not developed any longer.

The charmonium production in PYTHIA 8.1[80], which is the most recent version of PYTHIA, is no longer affected by the 'cluster' charmonia production from color reconnection. In addition, the production of  $J/\psi$  in the subhardest events is possible. Nevertheless, any hadronic activity directly connected with the  $J/\psi$ , which is not related to the fragmentation of the gluons in the Feynman diagrams (implemented in the framework of NRQCD) is not yet present. In light of these open questions, a reasonable comparison of event generators is not very easy and more evolved. For this task, a deep investigation of the possibilities provided by the most recent developments and a fruitful exchange with the developers will be necessary. The observables presented here, especially in conjunction with larger statistics, can give very valuable input to event generators attempting to describe charmonium occurrences more accurately.

Despite the open questions connected with prompt  $J/\psi$  production, the correlation of  $J/\psi$  from B-decays should be modelled reasonably well by Monte Carlo event generators, since they are to a large extent determined by the decay kinematics of the involved B-hadrons and the hard  $b\bar{b}$ -pair production. However, since the contribution of B-decays is of the order of 10 % in the present sample, it is not expected that these  $J/\psi$ -mesons will have an impact within the present statistical uncertainties. Therefore, a comparison of the correlation with MC generated B-decays is not appropriate for the investigated event sample.

## – Chapter VII –

# Conclusion and Prospects

This study represents the first investigation of azimuthal  $J/\psi$ -hadron correlations at low transverse momenta of  $J/\psi$ . The required methodology is introduced including the necessary efficiency and acceptance corrections. In addition, a background subtraction approach is described and applied on data. A correlated behavior of the large number of charged tracks in the same event as the  $J/\psi$  could not be observed within the present statistical limitations. In future, larger  $J/\psi$ -samples will allow the study of  $J/\psi$ -hadron correlations more precisely and, in addition, more differentially. Especially the variation of the  $p_T$ -threshold for the associated charged tracks will be important to enhance the sensitivity of the measurement. The analysis of the correlation between the  $J/\psi$ -meson and the leading- $p_T$  track in the same event could provide important information as well. Furthermore, the investigation of different  $J/\psi$ - $p_T$ -regimes will be crucial.

At low- $p_T$ , the multiplicity dependent behavior of the correlations will be of particular interest: It offers the opportunity to investigate to which extent the large hadronic activity observed by ALICE [39] is induced by the  $J/\psi$ -production itself or inherits from additional soft activity. At high- $p_T$ ,  $J/\psi$ -hadron correlations provide additional information about the event topology and, hence, about the production mechanism. In conjunction with the knowledge of the contribution from non-prompt  $J/\psi$ -production from secondary vertexing, the measurement of the hadronic activity accompanying prompt  $J/\psi$ -mesons will be very interesting.

Furthermore, the results both at low and high- $p_T$  can be valuable input for a more appropriate description of  $J/\psi$  in event generators.

ALICE is well suited for the study of detailed event characteristics in  $J/\psi$ -events due to precision tracking over a large transverse momentum range. The accumulation of larger statistical samples can be achieved by EMCal triggers at  $p_T > 6-8$  GeV/ $c$  and by TRD triggers even down to  $p_T \approx 1-2$  GeV/ $c$  of  $J/\psi$ . EMCal triggered events have already been recorded during 2011 and 2012. The TRD trigger is currently running and will give

access to a substantial increase of  $J/\psi$ -statistics in the kinematical domain, which is uniquely exploited by ALICE at LHC.

# Appendix A: Mixed event correction

The mixed event divisions applied in this thesis are used to eliminate possible effects of efficiency and acceptance in the measured raw distributions. It is clear that the correction is not imperatively needed for the good homogeneity of the TPC-tracking and the statistical precision achieved so far. Nevertheless, the implementation of these corrections can serve as a baseline for future correlation works.

First, a careful explanation and justification of the use of this method is presented. Secondly, the role of mixed event pool categories for the proper correlation will be explained.

## Basic Formalism

In order to concentrate on the essential features, we will assume, that all effects, which are not related to  $\phi$  and  $\eta$ -dependent efficiency/acceptance are already corrected before this correction is applied and the total number of tracks is already corrected properly<sup>1</sup>. In addition, we will consider only the one dimensional case of  $\Delta\eta(\Delta\phi)$ -correlation and assuming that there is no bias introduced by possible  $\Delta\phi(\Delta\eta)$ -inhomogeneities. We assume that the full azimuth is covered but only limited ranges for the  $\eta$  acceptance. We look at these distributions, since more dimensional cases follow by combining

---

1. In this analysis, this is achieved by applying the weighting factors explained in the corresponding section.

both cases in analogy to the one-dimensional case. We therefore start with:

$$\frac{dN_{assoc.}}{d\eta}(\eta) = \langle \frac{dN_{assoc.}}{d\eta} \rangle_{\eta} \cdot \epsilon_{assoc.}(\eta) \quad (\text{VII.1})$$

$$\frac{dN_{e^+e^-}}{d\eta}(\eta) = \langle \frac{dN_{e^+e^-}}{d\eta} \rangle_{\eta} \cdot \epsilon_{e^+e^-}(\eta) \quad (\text{VII.2})$$

$$\text{with:} \quad (\text{VII.3})$$

$$\int \epsilon_{assoc.}(\eta) d\eta \langle \frac{dN_{assoc.}}{d\eta} \rangle_{\eta} = N_{assoc.perpair} \quad (\text{VII.4})$$

$$\int \epsilon_{e^+e^-}(\eta) d\eta \langle \frac{dN_{e^+e^-}}{d\eta} \rangle_{\eta} = N_{e^+e^-} \quad (\text{VII.5})$$

$$\text{And:} \quad (\text{VII.6})$$

$$\frac{dN_{assoc.}}{d\phi}(\phi) = \langle \frac{dN_{assoc.}}{d\phi} \rangle_{\phi} \cdot \epsilon_{assoc.}(\phi) \quad (\text{VII.7})$$

$$\frac{dN_{e^+e^-}}{d\phi}(\phi) = \langle \frac{dN_{e^+e^-}}{d\phi} \rangle_{\phi} \cdot \epsilon_{e^+e^-}(\phi) \quad (\text{VII.8})$$

$$\text{with:} \quad (\text{VII.9})$$

$$\int \epsilon_{assoc.}(\phi) d\phi = 2\pi \quad (\text{VII.10})$$

$$\int \epsilon_{e^+e^-}(\phi) d\phi = 2\pi \quad (\text{VII.11})$$

$$(\text{VII.12})$$

The averages are already corresponding to the true values by assuming that efficiency corrections are applied before. Therefore, the 'efficiencies' reflect only relative efficiencies.

With these ingredients, the corresponding  $\Delta\eta$ -distribution is easy to construct<sup>2</sup>:

---

2. The following correction ansatz relies on the assumption that the efficiencies for the associated tracks (dielectron) pairs on the efficiencies of the dielectron pairs (associated tracks) only via their dependence of the absolute value of their pseudorapidity (or this effect is already taken care by other means). In other terms, it is assumed the correction via random events is sufficient to correct for the observed and not yet resolved efficiency effects and that  $C_{phys}(\Delta\eta)$  factorize with the efficiency effects. Since there is no large variation of the track density as a function of the  $J/\psi$ -emission direction, this should be a completely valuable assumption.

$$\frac{dN_{SE,measured}}{d(\Delta\eta)} = \quad (VII.13)$$

$$\int_{-\infty}^{\infty} d\eta_{assoc.} \int_{-\infty}^{\infty} d\eta_{e^+e^-} \frac{dN_{assoc.}(\eta_{e^+e^-})}{d\eta} \frac{dN_{e^+e^-}(\eta_{assoc.})}{d\eta} \delta(\eta_{e^+e^-} - \eta_{assoc.} - \Delta\eta) \quad (VII.14)$$

$$\cdot \Theta^4 \cdot C_{phys}(\Delta\eta) \quad (VII.15)$$

$$= \langle \frac{dN_{e^+e^-}}{d\eta} \rangle_{\eta} \langle \frac{dN_{assoc.}}{d\eta} \rangle_{\eta} \cdot C_{phys}(\Delta\eta) \quad (VII.16)$$

$$\cdot \int_{-\infty}^{\infty} d\eta_{assoc.} \int_{-\infty}^{\infty} d\eta_{e^+e^-} \epsilon_{assoc.} \epsilon_{e^+e^-} \cdot \Theta^4 \delta(\eta_{e^+e^-} - \eta_{assoc.} - \Delta\eta) \quad (VII.17)$$

$$\text{with:} \quad (VII.18)$$

$$\Theta^4 = \Theta(\eta_{assoc.} - \eta_{start,assoc.}) \Theta(-(\eta_{assoc.} - \eta_{end,assoc.})). \quad (VII.19)$$

$$\Theta(\eta_{e^+e^-} - \eta_{start,e^+e^-}) \Theta(-(\eta_{e^+e^-} - \eta_{end,e^+e^-})) \quad (VII.20)$$

$$\text{And:} \quad (VII.21)$$

$$\frac{dN_{SE,measured}}{d(\Delta\phi)} = \quad (VII.22)$$

$$\int_0^{2\pi} d\phi_{assoc.} \int_0^{2\pi} d\phi_{e^+e^-} \frac{dN_{assoc.}(\phi_{e^+e^-})}{d\phi} \frac{dN_{e^+e^-}(\phi_{assoc.})}{d\phi} \delta(\phi_{e^+e^-} - \phi_{assoc.} - \Delta\phi) \quad (VII.23)$$

$$\cdot C_{phys}(\Delta\phi) \quad (VII.24)$$

$$= \langle \frac{dN_{e^+e^-}}{d\phi} \rangle_{\eta} \langle \frac{dN_{assoc.}}{d\phi} \rangle_{\phi} \quad (VII.25)$$

$$\cdot \int_0^{2\pi} d\phi_{assoc.} \int_0^{2\pi} d\eta_{e^+e^-} \epsilon_{assoc.} \epsilon_{e^+e^-} \quad (VII.26)$$

$$(VII.27)$$

In this notation, the contribution to the folding from finite  $\eta$ -acceptance is expressed by the  $\Theta$  functions and separated from the relative efficiency effects given in the  $\epsilon$  functions. The  $C_{phys}$  function corresponds to the correlation function defined in the analysis method part. It is important to note that the  $\Theta$  functions concerning  $\eta_{assoc.}(\eta_{e^+e^-})$  introduce also constraints for the integration boundaries of  $\eta_{e^+e^-}(\eta_{e^+e^-})$  after resolving the  $\delta$ -distribution. Therefore, one cannot just write the borders given by the  $\Theta$ -functions as the integral boundaries, since there are not independent of each other, i.e. in case of constant  $\epsilon$ , this is still a non-trivial effect encoded in the  $\Theta$ -functions, which is the common triangular shape seen in the  $\Delta\eta$  before the correction. In contrast to the  $\eta$ -formulae, in the corresponding expressions of the azimuthal distributions, the integration boundaries are independent of each other, since from every absolute  $\phi$  value for the dielectron pair (associated

track), every possible  $\Delta\phi$  value is still possible<sup>3</sup>. From this formulae, it is also directly clear, that one has only to correct for these efficiency effects in case of a  $\Delta\phi$ -distribution, if both  $\epsilon$ -functions are not constant, since if already one of the two distributions is constant, the whole integration gets trivial and will not introduce any bias in the  $\Delta\phi$  distribution.

The corresponding distribution for the mixed events looks the same except of the mixing  $C_{phys}$ , since this correlation cannot be present by definition, since the tracks and the dielectron pairs are taken from different events:

$$\frac{dN_{ME}}{d(\Delta\eta)} = \quad (VII.28)$$

$$\int_{-\infty}^{\infty} d\eta_{assoc.} \int_{-\infty}^{\infty} d\eta_{e^+e^-} \frac{dN_{assoc.}}{d\eta_{assoc.}} \frac{dN_{e^+e^-}}{d\eta_{e^+e^-}} \delta(\eta_{e^+e^-} - \eta_{assoc.} - \Delta\eta) \Theta^4 \quad (VII.29)$$

$$= \left\langle \frac{dN_{e^+e^-}}{d\eta} \right\rangle_{\eta} \left\langle \frac{dN_{assoc.}}{d\eta} \right\rangle_{\eta} \quad (VII.30)$$

$$\cdot \int_{-\infty}^{\infty} d\eta_{assoc.} \int_{-\infty}^{\infty} d\eta_{e^+e^-} \epsilon_{assoc.} \epsilon_{e^+e^-} \cdot \delta(\eta_{e^+e^-} - \eta_{assoc.} - \Delta\eta) \cdot \Theta^4 \quad (VII.31)$$

In this formulation, it is also immediately clear, how the normalization of the mixed-event distribution has to proceed, in order to correct the same event distribution correctly:

$$Corr_{ME} = \frac{\left\langle \frac{dN_{e^+e^-}}{d\eta} \right\rangle_{\eta} \left\langle \frac{dN_{assoc.}}{d\eta} \right\rangle_{\eta} \cdot (\eta_{end,e^+e^-} - \eta_{start,e^+e^-})}{\frac{dN_{ME}}{d(\Delta\eta)}} \quad (VII.32)$$

$$\text{And therefore:} \quad (VII.33)$$

$$\frac{dN_{SE,corrected}}{d(\Delta\eta)} = \frac{dN_{SE,measured}}{d(\Delta\eta)} \cdot Corr_{ME} \quad (VII.34)$$

$$= \left\langle \frac{dN_{e^+e^-}}{d\eta} \right\rangle_{\eta} \left\langle \frac{dN_{assoc.}}{d\eta} \right\rangle_{\eta} \cdot (\eta_{end,e^+e^-} - \eta_{start,e^+e^-}) \cdot C_{phys.}(\Delta\eta) \quad (VII.35)$$

$$= N_{e^+e^-} \left\langle \frac{dN_{assoc.}}{d\eta} \right\rangle_{\eta} \cdot C_{phys.}(\Delta\eta) \quad (VII.36)$$

In case of a homogeneous tracking efficiency, the normalization factor of the correction factor reduces to:

$$\left\langle \frac{dN_{e^+e^-}}{d\eta} \right\rangle_{\eta} \left\langle \frac{dN_{assoc.}}{d\eta} \right\rangle_{\eta} \cdot (\eta_{end,e^+e^-} - \eta_{start,e^+e^-}) = \frac{dN_{ME,hom}(\Delta\eta = 0)}{d(\Delta\eta)} \quad (VII.37)$$

---

3. assuming that the detector has full azimuthal angle coverage.

And therefore the correction factor to:

$$Corr_{ME,hom} = \frac{\frac{dN_{ME}(\Delta\eta=0)}{d(\Delta\eta)}}{\frac{dN_{ME}}{d(\Delta\eta)}} \quad (\text{VII.38})$$

This is due to the fact, that that there is no influence of the  $\Theta$  functions for the central  $\Delta\eta$  bin and the  $\epsilon$  functions are 1 in this special case. In case of the azimuthal correlations assuming a full coverage in azimuth the following formulae for the normalization is valid, since there is no effect from the finite acceptance:

$$\left\langle \frac{dN_{e^+e^-}}{d\phi} \right\rangle_{\phi} \left\langle \frac{dN_{assoc.}}{d\phi} \right\rangle_{\phi} \cdot 2\pi = \left\langle \frac{dN_{ME}}{d(\Delta\phi)} \right\rangle_{\phi} \quad (\text{VII.39})$$

$$\text{And therefore:} \quad (\text{VII.40})$$

$$Corr_{ME} = \frac{\left\langle \frac{dN_{ME}}{d(\Delta\eta)} \right\rangle_{\phi}}{\frac{dN_{ME}}{d(\Delta\phi)}} \quad (\text{VII.41})$$

Naturally, there is no need for a relative correction by mixed events for the azimuthal correlation, if the tracking efficiency is homogeneous as a function of  $\phi$ .

## Role of pool categories

By applying the formalism developed and correcting the whole same event distribution by mixed event distributions retrieved from the full same event ensemble of associated tracks and dielectron pairs, the intended correction of the  $\phi$ - and  $\eta$ -efficiency and acceptance connected effects is only accurate, if the  $\phi$ - and  $\eta$ -efficiency maps are only functions of  $\phi$  and  $\eta$  and constant as a function of any other event specific, track specific or dielectron pair specific variable. This is generally not the case.

Therefore, one has to consider possible further corrections. Correcting subsets of same event distributions with mixed event distributions constructed from the same same event subsets are an appropriate tool to adress this issue. The division in this case is in done separately for every category and the distributions are added together afterwards by respecting their relative statistical weight. Usually, the term mixing pool categories is used for this kind of subevent samples. First, it is necessary to know, which kind of variable dependence can be corrected by this technique and which can't be corrected. Secondly, it is important to address, which observable is reasonable to be used for this categorization of events and subsequently mixing in these categories. It is only possible to use the pool categories for correcting properties, which are:

- characteristic for the event

- characteristic for the dielectron pair<sup>4</sup>
- characteristic for the leading- $p_T$  track in case of the leading- $p_T$  track-dielectron analysis

It is not possible with this method to correct for effects, which are characteristic for the charged tracks due to the fact that these effects are not caused by properties which distinguish one specific dielectron occurrence from another.

Secondly, there are two approaches to select reasonable variables for these mixing categories<sup>1</sup>:

- variables, which have an influence on the  $\eta$  and/or  $\phi$  efficiency maps
- variables, which have an influence on the physical shape  $C_{phys}$  or the number of correlated associated tracks per dielectron pair

One has only to correct for variables, which fulfill both criteria. We discuss for illustration only the dependence on one additional variable  $a$  and the  $\eta$  efficiencies.

In case that the  $\phi$  and  $\eta$ -efficiency is not a function of the additional variable, it is clear that there is no need for a further correction, since the average over the additional variable to be considered is properly done also if it influences the shape of the correlation. If the  $\phi$  and/or  $\eta$  efficiency depends on event or dielectron specific variables in addition to the  $\phi$  and  $\eta$  values of the associated tracks or of the dielectron pair, it is instructive to explain the situation by introducing generalized efficiencies in the additional observable  $a$  to be considered with the following properties:

$$\int da \epsilon_{e^+e^-}^{gen.}(\eta, a) \epsilon_{assoc.}^{gen.}(\eta, a) = \epsilon_{e^+e^-}(\eta) \epsilon_{assoc.}(\eta) \quad (\text{VII.42})$$

The equality is only right for the product and not for the individual factors, since the efficiencies appear only together in one specific dielectron occurrence.

Furthermore, we assume that  $C_{phys}(\Delta\eta)$ , the number of associated tracks per dielectron pair and the efficiencies show a dependence on the variable  $a$ , which is the most general case. We consider the case that the mixed event categories are chosen in a way that the variable  $a$  does not influence  $C_{phys}$ ,  $\epsilon_{e^+e^-}(\eta)$  and  $\epsilon_{assoc.}(\eta)$  within one single mixed event category. The

---

4. For the leading- $p_T$  track correlations, this is conceptually the same, for the dielectron correlations allowing multiple counting of a single event by multiple dielectrons in the event it is not the same.

1. Theoretically, the consideration of all possible variables is the best choice, but this is in the experiment due to limited statistics not possible.

boundaries of the mixing categories are denoted with  $a_i$ ,  $i \in [0, n]$ .

$$\frac{dN_{SE,corrected}}{d(\Delta\eta)} = \sum_{j=1}^n \frac{dN_{SE,measured,[a_{j-1},a_j]}}{d(\Delta\eta)} \cdot Corr_{ME,[a_{j-1},a_j]} \quad (\text{VII.43})$$

$$= \sum_{j=1}^n C(\Delta\eta, [a_{j-1}, a_j]) N_{e^+e^-}([a_{j-1}, a_j]) < \frac{dN_{assoc.}}{d\eta} >_{\eta}([a_{j-1}, a_j]) \quad (\text{VII.44})$$

By neglecting this dependencies on additional variables, the result will be biased, since the efficiency folding does not factorize with the physical shape and the number of associated tracks.

Possible examples for  $a$  in our case are:

- event properties: Vertex position, multiplicity
- dielectron properties: mass, opening angle,  $\Delta\phi_{e^+e^-}$ ,  $p_T$ , *polarization*

In the case of this analysis, finally only the invariant mass of the dielectron pair was considered as a mixing category, since a strong dependence of  $C_{phys}$  is observed. Naturally, also other observables like the opening angle in the transverse plane could be considered, since they have also a major impact on the efficiency map and are assumed to have a certain influence on the shape of the correlation, since this angle is strongly correlated with the transverse momentum<sup>5</sup>. Since the charged track efficiency is very homogeneous, the effect of the mixed event correction is small compared to the overall statistical error, which limit also the dimensions of mixed event categories. Therefore, only the mass was considered as a mixed event category. In future works, especially in case that the tracking efficiency exhibits a less optimal behaviour, certainly further observables have to be considered to guarantee a reliable correction by mixed events.

---

5. A binning in the transverse momentum instead, would also be an alternative.



# Appendix B: Influence of internal and external Bremsstrahlung on the measurement of $\phi_{J/\psi}$

Due to the fact that not a  $J/\psi$ , but a dielectron is detected and due to the non-negligible QED NLO internal bremsstrahlung and also the real bremsstrahlung induced at the passage of electrons through the detector material, it is necessary to investigate, whether the measurement of the azimuthal angle of a dielectron pair is significantly deviated from the azimuthal angle of the  $J/\psi$ .

Being only interested in an upper bound for the influence of this effect, the most extreme case is considered, namely a dielectron pair with a invariant mass of  $2.92 \text{ GeV}/c^2$ , which is the lower bound of the signal extraction region. The effect is also only treated by assuming that the tracking of dielectron is not affected by the emission of the photon and that the  $\phi$  measurement of electrons doesn't suffer from the effect.

First, the energy of the photon in the  $J/\psi$  rest frame is calculated using the four-momenta of the dielectron pair  $p_{e^+e^-}$  and of the photon  $p_\gamma$ :

$$m_{J/\psi}^2 = (p_{e^+e^-} + p_\gamma)^2 = m_{e^+e^-}^2 + 2E_\gamma(E_{e^+e^-} - |\vec{p}_{e^+e^-}|) \quad (\text{VII.45})$$

$$E_\gamma = \frac{m_{J/\psi}^2 - m_{e^+e^-}^2}{2 \cdot m_{J/\psi}} \quad (\text{VII.46})$$

It was exploited that the three-momentum of the dielectron pair and the one of the photon have to balance each other in this particular frame. The numerical evaluation gives<sup>6</sup>:  $E_\gamma = |\vec{p}_{e^+e^-}c| = 0.174 \text{ GeV}$ . Secondly, we consider the case, which results on the largest impact on the angle for the consideration of the kinematics in the lab frame. In order to determine the largest possible  $\phi_{e^+e^-} - \phi_{J/\psi}$  value, we assume that the decay plane, i.e. the plane spanned by the three-momentum of the  $J/\psi$  and the three-momentum

---

6. A mass  $m_{J/\psi}$  of  $3.1 \text{ GeV}/c^2$  was used. The intrinsic width is not important for the estimate, since it is roughly 2000 times smaller than the considered difference in invariant mass.

of the dielectron pair, is the plane transverse to the beam axis<sup>7</sup>. Since we want to keep the calculation as compact as possible, we are defining the unit vector of the  $J/\psi$  momentum as the x-axis without loss of generality. Therefore, the maximization of  $\phi_{e^+e^-} - \phi_{J/\psi}$  under the assumption of a positive projection of the dielectron pair momentum on the  $J/\psi$  momentum ( $p_{x,e^+e^-} > 0$ ) is corresponding to (all momenta are labframe momenta):

$$\text{minimize: } \cos(\phi_{e^+e^-} - \phi_{J/\psi}) = \frac{\vec{p}_{J/\psi} \cdot \vec{p}_{e^+e^-}}{|\vec{p}_{J/\psi}| |\vec{p}_{e^+e^-}|} \quad (\text{VII.47})$$

$$= \frac{\vec{p}_{T,J/\psi} \cdot \vec{p}_{T,e^+e^-}}{|\vec{p}_{T,J/\psi}| |\vec{p}_{T,e^+e^-}|} = \frac{p_{x,e^+e^-}}{\sqrt{p_{x,e^+e^-}^2 + p_{y,e^+e^-}^2}} \quad (\text{VII.48})$$

$$\text{maximize: } \frac{|p_{y,e^+e^-}|}{|p_{x,e^+e^-}|} \quad (\text{VII.49})$$

, where the last step is based on the monotonic behaviour of all involved functions in the relevant range. For the determination of the situation, which leads to the most extreme case, it is useful to express the labframe as a function of the momenta in the  $J/\psi$  restframe, since the value of the total momentum is already determined in this frame:

$$\frac{|p_{y,e^+e^-}|}{|p_{x,e^+e^-}|} = \frac{|p_{y,e^+e^-,rest}|}{|p_{x,e^+e^-,rest}\gamma + \gamma\beta E_{rest,e^+e^-}|} \quad (\text{VII.50})$$

$$\text{With:} \quad (\text{VII.51})$$

$$\gamma\beta = \frac{|\vec{p}|_{J/\psi,lab}}{m_{J/\psi}} = \frac{p_{x,J/\psi,lab}}{m_{J/\psi}}, \gamma = \frac{E_{lab,J/\psi}}{m_{J/\psi}} \quad (\text{VII.52})$$

$$\text{And:} \quad (\text{VII.53})$$

$$\frac{|p_{y,e^+e^-}|}{|p_{x,e^+e^-}|} = \frac{\sqrt{const - p_{x,e^+e^-,rest}^2}}{|p_{x,e^+e^-,rest}\gamma + \gamma\beta E_{rest,e^+e^-}|} \quad (\text{VII.54})$$

Since  $\beta E_{rest,e^+e^-} \gg p_{x,e^+e^-,rest}$  is valid for the relevant phase space of considerable momenta of  $J/\psi$ <sup>8</sup>, we can approximately assume for the estimate of the effect, that:

$$\frac{|p_{y,e^+e^-}|}{|p_{x,e^+e^-}|} \text{ is maximized for minimal } p_{x,e^+e^-,lab} \quad (\text{VII.55})$$

The result is that in this approximation the most extreme case corresponds to a  $J/\psi$ -flight direction perpendicular to the emission direction of

7. There are also configurations with larger angles between the dielectron pair and the  $J/\psi$ , if one considers the possibility that the projection of the dielectron momentum on the  $J/\psi$  momentum has not a positive sign, which is occurring only for extremely small transverse momenta of the  $J/\psi$ .

8. Equality is occurring with a dielectron invariant mass choice of 2.92 for:  $p_{J/\psi} = 0.2$  GeV/c; for  $p_{J/\psi} = 1.0$  GeV/c we have already:  $\beta E_{rest,e^+e^-} \approx 14 p_{x,e^+e^-,rest}$

the photon in the  $J/\psi$  restframe ( $p_{x,e^+e^-,rest} = 0$ ). The estimate follows straightforwardly:

$$\cos[(\phi_{e^+e^-} - \phi_{J/\psi})_{max}] = \quad (VII.56)$$

$$\frac{\beta\gamma E_{e^+e^-,rest}(=p_{x,e^+e^-,lab})}{\sqrt{E_{\gamma,rest}^2(=p_{y,e^+e^-,lab}^2 = p_{y,e^+e^-,rest}^2) + \beta^2\gamma^2 E_{e^+e^-,rest}^2(=p_{x,e^+e^-,lab}^2)}} \quad (VII.57)$$

A numerical evaluation yields for a  $J/\psi$ -momentum of 1 GeV/c (2 GeV/c, 10 GeV/c) and a dielectron mass of 2.92 GeV/c to:

$$(\phi_{e^+e^-} - \phi_{J/\psi})_{max} = 11.0^\circ (5.4^\circ, 1.1^\circ)$$

These values are smaller than the correlation bin width ( $22.50^\circ$ ), but could in principle alter the result significantly. However, it is important to note, that the most extreme case assuming the largest spread in invariant mass was assumed, which is not representative for the dielectron sample in this measurement. For an invariant mass of  $3.0 \text{ GeV}/c^2$  of the dielectron pair and the corresponding photon energy, which still applies only for a fraction of the selected signal dielectron pairs, one retrieves for a  $J/\psi$  momentum of 1 GeV/c (2 GeV/c, 10 GeV/c)

$$(\phi_{e^+e^-} - \phi_{J/\psi})_{max} = 5.6^\circ (2.8^\circ, 0.56^\circ).$$

In addition, these values does not correspond to an proper average over the spatial directions, but for the upper limit configuration. If we still assume that the  $J/\psi$  is emitted in the plane transverse to the beam axis, preserving the convention this direction is the x-axis and still assume that the dielectron pair momentum is in the restframe of the  $J/\psi$  perpendicular to the x-axis, but allow that the dielectron pair momentum has also a component in z- direction, we can allow for 'rotation' of the dielectron pair around the  $J/\psi$ - direction. We can easily derive an equally weighted average of the  $(\phi_{e^+e^-} - \phi_{J/\psi})_{max}$ , since the formulae stated above for  $(\phi_{e^+e^-} - \phi_{J/\psi})$  is in this case the correct formulae for the  $\cos[(\Delta\Theta)_{max}]$ <sup>9</sup>:

$$\text{Defining: } x = \frac{p_{y,e^+e^-}}{\sqrt{p_{y,e^+e^-}^2 + p_{z,e^+e^-}^2}} \quad (VII.58)$$

$$(\text{These quantities are equal in rest- and labframe}) \quad (VII.59)$$

$$\text{And: } c = E_{\gamma,rest}/p_{x,e^+e^-,lab} \quad (VII.60)$$

$$\langle \cos(\phi_{e^+e^-} - \phi_{J/\psi})_{max} \rangle_{2D} = \int_0^1 \frac{1}{\sqrt{1 + (c \cdot x)^2}} dx \quad (VII.61)$$

$$\text{A substitution and evaluation yield to:} \quad (VII.62)$$

$$\langle \cos(\phi_{e^+e^-} - \phi_{J/\psi})_{max} \rangle_{2D} = \frac{1}{c} [\text{arcsinh}(c)] \quad (VII.63)$$

---

9.  $\Delta\Theta$  denotes the opening angle between the dielectron pair and the  $J/\psi$  in three dimension.

This calculation results in a value for an average azimuthal angle difference for  $m_{e^+e^-} = 2.92 \text{ GeV}/c^2$  and for a  $1 \text{ GeV}/c$  ( $2 \text{ GeV}/c$ ,  $10 \text{ GeV}/c$ )  $J/\psi$ :

$$((\phi_{e^+e^-} - \phi_{J/\psi})_{max,2D} = 6.2^\circ (3.1^\circ, 0.6^\circ))$$

And for  $m_{e^+e^-} = 3 \text{ GeV}/c^2$  for a  $J/\psi$  momentum of  $1 \text{ GeV}/c$  ( $2 \text{ GeV}/c$ ):

$$((\phi_{e^+e^-} - \phi_{J/\psi})_{max,2D} = 3.2^\circ (1.6^\circ, 0.32^\circ))$$

Therefore, the resulting distortion of the observed distributions can be neglected for this first study. In future, these effects should be investigated in more detail in Monte Carlo studies for more precise investigations of  $J/\psi$ -correlations and it might be necessary to restrict the invariant mass range of the  $J/\psi$ , especially if it is intended to use a smaller binning for the  $\Delta\phi$  between the  $J/\psi$  and the charged tracks.

# Bibliography

- [1] S.L. Glashow.  
Partial Symmetries of Weak Interactions.  
*Nucl.Phys.*, 22:579–588, 1961.
- [2] S. Weinberg.  
A Model of Leptons.  
*Phys.Rev.Lett.*, 19:1264–1266, 1967.
- [3] D. J. Gross and F. Wilczek.  
Ultraviolet behavior of non-abelian gauge theories.  
*Phys.Rev.Lett.*, 30(26):1343–1346, 1973.
- [4] H. D. Politzer.  
Reliable perturbative results for strong interactions?  
*Phys.Rev.Lett.*, 30(26):1346–1349, 1973.
- [5] A. Djouadi.  
The Anatomy of electro-weak symmetry breaking. I: The Higgs boson  
in the standard model.  
*Phys.Rept.*, 457:1–216, 2008.
- [6] G. Aad et al.  
Observation of a new particle in the search for the Standard Model  
Higgs boson with the ATLAS detector at the LHC.  
*Phys.Lett.B*, 716:1–29, 2012.
- [7] S. Chatrchyan et al.  
Observation of a new boson at a mass of 125 GeV with the CMS ex-  
periment at the LHC.  
*Phys.Lett.B*, 716:30–61, 2012.
- [8] P. Braun-Munzinger and J. Stachel.  
The quest for the quark-gluon plasma.  
*Nature*, 448:302–309, 2007.

- [9] R. Aaij et al.  
Measurement of the CP-Violating Phase  $\phi_s$  in the Decay  $B_s^0 \rightarrow J/\psi\phi$ .  
*Phys.Rev.Lett.*, 108:101803, 2012.
- [10] T. Matsui and H. Satz.  
 $J/\psi$  suppression by quark-gluon plasma formation.  
*Phys.Lett.B*, 178:416–422, 1986.
- [11] F. Karsch and H. Satz.  
The spectral analysis of strongly interacting matter.  
*Z.Phys.C*, 51:209–224, 1991.
- [12] L. Kluberg and H. Satz.  
Color Deconfinement and Charmonium Production in Nuclear Collisions.  
2009.  
arXiv:hep-ph/0901.3831.
- [13] X. Zhao and R. Rapp.  
Medium Modifications and Production of Charmonia at LHC.  
*Nucl.Phys.A*, 859:114–125, 2011.
- [14] B. Chen, K. Zhou, and P. Zhuang.  
Mean Field Effect on  $J/\psi$  Production in Heavy Ion Collisions.  
*Phys.Rev.C*, 86:034906, 2012.
- [15] P. Braun-Munzinger and J. Stachel.  
(Non)thermal aspects of charmonium production and a new look at  $J/\psi$  suppression.  
*Phys.Lett.B*, 490:196–202, 2000.
- [16] A. Andronic, P. Braun-Munzinger, K. Redlich, and J. Stachel.  
Evidence for charmonium generation at the phase boundary in ultra-relativistic nuclear collisions.  
*Phys.Lett.B*, 652:259–261, 2007.
- [17] B. Abelev et al.  
Upgrade of the ALICE Experiment Letter Of Intent.  
2012.  
CERN-LHCC-2012-012 ; LHCC-I-022.
- [18] P. Braun-Munzinger and K. Redlich.  
Charmonium production from the secondary collisions at LHC energy.  
*Eur.Phys.J.C*, 16:519–525, 2000.
- [19] B. Abelev et al.  
 $J/\psi$  suppression at forward rapidity in Pb-Pb collisions at  $\sqrt{s_{NN}} =$

- 2.76 TeV.  
*Phys.Rev.Lett.*, 109:072301, 2012.
- [20] J. Wiechula for the ALICE collaboration.  
Nuclear modification of  $J/\psi$  production in Pb-Pb collisions at  $\sqrt{s_{NN}} = 2.76$  TeV.  
arXiv:hep-ex/1208.6566, 2012.
- [21] N. Brambilla, S. Eidelman, B.K. Heltsley, R. Vogt, G.T. Bodwin, et al.  
Heavy quarkonium: progress, puzzles, and opportunities.  
*Eur.Phys.J.C*, 71:1534, 2011.
- [22] K. Aamodt et al.  
Rapidity and transverse momentum dependence of inclusive  $J/\psi$  production in  $pp$  collisions at  $\sqrt{s} = 7$  TeV.  
*Phys.Lett.B*, 704:442–455, 2011.
- [23] J.-E. Augustin et al.  
Discovery of a Narrow Resonance in  $e^+e^-$  Annihilation.  
*Phys.Rev.Lett.*, 33:1406–1408, 1974.
- [24] J.J. Aubert et al.  
Experimental Observation of a Heavy Particle J.  
*Phys.Rev.Lett.*, 33:1404–1406, 1974.
- [25] T. Appelquist and H. D. Politzer.  
Heavy quarks and  $e^+e^-$  annihilation.  
*Phys.Rev.Lett.*, 34:43–45, 1975.
- [26] J. Beringer et al.  
Review of Particle Physics (RPP).  
*Phys.Rev.D*, 86:010001, 2012.
- [27] R. K. Ellis, W. J. Stirling, and B.R. Webber.  
QCD and collider physics.  
*Camb.Monogr.Part.Phys.Nucl.Phys.Cosmol.*, 8:1–435, 1996.
- [28] S. Bethke.  
Experimental Tests of Asymptotic Freedom.  
*Prog.Part.Nucl.Phys.*, 58:351–386, 2006.  
arXiv:hep-ex/0606035v2.
- [29] G. T. Bodwin, E. Braaten, and G. P. Lepage.  
Rigorous QCD analysis of inclusive annihilation and production of heavy quarkonium.  
*Phys.Rev.D*, 51:1125–1171, Feb 1995.

- [30] E. Eichten, K. Gottfried, T. Kinoshita, K. D. Lane, and T. M. Yan.  
Charmonium: The model.  
*Phys.Rev.D*, 17:3090–3117, 1978.
- [31] F. Abe et al.  
Inclusive  $J/\psi$ ,  $\psi(2S)$  and  $b$  quark production in  $\bar{p}p$  collisions at  $\sqrt{s} = 1.8$  TeV.  
*Phys.Rev.Lett.*, 69:3704–3708, 1992.
- [32] J.P. Lansberg.  
 $J/\psi$  production at  $\sqrt{s} = 1.96$  and 7 TeV: Color-Singlet Model, NNLO\* and polarisation.  
*J.Phys.G*, 38:124110, 2011.
- [33] J.-P. Lansberg.  
Quarkonium production in the LHC era: QCD correction and new observables.  
In *ICHEP 2012 proceedings- to be published*, 2012.
- [34] M. Butenschoen and B. A. Kniehl.  
World data of  $J/\psi$  production consolidate nonrelativistic QCD factorization at next-to-leading order.  
*Phys.Rev.D*, 84:051501, 2011.
- [35] Y.-Q. Ma, K. Wang, and K.-T. Chao.  
A complete NLO calculation of the  $J/\psi$  and  $\psi'$  production at hadron colliders.  
*Phys.Rev.D*, 84:114001, 2011.
- [36] P. Sun, C. P. Yuan, and F. Yuan.  
Heavy Quarkonium Production at Low  $p_t$  in NRQCD with Soft Gluon Resummation.  
2012.  
arXiv:hep-ph/1210.3432.
- [37] V.A. Saleev, M.A. Nefedov, and A.V. Shipilova.  
Prompt  $J/\psi$  production in the Regge limit of QCD: From Tevatron to LHC.  
*Phys.Rev.D*, 85:074013, 2012.
- [38] N. P. Zotov.  
Small x physics and hard QCD processes at LHC.  
*PoS, QFTHEP2011:010*, 2011.
- [39] B. Abelev et al.  
 $J/\psi$  production as a function of charged particle multiplicity in pp collisions at 7 TeV.  
*Phys.Lett.B*, 712(3):165 – 175, 2012.

- [40] S. Porteboeuf and R. Granier de Cassagnac.  
J/ $\psi$  yield vs. multiplicity in proton-proton collisions at the LHC.  
*Nucl.Phys.Proc.Suppl.*, 214:181–184, 2011.
- [41] M. Strikman.  
Remarks on the observation of high multiplicity events at the lhc.  
*Phys.Rev.D*, 84:011501, Jul 2011.
- [42] D. Acosta et al.  
Measurement of the J/ $\psi$  meson and  $b$ -hadron production cross sections in  $p\bar{p}$  collisions at  $\sqrt{s} = 1960$  GeV.  
*Phys.Rev.D*, 71:032001, 2005.
- [43] S. Abachi et al.  
J/ $\psi$  production in pp collisions at  $\sqrt{s} = 1.8$  TeV.  
*Phys.Lett.B*, 370(1–2):239 – 248, 1996.
- [44] A. Adare et al.  
J/ $\psi$  Production versus Transverse Momentum and Rapidity in  $p + p$  Collisions at  $\sqrt{s} = 200$  GeV.  
*Phys.Rev.Lett.*, 98:232002, Jun 2007.
- [45] B. Abelev et al.  
J/ $\psi$  production at high transverse momentum in p+p and Cu+Cu collisions at  $\sqrt{s_{NN}} = 200$  GeV.  
*Phys.Rev.C*, 80:041902, 2009.
- [46] L. Adamczyk et al.  
J/ $\psi$  production at high transverse momenta in  $p + p$  and Au+Au collisions at  $\sqrt{s_{NN}} = 200$  GeV.  
2012.  
arXiv:nucl-ex/1208.2736.
- [47] G. Aad et al.  
Measurement of the differential cross-sections of inclusive, prompt and non-prompt J/ $\psi$  production in proton-proton collisions at  $\sqrt{s} = 7$  TeV.  
*Nucl.Phys.B*, 850:387–444, 2011.
- [48] V. Khachatryan et al.  
Prompt and non-prompt J/ $\psi$  production in pp collisions at  $\sqrt{s} = 7$  TeV.  
*Eur.Phys.J.C*, 71:1575, 2011.
- [49] R. Aaij et al.  
Measurement of J/ $\psi$  production in pp collisions at  $\sqrt{s} = 7$  TeV.  
*Eur.Phys.J.C*, 71:1645, 2011.

- [50] B. Abelev et al.  
Measurement of prompt and non-prompt  $J/\psi$  production cross sections at mid-rapidity in  $pp$  collisions at  $\sqrt{s} = 7$  TeV.  
2012.  
arXiv:hep-ex/1205.5880.
- [51] F. Abe et al.  
Production of  $J/\psi$  Mesons from  $\chi_c$  Meson Decays in  $p\bar{p}$  Collisions at  $\sqrt{s} = 1.8$  TeV.  
*Phys.Rev.Lett.*, 79:578–583, Jul 1997.
- [52] R. Aaij et al.  
Measurement of the cross-section ratio  $\sigma(\chi_{c2})/\sigma(\chi_{c1})$  for prompt  $\chi_c$  production at  $\sqrt{s} = 7$  TeV.  
*Phys.Lett.B*, 714:215–223, 2012.
- [53] S. Chatrchyan et al.  
Measurement of the relative prompt production rate of  $\chi(c2)$  and  $\chi(c1)$  in  $pp$  collisions at  $\sqrt{s} = 7$  TeV.  
2012.  
arXiv:hep-ex/1210.0875.
- [54] P. Faccioli.  
Questions and prospects in quarkonium polarization measurements from proton-proton to nucleus-nucleus collisions.  
*Mod.Phys.Lett.A*, 27:1230022, 2012.
- [55] T. Affolder et al.  
Measurement of  $J/\psi$  and  $\psi(2S)$  polarization in  $p\bar{p}$  collisions at  $\sqrt{s} = 1.8$  TeV.  
*Phys.Rev.Lett.*, 85:2886–2891, 2000.
- [56] A. Abulencia et al.  
Polarization of  $J/\psi$  and  $\psi(2S)$  mesons produced in  $p\bar{p}$  collisions at  $\sqrt{s} = 1.96$  TeV.  
*Phys.Rev.Lett.*, 99:132001, 2007.
- [57] A. Adare et al.  
Transverse momentum dependence of  $J/\psi$  polarization at midrapidity in  $p + p$  collisions at  $\sqrt{s} = 200$  GeV.  
*Phys.Rev.D*, 82:012001, 2010.
- [58] B. Abelev et al.  
 $J/\psi$  polarization in  $pp$  collisions at  $\sqrt{s}=7$  TeV.  
*Phys.Rev.Lett.*, 108:082001, 2012.

- [59] C. Albajar et al.  
High transverse momentum  $J/\psi$  production at the CERN proton-antiproton collider.  
*Phys.Lett.B*, 200(3):380 – 390, 1988.
- [60] J.-P. Lansberg.  
Quarkonium production at high-energy hadron colliders: A Systematic gauge-invariant approach to relativistic effects of  $J/\psi$ ,  $\psi'$  and  $\Upsilon$  production.  
2005.  
arXiv:hep-ph/0507175.
- [61] A. C. Kraan.  
Experimental Aspects of Heavy Quarkonium Production at the LHC.  
*AIP Conf.Proc.*, 1038:45–54, 2008.
- [62] L. (ed.) Evans and P. (ed.) Bryant.  
LHC Machine.  
*J.Instrum.*, 3:S08001, 2008.
- [63] K. Aamodt et al.  
The ALICE experiment at the CERN LHC.  
*J.Instrum.*, 3:S08002, 2008.
- [64] G. Aad et al.  
The ATLAS Experiment at the CERN Large Hadron Collider.  
*J.Instrum.*, 3:S08003, 2008.
- [65] S. Chatrchyan et al.  
The CMS experiment at the CERN LHC.  
*J.Instrum.*, 3:S08004, 2008.
- [66] <http://lpc.web.cern.ch/lpc/>, 09 2012.
- [67] K. Aamodt et al.  
Production of pions, kaons and protons in pp collisions at  $\sqrt{s} = 900$  GeV with ALICE at the LHC.  
*Eur.Phys.J.C*, 71:1655, 2011.
- [68] J. Alme, Y. Andres, H. Appelshauser, S. Bablok, N. Bialas, et al.  
The ALICE TPC, a large 3-dimensional tracking device with fast read-out for ultra-high multiplicity events.  
*Nucl.Instrum.Meth.A*, 622:316–367, 2010.
- [69] A. Kalweit.  
*Production of light flavor hadrons and anti-nuclei at the LHC*.  
PhD thesis, TU Darmstadt Fachbereich Physik, Darmstadt, Juli 2012.

- [70] B. Abelev et al.  
Measurement of electrons from semileptonic heavy-flavour hadron decays in pp collisions at  $\sqrt{s} = 7$  TeV.  
2012.  
arXiv:hep-ex/1205.5423.
- [71] A. Spiridonov.  
Bremsstrahlung in Leptonic Onia Decays: Effects on Mass Spectra.  
DESY-04-105.
- [72] D. Acosta et al.  
Measurement of the  $J/\psi$  meson and  $b$ -hadron production cross sections in  $p\bar{p}$  collisions at  $\sqrt{s} = 1960$  GeV.  
*Phys.Rev.D*, 71:032001, 2005.
- [73] B. Abelev et al.  
Underlying Event measurements in pp collisions at  $\sqrt{s} = 0.9$  and 7 TeV with the ALICE experiment at the LHC.  
*J. High Energy Phys.*, 1207:116, 2012.
- [74] M. Kweon.  
private communication.
- [75] A. Adare for the ALICE collaboration.  
Triggered di-hadron correlations in Pb-Pb collisions from the ALICE experiment.  
*J.Phys.G*, 38:124091, 2011.
- [76] K. Aamodt et al.  
Harmonic decomposition of two particle angular correlations in Pb-Pb collisions at  $\sqrt{s_{NN}} = 2.76$  TeV.  
*Phys.Lett.B*, 708(3-5):249 – 264, 2012.
- [77] S. Vallero.  
*Study of the Underlying Event in pp collisions with the ALICE detector at the LHC.*  
PhD thesis, 2012.
- [78] M. Ivanov.  
private communication.
- [79] T. Sjöstrand, S. Mrenna, and P. Skands.  
PYTHIA 6.4 Physics and Manual.  
*J. High Energy Phys.*, 05:026, 2006.
- [80] T. Sjöstrand, S. Mrenna, and P. Skands.  
A Brief Introduction to PYTHIA 8.1.  
*Comput. Phys. Commun.*, 178:852–867, 2008.

- [81] K. Aamodt et al.  
Charged-particle multiplicity measurement in proton-proton collisions at  $\sqrt{s} = 7$  TeV with ALICE at LHC.  
*Eur.Phys.J.C*, 68:345–354, 2010.
- [82] M. Bahr, S. Gieseke, M. A. Gigg, D. Grellscheid, K. Hamilton, O. Latunde-Dada, S. Platzer, P. Richardson, M. H. Seymour, A. Sherstnev, J. Tully, and B. R. Webber.  
Herwig++ Physics and Manual.  
*Eur.Phys.J.C*, 58:639–707, 2008.
- [83] K. Werner.  
The hadronic interaction model EPOS.  
*Nucl.Phys.B*, 175-176:81–87, 2008.  
Proceedings of the XIV International Symposium on Very High Energy Cosmic Ray Interactions.
- [84] S. Porteboeuf-Houssais.  
private communication.



# Acknowledgements

First of all, I want to thank Prof. Dr. Johanna Stachel for the opportunity to work in this interesting field of research, the supervision of my thesis and her support during my thesis.

Furthermore, I would like to thank Prof. Dr. Hans-Christian Schultz-Coulon for reading and evaluating my thesis.

I am very grateful for all the discussion and help by the Jpsi2ee physics-analysis group and its members Dr. Anton Andronic, Dr. Ionut Arsene, Dr. Antonin Maire, Dr. Jens Wiechula, Prof. Dr. Christoph Blume, Dr. Giuseppe Bruno, Dr. Fiorella Fionda and Julian Book.

Furthermore, thanks go to the physics-working group on correlations and especially Dr. Jan Fiete Grosse-Oetringhaus and Dr. Sara Vallero for their support with the correlations framework and many discussions and advices. I greatly appreciate the support by the TPC experts Dr. Alexander Kalweit and Dr. Marian Ivanov.

Moreover, I would like to thank Dr. Sarah Porteboeuf-Houssais for the discussion on the implementation of charmonia in current event generators.

I would like to thank Dr. Yvonne Pachmayer, Jochen Klein, Dr. Ionut Arsene and Dr. Antonin Maire for proofreading my thesis.

Dr. MinJung Kweon, Felix Reidt, Johannes Stiller and Martin Völkl deserve thanks for the many interesting discussions and help.

Many thanks go to Dr. Ilya Selyuzhenkov for saving my computer's hard disk.

This work has been supported supported by the Studienstiftung des Deutschen Volkes and the Federal Ministry of Education and Research under promotional reference 06HD197D.



## **Erklärung:**

Ich versichere, dass ich diese Arbeit selbständig verfasst und keine anderen als die angegebenen Quellen und Hilfsmittel benutzt habe.

Heidelberg, den 23. Oktober 2012

Unterschrift: .....  
Michael Winn